Circuits and mechanisms controlling SW-REM alternation in sleep

Dissertation
zur Erlangung des Doktorgrades
der Naturwissenschaften

vorgelegt beim Fachbereich Biowissenschaften
der Johann Wolfgang Goethe - Universität
in Frankfurt am Main

von Hua-Peng Liaw
aus Taiwan

Frankfurt 2021
(D 30)

vom Fachbereich Biowissenschaften der

Johann Wolfgang Goethe - Universität als Dissertation angenommen.

Dekan:

Prof. Dr. Sven Klimpel

Gutachter:

Prof. Gilles Laurent

Neural Systems and Coding

Max Planck Institute for Brain Research, Frankfurt am Main

Prof. Dr. Jochen Röper

Institut für Physiologie II (Sinnes- und Neurophysiologie)

Johann Wolfgang Goethe University, Frankfurt am Main

Datum der Disputation: 16/03/2022

Contents

Abstract

Sleep is one of the fundamental requirements of all animals from nematodes to humans. It appears in different formats with shared features such as reduced muscle activities and reduced responsiveness to the environment. Despite the long history of sleep research, why a brain must be taken offline for a large portion of each day remains unknown. Moreover, sleep research focused on mammals and birds reveals two stages, rapid-eye-movement (REM) and slow-wave (SW) sleep, alternating during sleep. Whether these two stages of sleep exist in other vertebrates, particularly reptiles, is debated, as is the evolution of sleep in general.

Recordings from the brain of a lizard, the Australian bearded dragon *Pogona vitticeps*, indicate the presence of two electrophysiological states and provides a better picture of their sleep. Local field potential (LFP) signals, head velocity, eye movements, and heart rate during sleep match the pattern of REM and SW sleep in mammals. The SW and REM sleep patterns that we observed in lizards oscillated continuously for 6 to 10 hours with a period of 80-100 seconds when the ambient temperature was ~27°C. Lizard SW dynamics closely resemble those observed in rodent hippocampal CA1, yet originated from a brain area, the dorsal ventricular ridge (DVR), that does not correspond anatomically or transcriptomically to the mammalian hippocampus. This finding pushes back the probable evolution of these dynamics to the emergence of amniotes, at least 300 million years ago.

Unlike mammals and birds, REM and SW sleep in lizards occupy an almost equal amount of time during sleep. The clock-like alternation between these two sleep states was found initially by measuring the power modulation of two frequency bands, delta and beta. I recorded the full-band LFP and found an infra-slow oscillation (ISO) in the frequency range between 5 and 20 milli-Hz during sleep. The magnitude of ISO increased during sleep and decreased during both wakefulness and arousal during sleep. The up- and down-states of ISO were synchronized with the sleep state alternating rhythm but with a significant time lag dependent on the locations of the recording electrodes. Multi-site LFP recordings indicated that this ISO is a putative propagation wave sweeping extremely slowly, 30-67 µm/sec, from the posterior-dorsal pole to the anterior-ventral pole of the DVR.

Previous studies in other animals showed that brainstem areas such as the locus coeruleus, laterodorsal tegmentum, and periaqueductal gray are involved in sleep states regulation. It is sadly impossible to carry out *in vivo* recordings in the lizard brainstem without severely affecting them and their quality of life. I thus carried out *ex vivo* recordings in both DVR and brainstem.

Pharmacological stimulation of the brainstem could reversibly silence one distinct EEG pattern characteristic of SW sleep, the sharp-wave and ripple complex, in DVR. An ISO could be recorded simultaneously in both DVR and brainstem. From data collected in both intact and split *ex vivo* brains, I concluded that there are independent ISO generators in at least two areas, the brainstem and the telencephalon. Their signals may normally be synchronized by long-range connections. The DVR ISO leads the brainstem ISO by ~29 sec. Optogenetic stimulation of brainstem neurons was able to disrupt the ISO in DVR reversibly.

In conclusion, the lizard brain offers a relatively simple model system to study sleep. Despite a diversity of results in different lizard species, my results revealed a number of new findings. Relevant for sleep research in general: 1) REM and SW sleep exist in a reptile. Since they also exist in birds and mammals, they probably existed in their common amniote ancestor, if not earlier. 2) REM and SW occupy equal amounts of time during sleep (50% duty cycle), a unique feature among all described sleep electrophysiological patterns, suggesting the possible existence of a simple central pattern generator of sleep, possibly ancestral. 3) I discovered the existence, in the local field potential, of an infra slow oscillation with extremely slow propagation, locked to the SW-REM alternating rhythm. The causes and mechanisms of this ISO remain to be understood. To my knowledge, the correlation between sleep states and a slow rhythm has only been reported in human scalp EEG recordings so far.

Zusammenfassung

Einleitung:

Schlaf ist eine grundlegendes Bedürfnis für alle Tiere, vom Fadenwurm bis zum Menschen. Er tritt in unterschiedlichen Formen auf und weist gemeinsame Merkmale auf wie reduzierte Muskelaktivität, reduzierte Interaktionen mit der Umgebung, schnelle Reversibilität, und homöostatische Regulierung (Piéron, 1913). Trotz der langen Geschichte der Schlafforschung ist nach wie vor unklar warum das Gehirn für einen großen Teil des Tages in einen Ruhemodus übergeht.

Zu Beginn des 20. Jahrhunderts wurde der Schlaf als kontinuierlicher Zustand niedriger Aktivität untersucht (Kleitman, 1929), bis Loomis et al. den menschlichen Schlaf erstmals auf der Grundlage von Elektroenzephalographie (EEG)-Mustern in fünf Phasen unterteilten (Loomis et al., 1937). Bei anderen Säugetieren und Vögeln wird das Schlaf-EEG in der Regel in zwei Zustände unterteilt: REM-Schlaf (Rapid-Eye-Movement) und SW-Schlaf (Slow-Wave), auf der Grundlage von EEG-, EMG- und EOG-Signalen. Diese beiden Zustände sind bei Säugetieren und Vögeln eindeutig nachgewiesen worden (Low et al., 2008; Siegel, 2008). Ob die beiden Schlafstadien auch in Reptilien existieren, beziehungsweise ihr evolutionärer Ursprung, war jedoch umstritten.

Säugetiere und Vögel teilen sich einen Amniotenvorfahr, trennten sich jedoch vor über 300 Millionen Jahren (Striedter, 2016). Weil diese beiden Gruppen die einzigen Homöothermen unter den lebenden Wirbeltieren sind wurde vermutet dass sich der Zweistufenschlaf unabhängig voneinander entwickelt hat, und zwar aufgrund gemeinsamer Zwänge und selektiven Drucks in Verbindung mit der Homöothermie (Hobson, 2005;Libourelund Herrel, 2016). Wenn REM- und SW-Schlaf jedoch auch in anderen Zweigen des Amniotenstammbaums vorkommen, z. B. bei nicht-avianischen Reptilien, könnten die elektrophysiologischen Signaturen dieser beiden Stadien von einem gemeinsamen Vorfahren geerbt worden sein. Frühere Arbeiten, an denen verschiedene Reptilienarten beteiligt waren, lieferten unterschiedliche und teilweise widersprüchliche Ergebnisse (Libourel und Herrel, 2016).

Wir haben das lokale Feldpotential (LFP), die Herzfrequenz sowie die Kopf- und Augenbewegungen während des Schlafs im Gehirn einer Echse, der australischen Bartagame *Pogona vitticeps,* erneut untersucht. Die Ergebnisse bestätigten die Existenz von verhaltensbedingtem Schlaf. Darüberhinaus konnten wir zeigen dass schlafbezogenen LFP-

Muster jenen ähneln, die im Schlaf von Säugetieren aufgezeichnet werden (Shein-Idelson et al., 2016). Der REM- und der SW-Schlaf nehmen in Echsen fast die gleiche Zeitspanne während des Schlafs ein. Der taktähnliche Wechsel zwischen diesen beiden Schlafzuständen wurde zunächst durch Messung der Leistungsmodulation von zwei Frequenzbändern, Delta und Beta, festgestellt. Ich zeichnete das Vollband-LFP auf und fand eine Infra-Slow-Oszillation (ISO) im Frequenzbereich zwischen 5 und 20 Milli-Hz während des Schlafs.

ISO, definiert als langsame und periodische Fluktuation des elektrischen Potenzials, wurde erstmals 1957 von Aladjalova anhand von EEG-Aufzeichnungen in frei beweglichen Kaninchen beschrieben (Aladjalova, 1957). Statt die elektrischen Potenziale direkt zu messen, berichten viele Studien über die langsamen Oszillationen, indem sie die zyklische Veränderung schneller neuronaler Aktivitäten wie Aktionspotenziale (Albrecht et al., 1998; Penttonen et al., 1999; Ruskin et al., 1999) und verschiedener Gehirnwellen (Drew et al., 2008; Lázár et al., 2019; Novak et al., 1992) messen. Trotz der Beobachtung von ISOs in verschiedenen Spezies und Frequenzbereichen wurden ISOs jahrzehntelang weitgehend ignoriert, meist aus technischen Gründen. Die meisten EEG-Aufzeichnungen werden heute mit wechselstromgekoppelten Verstärkern durchgeführt, bei denen der Niederfrequenzfilter auf 0,5 Hz oder höher eingestellt ist, um unerwünschtes Rauschen wie Bewegungsartefakte zu eliminieren. Solche Filter unterdrücken jedoch auch langsame (<0,1 Hz) Rhythmen und können, je nach Filtertyp, niederfrequente Signale verzerren.

In meiner Dissertation untersuche ich die Existenz von ISO in *In-vivo*- und *Ex-vivo*-Aufnahmen. Die Phase der ISOs korreliert in *in* vivo-Aufnahmen auch robust mit Schlafzuständen. Der langsame Rhythmus kann im Hirnstamm und den bilateralen DVRs in intakten und gespaltenen *ex vivo* Gehirnen aufgezeichnet werden. Über die Mechanismen der ISO-Erzeugung ist nur sehr wenig bekannt. Ich stelle drei Hypothesen auf, darunter 1) die Gesamtaktivität von Neuronen und diffundierenden Faktoren; 2) Leitfähigkeitsänderungen durch Abfallbeseitigungsmechanismen; 3) extrazelluläre Potenzialänderungen, die durch den intrakraniellen Druck ausgelöst werden.

Ergebnisse:

Die weithin akzeptierte Definition von Schlaf basiert auf verhaltensbezogenen und kortikalen elektrophysiologischen Mustern. Ich habe die für Nagetiere entwickelten Methoden und Geräte für Aufzeichnungen in Echsen angepasst. Wir bestätigten zunächst die Existenz des Verhaltensschlafs durch gleichzeitige Aufzeichnung der Herzfrequenz, der

Kopfdrehgeschwindigkeit und der Augenbewegungen. Der Verhaltensschlaf ist eng mit dem Hell-Dunkel-Zyklus verbunden und bei allen Echsen und in allen Nächten sehr ähnlich. Das DVR-LFP während des Verhaltensschlafs konnte in zwei Spektralcluster unterteilt werden. Die dominante Frequenz des einen Clusters liegt unter 4 Hz. Der andere Cluster zeigte eine Breitbandaktivität, die dem des Wachzustand ähnelt. Wir wählten die Leistung des Deltabandes (0,5-4 Hz) und des Betabandes (10-30 Hz), um diese beiden Cluster zu quantifizieren, und berechneten das Verhältnis von Delta- zu Beta-Leistung (und nicht das Verhältnis von Delta- zu Theta-Leistung, wie bei Ratten) über ein 10-Sekunden-Gleitfenster. Bei Aufzeichnungen über Nacht oszillierte das δ/β-Leistungsverhältnis regelmäßig und kontinuierlich mit einer Periode von 80-100 Sekunden. Die Periode der δ/β-Verhältnis-Oszillation ist temperaturabhängig und wird durch eine quadratische Gleichung gut angepasst.

Die SW-REM-Zustände wechseln sich während der ganzen Nacht sehr regelmäßig ab, ein Muster, das bisher nur selten beschrieben wurde, wenn überhaupt. Die stabile Periode des Schlafzustandswechsels deutet auf die Existenz eines langsamen Oszillators im DVR hin. Der langsame Rhythmus der δ/β-Band-Leistungsmodulation lässt sich erst nach mehreren Schritten der Datenverarbeitung erkennen, einschließlich Segmentierung, Spektralanalyse, Leistungsmittelung und Division. Ich untersuchte die Möglichkeit, das langsame, DC-ähnliche extrazelluläre Feldpotenzial während des Schlafs direkt aufzuzeichnen. Dabei entdeckte ich das ISO in einem Frequenzbereich zwischen 5 und 20 Milli-Hertz. Trotz der Unterschiede zwischen den Aufzeichnungen hinsichtlich der Umgebungstemperatur, und des Beginns und des Endes der Aufzeichnung, war die ISO-Leistung immer gut mit der Leistung des δ/β-Leistungsverhältnisses korreliert. Experimente in denen der Schlaf in der Mitte der Nacht gestört wurde bestätigten die Beziehung zwischen ISO und Schlafzuständen auf langen Zeitskalen.

Sowohl das δ/β-Leistungsverhältnis als auch ISO sind langsame periodische Signale. Das Scrolling-Kreuzkorrelogramm zeigt eine sehr stabile Beziehung zwischen ISO und dem δ/β-Verhältnis. Während des Schlafs blieben die Periode dieser beiden Signale und die Verzögerung zwischen ihnen weitgehend unverändert. Interessanterweise änderte sich bei einer Änderung der Umgebungstemperatur zwar die Periode, nicht aber die Amplitude der beiden Signale. Die Zeitabstände zwischen ihnen änderten sich nicht proportional.

Die führenden und nachlaufenden Signale (δ/β-Verhältnis oder ISO) änderten sich nicht im Laufe der Zeir, wenn sie von denselben Elektroden und in demselben Tier aufgezeichnet wurden. Allerdings konnte das führende Signal bei verschiedenen Tieren/Aufzeichnungen

unterschiedlich sein. Beim Vergleich von Signalen verschiedener Elektroden in einer Sonde mit mehreren Schäften bleibt die Verzögerung zwischen den δ/β-Verhältnissen gleich, aber die Verzögerung zwischen den ISOs weist erhebliche Verzögerungen auf, obwohl sie sehr ähnliche Amplituden und Wellenformen haben. Lange Verzögerungen zwischen den Elektroden bedeuten, dass die ISO eine sich ausbreitende Welle mit einer sehr langsamen Ausbreitungsgeschwindigkeit (30-67 µm/sec entlang verschiedener Achsen) ist, von posterior-dorsal nach anterior-ventral in der DVR.

Frühere Studien an anderen Tiermodellen haben gezeigt dass Hirnstammbereiche wie der Locus coeruleus (LC) und das laterodorsale Tegmentum (LDT) in hohem Maße an der Regulierung des Schlafzustands beteiligt sind. Aufgrund der technischen Schwierigkeiten untersuchte ich die Interaktion zwischen Hirnstamm und DVR durch Aufzeichnungen in einem isolierten (*ex vivo*) Gehirn. Ein isoliertes Gehirn befand sich 16-24 Stunden lang in einem "neutralen" Zustand, der sich nicht eindeutig in Schlaf, Wachzustand oder Anästhesie einteilen lässt. *Ex-vivo*-Aufnahmen ermöglichten mir die gleichzeitige Aufzeichnung des LFPs von bilateralen DVRs und homologen Hirnstammbereichen, die wahrscheinlich am Wechsel des Schlafzustands beteiligt sind. Aus den Ergebnissen unserer Konnektivitätsstudien geht hervor, dass der DVR weitreichende und direkte Inputs von LC und subC erhält. Die pharmazeutische Stimulation dieser Bereiche in einem isolierten Gehirn kann das ausgeprägteste EEG-Muster während des Schlafs, den sogenannten „Sharp-Wave and Ripple-Komplex“ im DVR reversibel inhibieren.

ISOs mit einem breiteren Frequenzbereich als bei In-vivo-Aufnahmen (0,7-50 mHz) gibt es in bilateralen DVRs und im Hirnstamm. Ihre Frequenzen sind in den verschiedenen Bereichen fast identisch, aber die zeitliche Verzögerungen zwischen dem Hirnstamm und den bilateralen DVRs sind ~29 Sekunden lang, wobei der DVR führend ist. In Übereinstimmung mit den *In-vivo*-Ergebnissen handelt es sich bei der Ex-vivo-ISO ebenfalls um eine sich ausbreitende Welle. Die Verzögerung zwischen oberflächlichen und tiefen Aufnahmestellen (700 um entfernt) beträgt nur 1,6 Sekunden und ist damit wesentlich kürzer als bei *In-vivo*-Aufnahmen.

Angesichts der offensichtlichen Koordination zwischen DVRs und dem Hirnstamm habe ich versucht herauszufinden, ob einer oder beide die Quelle der Oszillation sind, oder ob vielleicht ein vermeintlicher, wahrscheinlich verteilter Oszillator fehlt. Ich verwendete ein einfaches physikalisches Trennexperiment, um diese Fragen zu klären. ISOs waren im Vorderhirn und im Hirnstamm vor und nach dem Querschnitt vorhanden, aber die Verzögerungszeit zwischen den beiden Teilen wurde instabil. Außerdem habe ich das ChR2-infizierte Gehirn verwendet, um die

Interaktion zwischen diesen beiden ISO-Generatoren zu testen. Lichtreize im Hirnstamm sind in der Lage, den DVR-ISO mit einer langen (~30 Minuten) Latenzzeit zu unterbrechen.

Schlussfolgerung:

Das Echsengehirn bietet ein relativ einfaches Modellsystem zur Untersuchung des Schlafs. Trotz unterschiedlicher Ergebnisse bei verschiedenen Echsenarten haben meine Ergebnisse eine Reihe neuer Erkenntnisse gebracht, die für den Schlaf im Allgemeinen von Bedeutung sind. Erstens gibt es REM- und SW-Schlaf in einem Reptil. In Anbetracht der Tatsache, dass homologe Bereiche, die bei Säugetieren mit der Schlafregulation in Verbindung gebracht werden, schon sehr alt sind, könnte das Reptiliengehirn auf ein uraltes schlafregulierendes System hinweisen, das wahrscheinlich schon beim gemeinsamen Vorfahren der Amnioten, wenn nicht sogar früher, existierte. Reptilien könnten daher ein nützliches Modell für die Untersuchung des SW-REM-Schlafwechsels sein. Zweitens nehmen REM- und SW-Phasen während des Schlafs gleich viel Zeit in Anspruch (50 % Duty Cycle), ein einzigartiges Merkmal unter allen beschriebenen elektrophysiologischen Schlafmustern, was auf die mögliche Existenz eines einfachen zentralen Mustergenerators des Schlafs hindeutet, der möglicherweise auf einen Vorfahren zurückgeht. Drittens entdeckte ich im lokalen Feldpotenzial eine extrem langsam fortschreitende Infra-Slow-Oszillation, die mit dem SW-REM-Wechselrhythmus verbunden ist. Die Ursachen und Mechanismen dieses ISO müssen noch erforscht werden, aber sie verdienen zweifelsohne mehr Aufmerksamkeit. Meines Wissens wurde die Korrelation zwischen Schlafzuständen und einem langsamen Rhythmus bisher nur in EEG-Aufzeichnungen des menschlichen Scalps festgestellt (Marshall et al., 1998). Im Gegensatz zu meinen Ergebnissen wurde in diesem Bericht das wandernde Merkmal des ultradianen Rhythmus nicht erwähnt.

The work presented in chapter 3 (Figure 3.1-3.3 A) of the thesis was published in *Science*:

Science. 2016 Apr 29; 352 (6285):590-5.

Slow waves, sharp waves, ripples, and REM in sleeping dragons.

Mark Shein-Idelson, Janie M Ondracek, **Hua-Peng Liaw**, Sam Reiter, Gilles Laurent

PMID: 27126045 DOI: 10.1126/science.aaf3621

Abbreviations

AAV	Adeno associated virus	ICP	Intracranial pressure
ABP	Arterial blood pressure	ISF	Interstitial fluid
AC	Alternating current	ISO	Infra-slow oscillation
ADHD	Attention deficit hyperactivity disorder	LC	Locus coeruleus
AHP	Afterhyperpolarizing potential	LDT	Laterodorsal tegmentum
ATP	Adenosine triphosphate	LFP	Local field potential
BOLD	Blood oxygenation level-dependent	LH	Lateral hypothalamus
BSA	Bovine serum albumin	LPT	Lateral pontine tegmentum
CAR	Common average referencing	mHz	milli-Hertz
CBV	Cerebral blood volume	MI	Mutual inhibition
ChR2	Channelrhodopsin 2	PAG	Periaqueductal gray
CMOS	Complementary metal-oxide-semiconductor	PBS	Phosphate-buffered saline
CPP	Cerebral perfusion pressure	PBS-T	Phosphate-buffered saline with Triton
CSF	Cerebrospinal fluid	PEDOT	Poly(3,4-ethylenedioxythiophene)
DC	Direct current	PET	Positron emission tomography
DCx	Dorsal cortex	PFA	Paraformaldehyde
DSIP	Delta sleep-inducing peptide	PPT	Pedunculopontine tegmental nuclei
dSPM	Dynamical statistical parametric mapping	PSS	Poly sodium 4-styrene sulfonate
DVR	Dorsal ventricular ridge	REM	Rapid eye movement
ECoG	Electrocorticography	rms	Root mean square
EDOT	3,4-Ethylenedioxythiophene	RI	Reciprocal interaction
EEG	Electroencephalography	RN	Raphe nuclei
eLORETA	Exact low resolution brain electromagnetic tomography	RSN	Resting state network
EMG	Electromyography	SLD	Sublaterodorsal nucleus
EOG	Electro-oculography	Str	Striatum
FFT	fast Fourier transform	subC	Sub-coeruleus
fMRI	Functional magnetic resonance imaging	SW	Slow-wave
FTG	Gigantocellular tegmental field		

Chapter 1
Introduction

Sleep is a widespread behavior across the animal kingdom. Despite decades of intense study, the core functions of sleep remain a mystery. A sleeping animal endangers itself to potential predators and wastes precious time that it could use to forage for food and mates. There must therefore have been a great selective pressure to maintain this behavior throughout evolution. I will briefly introduce sleep and its evolution. My results on lizard sleep demonstrate the existence of a slow electrical rhythm that has rarely been reported in other animal models. These sections of my thesis introduce different brainwaves, including infra-slow oscillations.

1.1. Sleep

1.1.1 Phenomenology

Sleep is a naturally recurring, essential state across animals with a nervous system, from nematodes to humans. Historically, sleep is defined by multiple behavioral criteria. Despite a significant variation in sleep patterns, sleep meets most, though not all, of the following criteria: 1) reduced responsiveness to surrounding stimulations; 2) behavioral quiescence at a particular time of day, often accompanied by a preferred location and stereotypic posture; 3) rapid reversibility, which set sleep apart from hibernation, anesthesia, and coma; 4) homeostatic regulation after deprivation. The basis for such a behavioral definition of sleep was first provided by Piéron (Piéron, 1913).

Sleep was studied as a continuous low-activity state in the early 20th century (Kleitman, 1929). However, it is far from being just one passive, quiescent state. Sleep is an actively regulated and homeostatically controlled brain state that can be subdivided into different stages. Human sleep can be divided into four different stages based on electroencephalography (EEG), electromyography (EMG), and electro-oculography (EOG) signals (Iber et al., 2007). In all mammals, sleep can be divided into repeated cycles of rapid-eye-movement (REM) and non-REM sleep. As techniques improved over time, more information was integrated into stage scoring. Despite decades of research, it is still unknown why sleep is segregated or whether different states fulfill common functions shared by different animal species.

Electrophysiological features of the sleeping brain's activity were added to the behavioral definition of sleep after their discovery. Subsequently, EEG, EMG, and EOG were accepted as

valid methods to identify sleep in mammals. These techniques later allowed the identification of two distinct sleep states, REM and non-REM sleep, in mammals and birds. The emergence of sleep architectures varies significantly among species and is highly adapted to their living environments. Bottlenose dolphins, for example, display unihemispheric sleep, which presumably allows them to swim when half-sleeping (Mukhametov et al., 1977). In mallards ducks, the portion of unihemispheric sleep increases by more than 150% when exposure to predation increases (Rattenborg et al., 1999).

Loomis et al. first divided human sleep into five different states. These states were defined by the existence of alpha waves, spindles, and large random potentials (slow-wave activities or high-voltage waves in more recent reports) (Loomis et al., 1937). Although slow eye movements were reported in sleeping human subjects, REM sleep was first identified in 1951 while observing children's eye movements during sleep (Aserinsky, 1996; Aserinsky and Kleitman, 1953). It was described as a state with 10-20 minutes episodes of rapid, jerky eye movements interspersed among longer phases without ocular movement. REM sleep as a distinct sleep state was first systematically studied in human subjects (Aserinsky and Kleitman, 1953) and later in cats (Dement, 1958). Cortical activity during these phases resembled wake activity, challenging the notion that sleep is a uniformly low-activity state (Aserinsky, 1996; Loomis et al., 1937). The REM phase is also known as paradoxical sleep or sometimes desynchronized sleep because of physiological similarities with the awake states. Besides eye movements, REM sleep is accompanied by significant changes in many physiological parameters. The heart rate and blood pressure slightly increase but lose their regularity (Snyder et al., 1964), thermoregulation is suppressed or depressed (Parmeggiani, 2003), brain temperature increases (Kawamura and Sawyer, 1965), and cerebral blood flow increases (Revich et al., 1968). These phenomena occur in concert with a deep atonia in most skeletal muscles (Jouvet et al., 1959).

Non-REM sleep, also known as slow-wave (SW) sleep, is characterized by a relatively low frequency, large-amplitude EEG signal. In early research, it was used to measure the depth of natural sleep in humans, which is highest in the first part of sleep and declines in the course of the night. Blake and Gerard first reported that deep sleep in normal human subjects was regularly associated with a large regular potential wave at a frequency of 0.5-3 Hz (Blake and Gerard, 1937). In 1993, Steriade and his collaborators described a new type of slow oscillation in the thalamocortical system (Steriade et al., 1993a, 1993b, 1993c). They referred to this newly discovered rhythm as 'slow' oscillations. Their frequency below 1 Hz was lower than that of the delta rhythm (1–4 Hz) (Achermann and Borbély, 1997). Despite its modest name, the new pattern was catapulted to fame because it brought together basic and clinical investigations on

delta patterns (Achermann and Borbély, 1997), cortical spindles (Mölle et al., 2002), and K-complexes (Amzica and Steriade, 1997) of sleep.

1.1.2 Functions

The functions of sleep remain mysterious in neurobiology. There are currently two main hypotheses: one concerns high-order cognitive functions such as memory consolidation or brain plasticity, and the other focuses on housekeeping or restorative processes (Frank and Heller, 2019). Despite these sleep-related hypotheses, the question as to why the brain must be taken offline for a large portion of our daily lives remains unanswered.

The cognitive hypothesis proposes that sleep is essential for high-level brain functions such as learning and memory, as well as synaptic plasticity. The firing of place cells in hippocampal CA1, for example, corresponds to a specific location in a given environment. During sleep episodes following maze exploration, firing patterns ‘replay’ experienced sequences during sharp-wave ripples (SWR) as of the animal traveled through the same trajectory (Lee and Wilson, 2002). Synchronous 'play back' in cortical and hippocampal neurons during sleep has been hypothesized to be necessary for long-term memories (Walker and Stickgold, 2006). Indeed, selective suppression of hippocampal SWRs after training impairs spatial memory in rats (Girardeau et al., 2009).

The housekeeping and restorative hypothesis proposes that sleep governs the brain's basic needs, including maintaining brain energy metabolism, macromolecular biosynthesis, and removing metabolic waste. Adenosine, for example, is a central player in energy exchanges. Microdialysis studies in cats reveal that extracellular adenosine concentrations in the basal forebrain are 21% lower during SWS than in the awake state (Porkka-Heiskanen et al., 1997). Sleep also promotes the synthesis of proteins necessary for normal awake functions. The amounts of sleep are positively correlated with protein synthesis. This effect can be found in the cerebral cortex of rats (Ramm and Smith, 1990) and monkeys (Nakanishi et al., 1997). Elimination of metabolic waste is a relatively new hypothesis about sleep function. The highly polarized macrosystem of rapid interchange of cerebrospinal fluid (CSF) and interstitial fluid (ISF) has been called the ‘glymphatic system,’ based on its similarity to the lymphatic system in peripheral tissue and the critical role of glial AQP4 channels in fluid transport. The exchange is facilitated by the convective influx of CSF from the subarachnoid space into the periarterial space. The subsequent transport of CSF into the brain parenchyma is facilitated by AQP4 channels expressed in a highly polarized manner in astrocytic endfeet that ensheathe the brain

vasculature. CSF movement into the parenchyma drives convective interstitial fluid fluxes within the tissue toward the perivenous spaces surrounding the large deep veins. The ISF is collected in the perivenous space from where it drains out of the brain toward the cervical lymphatic system (Jessen et al., 2015).

1.2. The evolution of sleep

On the basis of our results from sleep recordings in lizards, we hypothesized that the REM and non-REM states of sleep were present already in the common ancestor of amniotes. This hypothesis engendered some debates (Libourel and Barrillot, 2020; Ungurean et al., 2020). This section reviews previous studies and theories about two sleep stages from an evolutionary perspective, focusing on amniotes. Amniotes were the first vertebrates with a life cycle possible outside of water. Mammals, birds, and reptiles diverged from amniotes hundreds of millions of years ago. Despite the structural difference, some brain areas, such as the hippocampus, are functionally conserved (Striedter, 2016). By studying an evolutionarily distinct species, we wish to identify general principles of neural circuits and understand the function of the brain.

Sleep is a common behavior in all vertebrates. Despite a long history of sleep research, most work focuses on mammals and birds. These two clades, which diverged from their common ancestor over 300 million years ago, both engage in SW and REM sleep. However, there are some differences between mammalian and avian sleep. Mammalian SW sleep usually contains sleep spindles, absent in birds. Mammalian REM sleep lasts several minutes or longer; avian REM sleep rarely lasts longer than 10 seconds (Lesku and Rattenborg, 2014). Due to the anatomical and electrophysiological differences between mammals and birds, it was often considered that the two stages of sleep evolved independently (Rattenborg et al., 2011). Moreover, it was thought that this convergent evolution of sleep was correlated with the appearance of homeothermy. A hypothesized alternation of SW and REM sleep, evolved from twilight sleep and daytime sleep, respectively, was thought to greatly improve the memory consolidation process (Lee Kavanau, 2002).

Despite repeated attempts, the REM and non-REM stages of sleep had not been demonstrated unequivocally in turtles and lizards until recently (Shein-Idelson et al., 2016). The two primary criteria, polygraphic and behavioral, both have limitations when evaluating sleep states. Sleep-related eye movements were observed in reptiles: two chameleons, *Ghameleo jacksoni* and *C. melleri.*, showed independent eye movements during sleep, although the brain's electric activity did not show two distinct patterns. The bursts of eye movements lasted 1-7 min and were

interrupted by periods devoid of eye movement of similar variable length (Tauber et al., 1966). Short bursts of eye movement during sleep were also present in other lizards, *Ctenosaura pectinate* (Tauber et al., 1968) and *Iguana iguana* (Ayala-Guerrero and Mexicano, 2008).

The observations of eye movement in lizards during sleep were all accompanied by a reported reduction in electric activity. These results led to one theory that tries to explain the evolution of two-stages sleep. The 'REM first' hypothesis proposed that the high-voltage slow waves characterizing SW sleep in mammals represent an evolutionary feature of more recent phylogenetic origin than the REM phase of sleep. Tauber et al. brought up the hypothesis by observing EEG and EOG signals from the lizard, *Ctenosaura pectinate.* Eye movement appeared 2-3 hours after sleep onset and recurred intermittently throughout the entire sleep period. The EEG amplitude and frequency were reduced during sleep without two distinct patterns (Tauber et al., 1968). Slow waves, typical of SW sleep in mammals, rely on the integrity of the neocortex and the anatomo-functional relationship between the thalamus and the neocortex (Jouvet, 1967). The reptilian brain is equally organized but with less developed higher structures than in mammals, such as the cerebral neocortex (Butler, 1980). Therefore, the absence of slow waves during quiet sleep may only imply the absence of the appropriate neurophysiological generators of this EEG activity, but not of sleep itself. This hypothesis has been supported by experimental evidence from sleep studies performed in decorticated cats, where slow waves were not present during behavioral sleep (Jouvet, 1962). Moreover, electrocorticography (ECoG) patterns of *in utero* recordings in the guinea pig fetus showed that SWS only appeared after cerebral maturation (Astic et al., 1973).

Another hypothesis, the 'SW first' hypothesis, suggests that REM sleep evolved after the start of the mammalian line. Allison et al. recorded cortical EEG throughout sleep in a living representative of the phylogenetically most ancient order of mammals, the echidna (*Tachyglossus aculeatus*, an egg-laying monotreme). They found that the animal had rare eye movements. The arousal threshold was elevated during SW sleep. However, the arousal threshold in low-voltage EEG sleep, which occurs immediately after the high-voltage state, was similar to that during awake periods. Taking into account the lack of theta activities in the hippocampus, the authors concluded that the low-voltage period was quiet waking but REM sleep (Allison and Goff, 1968; Allison et al., 1972). Several studies of reptiles supported this conclusion. EEG recording from iguanid lizards, *Ctenosaura pectinata* and *Iguana iguana* (W. F. Flanigan, 1973); young caimans, *Caimun sclerops* (Meglasson and Huggins, 1979; Warner and Huggins, 1978); all tortoises (Jouvet, 1965; Jouvet and Klein, 1964) and tiger salamander,

Ambystoma tigrinum (Lucas et al., 1969), all exhibited behavioral sleep. No periods of phasic motor or eye movement activity were seen that were reminiscent of REM sleep.

Studies in reptilian and mammalian sleep over the last decades have led to diverse, even conflicting, results. The EEG in the desert iguana, *Dipsosaurus dorsalis*, clearly demonstrated two-stage sleep with no recordable eye movements (Huntley, 1987). Another lizard, *Ctenosaura pectinate*, exhibited two-stage sleep and phasic eye movements. However, eye movement was associated with the period of high-voltage waves (Ayala-Guerrero and Huitrón-Reséndiz, 1991). The latter work on another monotreme, the duck-billed platypus *Ornithorhynchus anatinus*, reported vigorous rapid eye movements and bill and head twitching, reminiscent of REM sleep. However, EEG during behavioral REM-like sleep states displayed moderate and high-voltage cortical activity (Siegel et al., 1998, 1999). Sleep in ostriches, *Struthio camelus*, a member of the most basal group of living birds, showed a unique polygraphic pattern. Episodes of REM sleep were delineated by rapid eye movements, but forebrain activity slipped between REM-like and SW-like activities (Lesku et al., 2011). In conclusion, both 'SW first' and 'REM-first' hypotheses cannot comprehensively explain the limited but diversified data from previous reports.

By comparing neuroanatomical traits and EEG between reptiles and mammals, another hypothesis proposed that the reptilian active state became mammalian sleep. The basking behavior evolved into SW sleep, and general active behavior evolved into REM sleep. The reptilian 'rest period' remained in some mammalian species as shallow torpor (Nicolau et al., 2000; Rial et al., 2010). This hypothesis, particularly the part related to the SW sleep, was challenged by Niels Rattenborg. He argued that although the slow-wave activity in awake and active reptiles is similar to the one observed in mammals during SW sleep, this activity is less synchronized or lower in amplitude. Moreover, the reptilian dorsal cortex lacks the interconnectivity necessary to generate sleep-related slow waves in the EEG (Rattenborg, 2007). The long debate between Rial and Rattenborg, without powerful evidence from either side, is beyond the scope of my thesis.

Many former hypotheses are based on very limited behavioral and electrophysiological results. However, reptiles are highly diverse and have invaded all possible niches ranging from the marine environment to exclusively terrestrial and fossorial species. There are today some 11239 species of non-avian reptiles (www.reptile-database.org, data until 2020/12). Data on sleep is available for less than 0.24% of all reptiles (Libourel and Herrel, 2016). A recent study following our own compared sleep characteristics in two lizard species, *Pogona vitticeps* and *Salvator merianae*, demonstrating the diversity of sleep patterns with a close evolutionary relationship

(Libourel et al., 2018). There is little agreement on which theory should be taken. Maybe the question should not be whether non-avian reptiles show REM and SW sleep, but how these states appeared and evolved along the different branches of the amniote tree.

Studying sleep in reptiles presents some unique difficulties and challenges. First, reptiles are poikilotherm. It has been shown that sleep is strongly influenced by environmental variables such as lighting conditions and temperature (Berger and Phillips, 1995). These factors also strongly influence reptilian sleep. Walker and Berger recorded the EEG and other physiological signals from a turtle, *Testudo denticulata*. Two distinct EEG states similar to SW and REM sleep appeared during sleep. However, the arousal threshold was indifferent to the different states. All EEG spikes disappeared when the temperature was lowered to 16°C (Walker and Berger, 1973). Huntly recorded EEG patterns in the desert iguana, *Dipsosaurus dorsalis,* at 10, 20, and 30°C in different seasons. Total sleep increased with decreased day length and temperature. The amplitude and frequency of sharp waves decreased with temperature. 'Paradoxical sleep,' despite the fact that there is no recordable eye movement in this species, only occurred at 20 and 30°C (Huntley, 1987). Similar temperature-related changes were reported in the lizard, *Gallotia galloti* (De Vera et al., 1994). Another prolonged immobility state, hibernation, adds complexity to the study of sleep in poikilotherms. Mammals' EEG during hibernation is dominated by slow-wave-like oscillations or isoelectric with intermittent bursts of spindles (Andersen et al., 1960; Walker et al., 1977). Many experiments may thus need to be repeated with more accurate and better-controlled climate conditions.

Another factor that may bias sleep patterns is age. In mammals, sleep duration, especially REM sleep, decreases with age (Roffwarg et al., 1966). Most reptilian studies did not report on the animals' age and presumably used juveniles and adults. If REM sleep serves as an endogenous source of stimulation to assist in structural maturation and differentiation (Roffwarg et al., 1966), it might exist only *in ovo* and disappear soon after hatching. Corner reviewed periodic spontaneous motility during early development throughout the animal kingdom. In all species, the phasic and tonic activity alternations can be found *in ovo* and *in utero*. He hypothesized that the ultradian sleep rhythm in adult mammals is the evolutionary remnant of the shorter cycle of the rapid body movement during the late fetal or hatching stage in the embryo (Corner, 1977).

The currently accepted mammalian-centric definition of sleep, based on behavioral and cortical electrophysiological patterns, may cause difficulties when applied to all species in the same taxon, not to mention in different taxa. REM sleep is particularly difficult. At the behavioral level, eye movement, phasic motor automatisms, and muscle atonia are common criteria to evaluate

REM sleep. However, birds have the ability to perch, sometimes even only on one foot, throughout their REM sleep episodes. They do, however, show some form of muscle atonia in their neck muscles. That phenomenon is most visible in species with long necks, such as geese (Dewasmes et al., 1985). At the electrophysiological level, different types of electrodes, implantation locations, and parameters of recording equipment could affect recording results. The diversity of cortical EEG in different reptilian species is mentioned above. On the other hand, the neural circuits that apparently support mammalian REM sleep in the brainstem and hypothalamus are conserved in reptiles. State-specific neuronal discharges occur throughout the brainstem. Eiland et al. recorded reticular formation units during wakefulness and quiescence in box turtles. Unlike mammals, no recorded units showed consistent, cyclically occurring phasic events during quiescence (M. Eiland et al., 2001).

It is conceivable that the fundamental neural mechanisms of sleep are not basically different in mammals and other vertebrates. However, the approach to study the evolution of sleep has been strongly influenced and exclusively dependent on electrophysiological criteria. This approach was initially developed as a means of defining sleep in mammalian species. Thus, applying these criteria to sleep states across phylogeny with very different neuroanatomy, metabolism, and lifestyle may sometimes result in misidentification. It is almost always problematic when applied to the study of sleep in non-mammals. It would seem essential that electrographic measures always be interpreted within the framework of behavioral assessment. Subsequently, the electrographic features should be taken into consideration and compared. Our results in bearded dragons generated many discussions about the evolutionary origin of two-states sleep (Blumberg et al., 2020). A recent paper using zebrafish reported two sleep states using whole-body fluorescence imaging (Leung et al., 2019), pushing the potential origin of two-stages sleep further back in time. A comparative approach, including more phylogenetic groups, is therefore necessary to understand the evolution of sleep.

1.3. Introduction to neural oscillations

Brainwaves, or neural oscillations, are rhythmic patterns of neural activities in the brain. Oscillatory activity can be observed at different levels of organizations and is thought to play critical roles in processing and transferring neural information. At a single-neuron level, oscillations can appear either as fluctuations in membrane potential or as rhythmic patterns of action potentials, which have the potential to generate the oscillatory activation of post-synaptic neurons. At the level of neural ensembles, macroscopic oscillations can be seen from a

distance when large numbers of neurons act simultaneously. Different brain areas with their unique architecture and neural properties can give rise to oscillations at a different frequency than the firing frequency of individual neurons.

The earliest report on electric activities in the brain was a short abstract of about ten sentences in a presentation submitted to the British Medical Journal by Richard Caton in 1875. Little note seems to have been taken until intense polemics arose between physiologists in the 1890s about who should claim to be the founder of electroencephalography (Coenen et al., 2014). Neural oscillations in humans were first observed by Hans Berger in 1924. In his groundbreaking paper (Berger, 1929), he described two continuous oscillations. The large-amplitude, slower (average period of ~90 ms) rhythm induced by eye-closure in awake, calm subjects was named 'alpha' wave because he observed it first. Alpha wave with a rhythm between 8 and 12 Hz is often observed over the occipital cortex. It can be found in most awake conditions, but its power increases when the brain is in idling conditions such as during eye closure or muscle relaxation. The same phenomenon can also be observed during meditation when human subjects disengage from environmental stimulations (Schuman, 1980). Neural oscillations in a similar frequency range can be recorded over the motor cortex (mu rhythm) and the auditory cortex (tau rhythm). These rhythms are involved in the inhibition of planned actions and can be effectively blocked by acoustic stimulation, respectively (Lehtelä et al., 1997; Pfurtscheller and Neuper, 1994). Alpha activity decreases during REM sleep after selective REM sleep deprivation. However, its topographic distribution and time course are not affected. This suggests that alpha activity in the REM sleep EEG is a marker of REM sleep homeostasis (Roth et al., 1999).

Opposite to the alpha wave, Berger reported the 'beta' wave that was present when the eyes were open. It is a low-amplitude, faster (average period of ~35 ms) rhythm (Berger, 1929). Many classical observations have linked the beta wave to motor functions with a rhythm between 13 and 30 Hz. The beta wave, particularly pronounced during steady contractions, is attenuated by voluntary movements and highest during holding periods following movements (Engel and Fries, 2010). Recent studies found synchronized beta-band oscillation in both somatosensory and motor cortices. It may involve recalibrating the system following a movement and preparing for the next movement (Baker, 2007). Other proposed functions include but are not limited to top-down attentional processing (Buschman and Miller, 2007), preservation of the current brain state (Engel and Fries, 2010), and large-scale coupling in sensorimotor integration (Siegel et al., 2012).

Oscillations in the alpha/beta band are present in different animal models. For example, sleep spindles at 7-15 Hz occur in the cat neocortex and thalamus during the early stage of SW sleep. It is a waxing-and-waning oscillation that lasts 0.5-3 sec (Fuentealba and Steriade, 2005). In lizards, sleep spindles have not been observed in the DVR or cortex. The alpha/beta wave is the dominant signal during REM sleep. During awake states, no apparent beta oscillation appears in the cortex and DVR. Whether the beta oscillation appears in different brain areas is currently unknown.

Since the influential discoveries of Hans Berger, brainwaves have been documented in numerous species, from reptiles to birds to mammals. Dietsch demonstrated the existence of state-dependent, discrete frequency bands in the Fourier transform of raw EEG signals. This is the beginning of the classic EEG sub-bands that people still refer to today (Dietsch, 1932). The frequency ranges vary from very slow oscillations with periods of minutes (Aladjalova, 1957) to ultra-fast oscillations with frequencies reaching ~600 Hz (Curio et al., 1994). The first classification introduced by the International Federation of Societies for Electroencephalography and Clinical Neurophysiology (IFSECN) in 1974 has drawn evenly and somehow arbitrary borders between frequency bands. They are delta, <4 Hz; theta, 4-8 Hz; alpha, 8-13 Hz; beta, >13 Hz; gamma, (use of term discouraged) (IFSECN, 1974). The lack of consensus and clinically oriented guidelines have undergone multiple major changes and are still debated (Babiloni et al., 2020).

There are significant problems with brainwave classification, especially when applying them to different animal models. First, frequency bands below 0.1 Hz were not included and named due to technical reasons despite the low-frequency oscillations discovered in rabbits' cerebral cortex 17 years before the first guideline was formulated (Aladjalova, 1957). Slow oscillations with a frequency range lower than the delta wave received minimal attention since they were discovered. Second, rhythms generated by the same physiological machinery in different species often fall into different bands. The hippocampal theta wave, for example, was discovered in rabbits with a frequency of 4-6 Hz; they were named 'theta' waves (Green et al., 1960). However, hippocampal theta in rodents varies between 5 and 10 Hz. According to the guidelines, it should be called theta-alpha wave. A useful taxonomy would be able to represent the physiological similarities that give rise to oscillations in different species and different conditions. The absolute frequency bands should not be the only criteria. Unfortunately, this method is impractical now because the mechanisms underlying most brainwaves in different animal models are not well-known.

Despite this imperfect taxonomy, brainwaves are still one of the most important features in neuroscience research. Among all brainwaves, the most important rhythm related to sleep is the delta wave. It is attributed to the work of Gray Walter through his EEG recordings from cerebral tumor patients. He suspected that the delta wave was generated by cortical tissue in some phase of functional disturbance (Walter, 1936). Recent work connects the delta wave with the motivational processes associated with both reward and defense mechanisms, cognitive processes related to attention, and the detection of motivationally salient stimuli in the environment (Knyazev, 2012).

Loomis et al. first reported the link between delta waves and sleep in 1937. They classified human sleep into five states and also described sleep spindles during sleep. Although the name of delta wave did not appear in their publication, their later states D and E contain large random potentials, which occurred 0.5-3 times per second. Subjects were less responsive to sound and light stimuli and did not report dreaming during these states (Loomis et al., 1937). Delta waves can also be recorded in animal models during sleep. The signal, based on its frequency range and origin, can be divided into two components. First, the cortical delta. The detailed cellular mechanism of it is unknown, but it is possibly driven by intrinsically bursting neurons (Amzica and Steriade, 1998). Second, the thalamic delta. The long-lasting hyperpolarization of the thalamic relay neuron leads to slow cation current (I_h) activation. The depolarized membrane triggers rebound bursting, mediated by low-threshold Ca^{2+} current (I_T). Both I_h and I_T are inactivated during the burst. The membrane potential becomes hyperpolarized afterward and ready for the next cycle of oscillations (Steriade et al., 1993d). The corticothalamic feedback loop then synchronizes thalamic burst-firing and generates local field potentials in the thalamus (Volgushev et al., 2006).

The cellular mechanism of the delta wave is relatively clear in mammals. However, a similar mechanism might not apply to lizards. The properties of different ion channels and the interaction between the thalamus and the cortex are unclear there. Moreover, the EEG pattern of lizard SW sleep is not a continuous up-and-down state alternation but concatenated by EEG events very similar to SWRs in rats. SWRs are the signature of hippocampal CA1 in rats during SW sleep and awake resting. It is initiated by population bursts of pyramidal neurons in the hippocampal CA3. Synchronized activities reach CA1 via collaterals, cause depolarization of pyramidal cells in CA1, and give rise to negative extracellular waves, the sharp waves. The sparse firing of CA1 pyramidal neurons and inhibition by activated interneurons give rise to high-frequency oscillations (140-200 Hz), the ripples (Buzsáki, 2015). SWR-like events have been observed in other areas, including the piriform cortex and amygdala. SWR-like events in both

areas occur during SW sleep (Narikiyo et al., 2014; Ponomarenko et al., 2003). Two recent studies reported that slow-waves are generated in the claustrum and propagate to downstream areas in lizards and mice (Narikiyo et al., 2020; Norimoto et al., 2020). The mechanism of lizard SWR generation is unknown. Due to the lack of a layered structure in the DVR, it may differ from its rodent counterpart.

Brainwaves in any particular brain area do not always stay in the same frequency range. State-related frequency changes in the same area are a very common phenomenon. In the primate motor cortex, beta waves are pronounced during steady contractions and highest during holding periods following movement. During the preparation and execution of movements, beta oscillations are replaced by gamma oscillations (Donner et al., 2009; Engel and Fries, 2010). In the rat hippocampus, the theta wave is associated with exploratory movement and REM sleep. SWRs, in contrast, appear during awake rest, consummatory behaviors and SW sleep. These two oscillatory states largely determine the direction of information flow between the hippocampus and neocortex. They also affect gamma oscillations when interacting with connected areas (Buzsaki, 2011). Other brainwaves appear in different frequency ranges such as theta and gamma oscillations. Their functions are less related to sleep and beyond the scope of my study.

Neural tissue can generate oscillatory activities in many ways, driven by mechanisms within individual neuron types or by interactions between them. The frequency ranges defining brainwaves, as described above, have been decided somewhat arbitrarily, based on experimental observation. In 2003, Penttonen and Buzsaki first noticed that the mean frequencies of three independently generated hippocampal rhythms in rats, theta (4-10 Hz), gamma (30-80 Hz), and ripples (140-200 Hz), form a linear progression on a natural logarithmic scale (Penttonen and Buzsáki, 2003). They also extrapolated the linear relationship to other frequencies and estimated those of other expected classes. In the low frequency range, they designated slow 1 (0.7-2 sec/cycle), slow 2 (2-5 sec/cycle), slow 3 (5-15 sec/cycle) and slow 4 (15-40 sec/cycle). Their work supported the first publication on slow rhythms in rabbits by Aladjalova (Aladjalova, 1957). Slow rhythms will now be introduced next section.

1.4. infra-slow oscillations

Infra-slow oscillations (ISO), defined as slow and periodic electrical potential changes, were first described by Aladjalova in 1957. She recorded two rhythms: the faster one, with a period of 7-9 sec, from the frontal brain area, and the slower one, with a period of 1-1.5 min, from the

occipital area of one hemisphere. ISO frequencies and amplitude changed during phenobarbital-induced sleep (luminal sleep), after strong electrical stimulation, flickering illumination of the retina, and in different layers (Aladjalova, 1957). These supra-second oscillations were understudied for decades until the late 1990s. ISOs can be sub-divided into at least four groups based on the theoretically estimated ranges defined by Penttonen and Buzsáki (Penttonen and Buzsáki, 2003). Based on recording methodologies, ISOs can be found using blood oxygenation level-dependent (BOLD) imaging, direct measurement of electrical potentials, measurement of power modulation in different frequency bands, single- and multi-units recordings, and calcium imaging. Regardless of the method, in this section, ISOs refer to all slow rhythms whose frequencies are lower than that of the delta wave (<0.5 Hz).

As observed in rabbits, slowly fluctuating potentials have been reported in the cerebral cortex of conscious and lightly barbiturate-anesthetized cats (4-120 sec/cycle) (Norton and Jewett, 1965). In human subjects, cortical EEG during sleep show slow rhythms of 4-50 sec/cycle (Achermann and Borbély, 1997; Aladjalova, 1964; Vanhatalo et al., 2003). ISOs have been identified in the monkey's visual cortex (Leopold et al., 2003) and in the lateral geniculate complex, primary visual cortex, and dorsal raphe nucleus of rats (Filippov and Frolov, 2004; Filippov et al., 2004). These waves are so slow that they sometimes require direct current (DC) recording to produce undistorted signals or introduce compensatory current to avoid DC offsets that often exceed the amplifiers' range (Nasretdinov et al., 2017). The natural tendency of experienced electrophysiologists is to search for unanticipated artifacts and question the significance of these slow waves. However, slow spontaneous activities exist in many animals and even plants. The fresh-water algae, *Chara coralline* and *Nitella flexilis*, generate action potentials in response to mechanical stimulation, injury, or direct electrical stimulation. The duration of action potentials is about 1000-fold slower (several seconds) than those in the nerve and the conduction velocities are of the order of 1-2 cm/sec (Gaffey and Mullins, 1958; Johnson et al., 2002; Osterhout and Hill, 1940).

Instead of measuring electrical potentials directly, many studies report on the slow oscillations by measuring the cyclic change of faster neuronal activities such as action potentials and various brainwaves. In freely moving and urethane-anesthetized rats, the firing rate of lateral geniculate neurons showed oscillations with periods in the range of 40 to 100 sec (Albrecht and Gabriel, 1994; Albrecht et al., 1998). In the hippocampus, bursts of unit discharges reoccur within a range of 15 to 70 sec (Penttonen et al., 1999). Similar results were reported in the basal ganglia (Ruskin et al., 1999) and in locus coeruleus neurons (Akaike, 1982) of awake, immobilized rats. A comparative study in humans and mice shows that sigma (10-15 Hz) band

activities are modulated by a 0.02-Hz oscillation (Lecci et al., 2017). In humans, cortical multi-units activity revealed a rhythm of ~20 sec period (Moiseeva and Aleksanian, 1986). Furthermore, both theta- and alpha-band-power oscillations vary periodically every ~17 and ~42 sec at rest (Novak et al., 1992). The power of gamma oscillations also show a peak at 0.1 Hz (Drew et al., 2008). Such infra-slow fluctuations might be a phenomenon that reflects the change of macroscopic excitability in the underlying neural tissue (Elbert, 1993).

Despite the observation of ISOs in different species and frequencies, ISOs have been largely ignored for decades. Due to the potential benefits in diagnosis, prognosis, and treatment of clinical conditions, some reports have started to advocate the use of slow oscillations (Kovac et al., 2018). The neglect of ISOs occurred mostly for technical reasons. Most EEG recordings are now performed using AC-coupled amplifiers with the low-frequency filters set at 0.5 Hz or higher. This practice was introduced to eliminate unwanted noise such as motion artifacts. Several measures are highly recommended to avoid slow-drifting artifacts during prolonged recording of a very slow signal or DC-EEG recording. They include keeping the input current as low as possible (<1 pA) and using high impedance (>=10 GOhm) non-polarized electrodes (e.g., Ag/AgCl) (Bauer et al., 1989).

ISOs regained attention partly due to the discovery of so-called underlying resting-state networks (RSNs) (Biswal et al., 1995). Functional magnetic resonance imaging (fMRI) has been widely used to study brain regions showing task-related increases in neural activity. RSNs, by contrast, concern brain regions in which neural activity is higher during a baseline state than during an experimental task. The identification of RSNs results from the temporal correlations of the BOLD signal change between distinct brain areas (e.g., bihemispheric sensorimotor cortices). During resting states, coherent RSN patterns can be identified by having the most power at frequencies between 0.01 and 0.05 Hz (De Luca et al., 2006). Their synchronized fluctuation is interpreted as implying functional neuronal connections (Fox and Raichle, 2007; Mateo et al., 2017). There is more than one spatially distinct RSN in a resting brain image dataset, with each RSN having a distinct signal time-course (De Luca et al., 2006; Greicius et al., 2003). Some RSNs represent functionally related regions or anatomically connected areas previously identified. More recent work shows that the correlation between DC EEG and the BOLD signal varied substantially over time (Grooms et al., 2017).

Very little is known about the mechanisms of ISO generation. In general, slow oscillations involve larger neuronal areas, whereas higher frequency oscillations are more localized. The latter is generally explained by the low-pass filtering properties of brain tissue. However,

previous work suggests that anatomical connectivity plays a more important role than geometric distance (Buzsaki et al., 1988a). Moreover, masses or sheets of neurons showing a dominant orientation of the contained elements are especially advantageous for accumulated neural activity. Neural arbors are usually oriented perpendicularly to a layered structure. This parallel morphology allows fast electrical potentials to increase in intensity along neural arbors and become large extracellular field potentials. However, the mechanism of fast field-potential generation may not apply to ISOs. ISOs can be recorded in multiple non-layered structures such as the basal ganglia (Hutchison et al., 2004) and thalamus (He, 2003).

Thalamic glial cells may be a key to ISO generation in mammals. Multi-units extracellular recordings from cat thalamus slices demonstrated that ISOs at ~0.03 Hz were present in groups of closely situated neurons. Unlike the general concept that negative-going field potentials are associated with neuronal excitation, simultaneous intra- and extracellular recordings reveal that the negative peaks of extracellular field potential coincided with the onset of long-lasting hyperpolarizing intracellular potentials. This counter-intuitive phenomenon suggests that the ISOs do not reflect the synchronous fluctuation of membrane currents in populations of thalamic neurons but rather some separate, possibly non-neuronal process. The long-lasting hyperpolarizing potentials were not blocked by antagonists of ionotropic glutamate receptors, $GABA_{A,}$ and $GABA_B$ receptors, but reversibly abolished by Ba^{2+} that inhibits inwardly rectifying K^+ (K_{Ir}) current, and by the adenosine A1 receptor antagonist, DPCPX. One possible adenosine source leading to phasic A1-receptor activation and K_{Ir} channel opening is the degradation of adenosine triphosphate (ATP) following its release from glial cells. In support of this hypothesis, the ecto-ATPase inhibitor, ARL67156, reversibly converted the neuronal ISO into continuous firing (Lörincz et al., 2009). Another indirect supporting result is that thalamic astrocytes exhibit spontaneous intracellular Ca^{2+} oscillations at an average frequency of 0.019 Hz (Parri and Crunelli, 2001). These calcium waves lead to ATP release from individual astrocytes (Guthrie et al., 1999).

ISOs have an impact on both neuronal activity and behavior. The power of faster neuronal activities, including theta, alpha, and gamma oscillations, as well as multi- and single-unit activities, is modulated by the infra-slow cycle. Cross-frequency coupling implies that the infra-slow generator presumably modulates the functions of these faster oscillations. In freely-behaving rats, the phase of ISOs, calculated by the band-limited power of low-(0.5-9 Hz) and high-(40-100 Hz) frequency activities, contributed to the observed trial-to-trial variability of evoked responses by dynamically altering the generation of action potentials in response to postsynaptic depolarization (Dash et al., 2018). During a somatosensory detection task (HITs

and MISSes task), the performance of human subjects was strongly correlated with the phase, but not the amplitude, of infra-slow (0.01-0.1 Hz) EEG fluctuations. The phase of ISOs also robustly correlated with the phase of power modulation of all tested frequency bands between 1 and 40 Hz (Monto et al., 2008). When children were asked to engage in a reaction-time task, the ISO power (0.02-0.2 Hz) of DC-EEG decreased by ~20%. Attention-deficit-hyperactivity-disorder (ADHD) patients show ~10% lower ISO power than normal children, regardless of whether they have been resting or performing a task. ADHD patients also perform more poorly than normal children (Helps et al., 2010).

Cross-frequency coupling between ISOs and faster oscillations has also been observed during sleep. Two frequency bands, delta (0.5-4 Hz) and sigma (10-15 Hz), are most clearly and consistently modulated by ISOs (Lázár et al., 2019; Lecci et al., 2017). These two frequency bands contain the two most prominent features, 'slow oscillations' and sleep spindles, during SW sleep. These results suggest that the major SW-rhythm generators and presumably their functions are modulated by an ISO generator in the 0.01-0.1 Hz range. Beyond these time scales, human sleep is usually composed of the REM-SW sleep cycle. Each sleep cycle of alternating SW and REM sleep takes approximately 90 minutes, occurring 4-6 times in a good night's sleep. Polysomnographic recording reveals that the scalp DC potential decreases during the transition from REM to SW sleep and increases during the transition from SW to REM sleep. The cycle of an average DC potential is synchronized to sleep states alternation but with a time lag (Marshall et al., 1998). These results are very similar to the lizard ISO during sleep, as I will show in the results section.

In conclusion, there exists a considerable amount of data at the slow end of the frequency spectrum. However, these data have generated more questions than answers. ISOs undoubtedly deserve more attention. My work will hopefully participate in answering some of those questions.

Chapter 2
Materials and Methods

2.1) Electrode preparation and data acquisition

2.1.1) Tetrode drives

The 64-channel tetrodes drives were modified from the ultra-lightweight tetrode drive (flexDrive, Open Ephys) designed by Jakob Voigts et al. (Voigts et al., 2013). The design files and assembling instructions can be found on the open-ephys website (https://open-ephys-2gg5.squarespace.com/flexdrive). Due to our electric workshop's manufacturing constraints, the diameter of holes for gold pins had to be enlarged from 200 µm to 300 µm. The edge of the printed circuit board is 500 µm wider than in the original design.

The tetrode wire was manufactured by California Fine Wire with nickel-chrome (Stablohm 800) alloy and insulated with HML (or SML) and a VG Bond coat. The core diameter is 0.0005 inches, and the overall diameter is 0.00075 inches. When making a tetrode, the wire was folded twice, hung, and straightened with a lightweight clip. The folded wires were then twisted 100 times clockwise and 40 times counterclockwise. The twisted wires were glued together by slowly running a hot air gun at a distance of about 1 cm to slightly melt the VG Bond coating. A paper cone was attached to the tetrode drive, with a thin layer of epoxy applied to it.

All tetrodes were cut with fine scissors (RS-5915SC, Roboz) immediately before gold plating. The plating protocol is described by the Redish lab (Ferguson et al., 2009). The impedance of all the channels after gold plating was around 100 kOhm at 1000 Hz. All tetrodes were immersed in sterilized mineral oil for a few seconds to prevent oxidation after plating.

2.1.2) Silicon probes preparation

Silicon probes were ordered from NeuroNexus or Cambridge NeuroTech in different configurations and packages. Chronic probes were mounted onto the linear motor (customized or from Cambridge NeuroTech) with OptiBond, then further secured by UV-curing adhesive. The Omnetics connector was taped to the probe holder to prevent it from moving and damaging

shanks during implantation. Small connectors were soldered to the ground and reference cables for further connection during surgery.

The PEDOT plating protocol was modified from the protocol of the Harris lab at Janelia Research Campus (personal communication). In summary, 0.225% (w/v) of Poly sodium 4-styrene sulfonate (PSS, Sigma-Aldrich, product no: 243051) and 0.144% (w/v) 3,4-Ethylenedioxythiophene (EDOT, Sigma-Aldrich, product no: 483028) were added to double distilled water. The solution was stirred with a magnetic stir bar for 20-30 minutes at 300-500 rpm until the EDOT was incorporated into the PSS solution. The PSS/EDOT solution was placed in a vacuum desiccator with a pressure of 100 mBar for 10-15 min before use.

The silicon probe was connected to the nanoZ (White Matter LLC), and the tip was carefully placed in the PEDOT solution. The desired current was calculated to reach the current density of 2-3 mA/cm^2. Each plating cycle duration was 10, 10, 8, and 6 seconds, respectively, with a pause of at least 5 seconds in between. A positive current was injected into each channel in every plating cycle. Electrode impedance was 30-100 kOhm at 1000 Hz, depending on the electrodes' diameter, after four plating cycles. If necessary, PEDOT was redeposited on those sites that did not have a low enough impedance. For each electrode, impedance over different frequencies was tested in 1X PBS before and after plating. Data were saved for further reference.

Probes for *in vivo* recording do not need special labeling. For *ex vivo* recordings, a thin layer of DiI or DiO solution (Thermo-Fisher Scientific, catalog No.: V22885, V22886) will be applied to the non-electrode side on each shank of a silicon probe. Recording sites can be seen under florescence microscope after recording without staining.

2.1.3) Silicon probe cleaning

Silicon probes for acute recordings were used multiple times until the noise level increased significantly, or more than one-third of all channels were broken. After every recording, probes were submerged in 3% liquid detergent (Contrad-70, Decon Labs Inc.) overnight while gently stirring. The next morning, probes were cleaned with ddH2O before transferring them to 1% tergazyme solution (Sigma-Aldrich, product no. Z273287) overnight. All probes were then cleaned with ddH2O for at least 1 hour and air-dried for the next recording.

2.1.4) Data acquisition

All recordings were performed with Digital Lynx SX systems (Neuralynx Inc.) and HS-36 headstages. The headstages were connected to a lightweight shielded tether cable via an

adapter (ADPT-HS36-N2T-32, Neuralynx Inc.). Recordings were grounded and referenced against one of the reference wires separately.

Signals were sampled using a 24-bit analog-to-digital converter at 32000 or 20000 Hz with an input range of +/- 132 millivolts. The unfiltered data were stored in a signed 32-bit integer format on the hard drive (.nrd file). The raw data were then bandpass filtered at 0.1-9000 Hz with an input range based on the signal amplitude. The filtered signals were stored separately in a signed 16-bit integer format (.ncs files). Both data types are suitable for different analyses.

2.2) *In vivo* recording

2.2.1) Subjects

All experimental procedures were performed following the German animal welfare guidelines: permit no. V54- 19c 20/15- F126/1005 granted by the Regierungspraesidium Darmstadt (Dr. E. Simon).

All lizards used for *in vivo* implantation were 120-350 g at the time of surgery. Animals were individually housed in 77x65x55 cm (width x depth x height) terraria on a 12-12-h light-dark schedule. Sleep recordings were performed during the dark phase (at night). Animals had free access to dry herbs and water in the terrarium. Insects or worms were given twice a week, depending on the lizard's body weight.

2.2) Implantation

The implantation protocol of our publication (Shein-Idelson et al., 2016) was later modified. In summary, a lizard was administered analgesics (Butorphenol: 0.5 mg/kg s.c., Meloxicam: 0.2 mg/kg s.c.) and antibiotics (Marbocyl: 0.05 mg/kg s.c.) 12-16 hours before surgery. On the day of surgery, the animal was initially anesthetized in an airtight box containing an open tube stuffed with isoflurane-saturated tissue paper. Once the lizard lost its righting reflex, the anesthesia was maintained with isoflurane (1-3 vol. %) after intubation. The breathing rate was set to 8-9 breaths per minute with 6-12 ml air. When the corneal reflex disappeared, the head was fixed in a stereotactic apparatus. Body temperature was monitored and maintained at 30°C by an esophageal probe and a heating pad (Homeothermic Monitoring System, Harvard Apparatus). The heart rate was monitored using a Doppler flow detector (model 811-B, Parks Medical Electronics, Inc.). The eyes were protected by ointment (Vidisic, Bausch & Lomb GmBH)

and hand-made aluminum eye patches. The skin around the skull was disinfected with a 10% Povidone-iodine solution twice before removal with a scalpel. Residual tissue was removed using a 3% hydrogen peroxide wash. A thin layer of UV-curing glue (OptiBond All-in-one, Kerr) was applied to the skull after drying its surface.

A large craniotomy was drilled to maximize brain exposure, especially the posterior part of the forebrain, without damaging the pineal eye. Ground and reference wires were immersed into the cerebrospinal fluid and secured on the skull with a UV-curing adhesive after carefully removing the dura and arachnoid layers. The pia was removed gently over the area of electrode insertion (usually over medial/dorsal-medial cortex).

Probes were mounted on a flattened needle or a nano-Drive (Cambridge NeuroTech) and secured to its holder. The probe was then slowly lowered into the tissue stereotaxically, to a depth of 1-1.4 mm. After probe insertion, motors or holders were secured onto the skull by UV-curing adhesive. The brain was covered with a thin layer of the artificial dura (DOWSIL™ 3-4680, Dow Inc.) (Jackson and Muthuswamy, 2008) and Vaseline. The exposed skull, ground, reference wires, and motors were covered with a layer of UV-curing adhesive and dental cement.

After surgery, the lizard was released from the stereotaxis. The ventilator and endotracheal tube remained until autonomous breathing started. A lizard usually takes more than 30 minutes to fully recover from anesthesia (regain spontaneous movement and normal body posture). After recovery from anesthesia, the lizard was returned to its terrarium with an ad-lib feeding schedule. Analgesics, antibiotics, and saline were given every other day until five days after the surgery day.

2.2.3) Behavioral recordings

About 1 to 2 hours before the dark phase, the animal was placed in a familiar sleep box (20 x 30 x 40 cm, width x depth x height) in a quiet, electromagnetic-radiation shielded room. The animal was recorded continually by video and physiological monitoring over 16 - 18 hours until the next morning. The light-dark cycle (12 hours light, 12 hours dark) remained unchanged and synchronized to the terrarium. An overhead infrared light was used to illuminate the experimental arena.

The floor of the sleep box was an aluminum breadboard with water channel (MBC 3030M, Thorlabs). The temperature was controlled by a heating thermostat (Alpha A6, Lauda) which pumps warm water through the water channels. Depending on the experimental purpose, the

temperature was set between 23 and 31 °C. The temperature was recorded using a thermistor probe (TSP-TH, Thorlabs) placed on the breadboard's surface.

The animal's behavior was monitored with digital cameras (acA1920-155uc, Basler) at 20 or 40 frames per second. The infrared filter in the camera was removed to record during the dark period. TTL pulses sent by the camera synchronized the video and electrophysiological signals.

2.2.4) Micro-lesions and transcardial perfusion

After the period of chronic recording was over, the animal was deeply anesthetized with an overdose of ketamine (180 mg/kg, i.m.) and Midazolam (6 mg/kg, i.m.). A supplementary dose of Pentobarbital (30 mg/kg, i.p.) was administered 15-30 minutes later. After the corneal reflex disappeared, a 10-second positive current was applied to selected sites through the plating adapter. The equation to calculate the charge is: $\mu A*10(sec)/area(\mu m^2) = 0.15 (\mu C/\mu m^2)$.

The animal was perfused transcardially with 80-100 ml PBS, followed by 50-60 ml of 4% paraformaldehyde in PBS (Hoops, 2015). The intact head was then detached from the body and placed in 4% paraformaldehyde in PBS at 4°C for 36-48 hours. After post fixation, the brain was removed and prepared for sectioning and staining.

2.3) *In vitro* recordings

2.3.1) Ringer's solution

The Ringer's solution was freshly prepared in the morning of the recording day. The recipe was initially used in the slice recordings from snakes (Dantzler, 1969). It proved suitable for lizard retinal recordings of up to 30 hours (Stirling et al., 1998). The solution contained NaCl 126 mM, KCl 3 mM, $NaHCO_3$ 24 mM, NaH_2PO_4 0.72 mM, $MgSO_4$ 1.2 mM, $CaCl_2$ 1.8 mM, D-glucose 10 mM.

All components, except for $MgSO_4$ and $CaCl_2$, were added to double-distilled water. The solution was then gassed with carbogen (95% oxygen and 5% CO_2) for 15-20 minutes. $MgSO_4$ and $CaCl_2$ were added to the solution after the pH reached 7.4-7.5. During the entire *ex vivo* recording, the Ringer's solution was bubbled with carbogen and kept at room temperature (22-25°C), unless noted otherwise.

2.3.2) Whole-brain preparation

A lizard weighing 100 to 400 g at the time of sacrifice was initially anesthetized in an airtight box containing an open tube stuffed with sevoflurane-saturated tissue paper until the corneal reflex disappeared. After decapitation and jaw removal, a carotid artery perfusion was done using lizard Ringer's solution for 15-20 minutes. The rate of perfusion was 50-60 drops per minute.

The brain was removed from the skull in the Ringer's solution together with the spinal cord. The cerebellum, cortices of both forebrain lobes, pineal eye, and pia mater were removed. The preparation was pinned to an agarose 4% plate and transferred to a recording chamber perfused with oxygenated Ringer's solution at a rate of 4.5 ml per minute. The liquid level in the bath was kept constant by fine-tuning the speed of input and output of the peristaltic pump. The preparation was left to equilibrate at room temperature (22-25 °C) for at least 1 hour before recording or manipulation started.

2.3.3) Slice preparation and recording

A lizard was anesthetized by sevoflurane until the corneal reflex disappeared. The brain was removed in ice-cold Ringer's solution. Immediately after brain extraction, sections of 500 micrometers thickness were sliced using a vibratome (VT1200S, Leica) in an ice-cold Ringer's solution. All slices were then transferred to an oxygenated Ringer's solution at room temperature for at least 1 hour before recording.

During recording, each slice was anchored with a nylon mesh (ALA HSG-MEA-5B, Multichannel System) on a 252-channel extracellular recording system (USB-MEA256-System, Multichannel system). The multi-electrode array has 252 glass embedded titanium-nitrate electrodes with 10 or 30 µm electrode diameter and 60 or 100µm electrode spacing. The sampling rate used for extracellular recordings was 32kHz.

2.3.4) Optogenetics

The retrograde AAV virus (Tervo et al., 2016), AAV2/rg Syn-ChR2(H134R)-GFP (#58880, Addgene), was co-injected with Alexa dyes bilaterally into DVR under anesthesia (see section 2.2.2). After 4 to 8 weeks of incubation, the animal was sacrificed (see section 2.3.3). The brain was removed under red light to avoid activating channelrhodopsin 2 (ChR2) before recording.

After probes insertion, an optic fiber (CFML14L10, Thorlabs or LambdaB, Optogenix) was placed on the brain surface or inserted into the targeted area. The optic fiber was connected to a blue

light LED (M470F3, Thorlabs). The target area was stimulated with 3 rounds of a 2ms pulse at 20-50 Hz for 12 seconds (10 seconds pause). The light power was 6.5 to 26.8 mW/mm^2. The duration between repetitive stimulation bursts was at least three hours. The infection efficiency of the retrograde virus varied greatly between individuals, needing to be checked post hoc by immunohistochemistry.

2.3.5) Pharmacology

Bicuculline was mixed with Alexa Fluor 647 and diluted to its final concentration (2mM) in Ringer's solution. The mixture was front-filled into a glass pipette with a tip opening of 30-40 µm in diameter. After the baseline recording, the glass pipette was slowly advanced to the target area. The pressure injection speed was 5-10 nl per minute, and the volume per injection was 20 nl. After the injection pump stopped, the glass pipette stayed in the injected area for 7-10 minutes before being retracted and extracted from the brain.

2.4) Histology

2.4.1) Fixation and sectioning

In vivo brains were prepared as described in section 2.2.3. *Ex vivo* brains and slices were kept in 4% PFA at 4°C for 24 to 36 hours and then transferred to PBS before sectioning. The spinal cord of intact brains was removed after fixation. The brain was cut coronally between the forebrain and the midbrain. The brain's anterior and posterior halves were embedded separately in 4 to 4.5 % low-melting agarose. Coronal sectioning was performed on a vibratome (VT1200S, Leica) with a section thickness ranging between 50 and 100 µm.

The thick slices from slice recordings (section 2.3.3) were embedded in agarose and resliced using a vibratome. Final slice thickness was between 50 and 70 µm.

2.4.2) Immunohistochemistry on brain sections

The sections were collected in 24-well plates in PBS. To block unspecific binding sites, PBS was replaced with 300 to 400 µl blocking solution (1% BSA in 0.5% PBS-T) and gently shaken overnight at 4°C. The sections were incubated with primary antibodies (hippocalcin, ab24560, Abcam, rabbit, 1:1,000; anti-GFP, A10262, Invitrogen, chicken, 1:1,000; ChAT, AB144P, Merck,

goat, 1:100; mTH, 22941, ImmunoStar, mouse, 1:100; rabTH, AB152, Merck, rabbit, 1:200) in blocking solution overnight at 4°C. After washing with PBST three times, the samples were incubated with appropriate secondary antibodies (1:500, all from Invitrogen) in blocking solution for 4 hours at room temperature, followed by three washes with PBS-T. Some slices were counterstained with NeuroTrace 435/455 blue-fluorescent Nissl stain (N21479, Invitrogen, 1:200) in PBS for 2 hours at room temperature. After rinsing with PBS, the sections were mounted with Dako Fluorescence Mounting Medium (S3023, Dako). Images were acquired by confocal microscopy (LSM 710, Carl Zeiss AG) using 10X or 20X objectives.

2.5) Data analysis

All data analysis was performed using Matlab 2018a.

2.5.1) Spectral analysis of LFP recorded during sleep

The filtered voltage traces as in section 2.1.4 were downsampled (250 Hz), low-pass filtered (100Hz), and binned (10 sec). A 2- to 4-hour section, occurring at least three hours after the onset of recording, was first used to evaluate the signal. The average normalized power spectrum (spectrum in each bin divided by the average over the entire section) for each bin was calculated using the Welch method (10-sec windows, 50% overlap). The correlation matrix between all bin pairs (frequency range 0-30Hz) was calculated and separated into two main groups using agglomerative clustering. The δ/β ratio on 10-sec bins (1-sec steps) was calculated by dividing the mean spectrum in the δ band (0.5-4 Hz) by the mean spectrum in the β band (10-30 Hz) in each bin.

2.5.2) Infra-slow oscillation

The unfiltered voltage traces as in section 2.1.4 were downsampled to 10 Hz. A Chebyshev (type 1) bandpass filter was used to remove the DC component that potentially came from the electronic devices. The filter was designed with the following parameters: highpass stop frequency = 1 milli-Hertz (mHz); highpass pass frequency = 2 mHz; lowpass pass frequency = 20 mHz; lowpass stop frequency = 25 mHz; stopband attenuation = 4 dB; passband ripple = 0.1 dB. The signals were zero-phase filtered with >1000 sec initial value padding on both ends of the data. The power of infra low oscillation and δ/β ratio were calculated by the moving root-mean-square within a window of 600 seconds and 60-sec steps.

2.5.3) Auto- and cross-correlation

The δ/β ratio and ISO were used to calculate auto- and cross-correlations. A scrolling auto-correlation was calculated on both time-series data (300-sec bin with 12-sec steps, or 1200-sec bin with 60-sec steps) and normalized in each bin.

The cross-correlation was calculated between the δ/β ratio and ISO or ISO from different channels. Both time-series data were binned into 600 or 1200 sec periods (60-sec step). The scrolling cross-correlation was calculated and smoothed with each bin. The highest peak was extracted from each cross correlogram and smoothed using a median filter (600-sec window).

2.5.4) Spike sorting

Spike sorting was performed in JRClust (Jun et al., 2017a). In summary, a smoothing slope filter (Savitzky-Golay) was applied to voltage traces to remove the local field potential (LFP). The local common average referencing (CAR) was used to remove external noise and artifacts. Noise was further removed by setting the fast Fourier transform (FFT) coefficients to zero, except for the narrow passing band around spikes (300-2000 Hz). Spikes were detected by measuring the slope of the voltage traces and identifying those that crossed a fixed threshold. A spiking event was assigned to the site showing the largest spike amplitude (compared to the adjacent electrodes, n=10 by default). Two features of each spiking event, space and time, were calculated for clustering. Space was the center-of-mass of each spiking event calculation by averaging the site coordinates weighted by their spike amplitudes. Time was a channel-covariance feature computed by projecting the spike waveforms onto the normalized waveform from the center site.

The clustering was done by searching the density peaks of the space and time distribution (Rodriguez and Laio, 2014). Auto-sorting results were manually verified and scored using a graphical user interface. All units used in the data analysis were separable from the background noise and neighboring clusters. Any spike that could not easily be assigned to a cluster was eliminated during the manually verified step.

Chapter 3
In vivo recording: Results

Extracellular recording in freely moving animals is one of the most popular techniques to understand the brain function. With minimal restrains of animal behaviors, scientists can access the neural activities when animals perform different tasks in a given environment. Numerous materials and devices with different usages, such as tetrodes, linear or matrix electrode arrays, CMOS-based electrodes, or portable microscopes, are commercially available. Different methods are suitable for different experimental conditions. There is no agreed-upon best method in system neuroscience, but each method has its own advantages and disadvantages.

I adapted methods and equipment developed for use with rodents to lizard recordings. The tetrodes and silicon probes both gave high-quality and reproducible results over multiple weeks. LFP recordings overnight showed that the neural activities during sleep are strikingly similar to those in mammals and birds. Figure 3.1-3.3 A are drawn from the results of a paper (Shein-Idelson et al., 2016) for which I performed most of the brain recordings and was second author. The following description focuses on the slow rhythm of SW and REM sleep alternation. Inspired by review papers published by the Buzsáki lab (Buzsáki and Draguhn, 2004; Penttonen and Buzsáki, 2003), I searched for ISO (Aladjalova, 1957) in the DVR. ISO could be reliably connected to sleep behavior and different sleep states at night. The relationship between ISO and sleep states hints at the existence of interesting yet unknown mechanisms in the lizard brain during sleep, and possibly during wake also.

3.1) Behavioral Sleep

Sleep can be defined as a reversible periodic state in which an animal loses consciousness of its surroundings. It is usually accompanied by a typical body posture, such as lying down with eyes closed, and revealing physiological features, such as decreasing body temperature and heart rate. We recorded multiple physiological features over the 18 to 20 hours centered in the middle of the night to determine behavioral sleep. Those features include head angle, eye movements, and heart rate.

Lizards spontaneously became drowsy soon after and sometimes before the beginning of the dark phase, typically at 7 pm. They settled into a position with a relaxed, horizontal sleeping posture with their heads resting on the floor. Their eyes remained closed during sleep. The heart rate decreased significantly to 20-30 bpm throughout the night, except for occasional peaks correlated with brief body repositioning (figure 3.1 A). These behavioral features were highly consistent across individuals and different environmental conditions, such as ambient temperatures and humidity. Behavioral sleep was closely aligned with the light-dark cycle, but the transition to behavioral sleep often anticipated the onset of darkness.

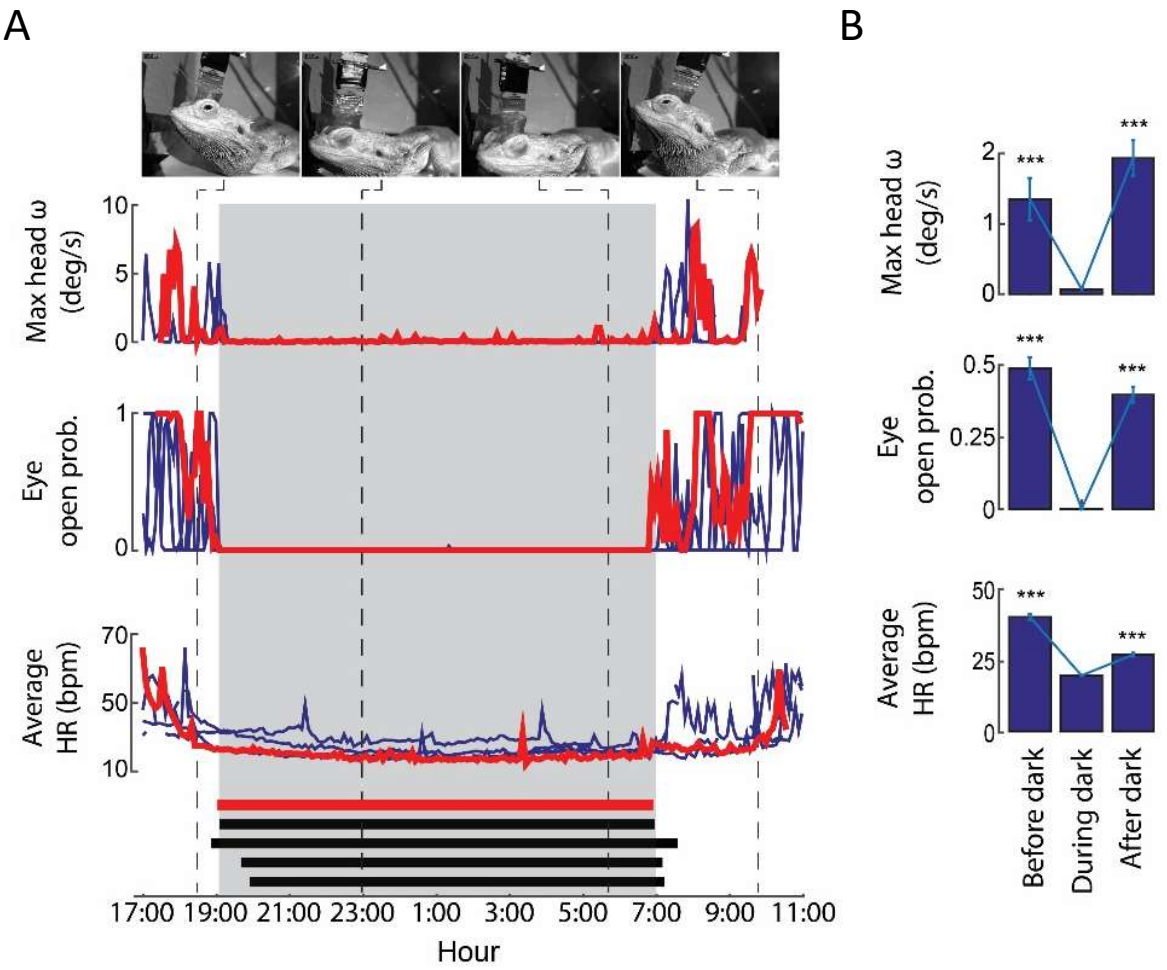

Figure 3.1: Behavioral sleep in lizards
(A) Behavioral and physiological parameters used to assess behavioral sleep state in *Pogona*. Red traces: the animal pictured; Blue traces: other nights and animals; Gray shaded area: time of darkness. All plots are peak values in successive 5-min periods). The top row includes representative photographs illustrating the awake (far left and far right) and sleep (middle) states. The second row shows maximum head angular velocity during and around night time (n = 3 recordings). The third row shows the probability of the eye contralateral to LFP recording being open (n = 4 recordings). The fourth row shows the heart rate (HR) (n = 5 recordings from three animals). Trace interruptions (in awake segments) are due to animal movements, preventing reliable HR measurement. The bars (bottom) indicate the periods defined as behavioral sleep, determined as the intersection of rest periods, as assessed from the above physiological and behavioral parameters (n = 5 recordings from three animals). **(B)** Means and standard error of the variables in (A), calculated over successive 5-min segments before, during, and after dark. ***P < 0.001; two-tailed t-test with Bonferroni correction. (figure modified from (Shein-Idelson et al., 2016))

3.2) Two states sleep at night

The most noticeable physiological changes observed during sleep occurred in the brain. Sleep EEGs from birds to mammals can be roughly divided into two states: REM and SW sleep. We recorded electrophysiological signals as LFPs from DVR during behavioral sleep (figure 3.2 A). The signals showed a periodic activity of signals with different amplitudes (figure 3.2 B). In the sleep EEG of mammals, one observes sleep spindles, around 10 to 15Hz, during SW sleep, and theta wave, around 6 to 10 Hz, during REM sleep. Both were undetectable in the lizard DVR. Yet, the nocturnal DVR LFP could be divided into two spectral clusters (figure 3.2 C). The frequency at which the mean spectral curves of these two components intersected was around 4 Hz (figure 3.2 D), defining a low-frequency spectral cluster (<4Hz, delta band) and a broadband cluster closer to activity recorded in the awake state. By analogy with metrics used with rodents, we chose the 10 to 30 Hz (beta band) to quantify the broadband cluster. The sleep states can be discriminated easily by dividing the power in the delta band by that in the beta band (δ/β ratio) instead of the ratio of delta to theta as in rats where theta is prominent in hippocampus during REM sleep. (Csicsvari et al., 1999; Louie and Wilson, 2001; van Luijtelaar and Coenen, 1984).

Under a 12/12 (light/dark) cycle, lizards slept 6 to 10 hours every night (figure 3.2 E). During sleep, the δ/β ratio oscillated regularly with a period of 80 to 100 seconds at 27°C ambient room temperature (figure 3.2 F). The slow alternation (high then low delta power) started shortly after the onset of the dark (light off) phase. It continued uninterrupted until 1 to several hours before the end of the dark phase. The amplitude of the δ/β ratio decreased throughout the end of the dark phase predicting the transition to wake.

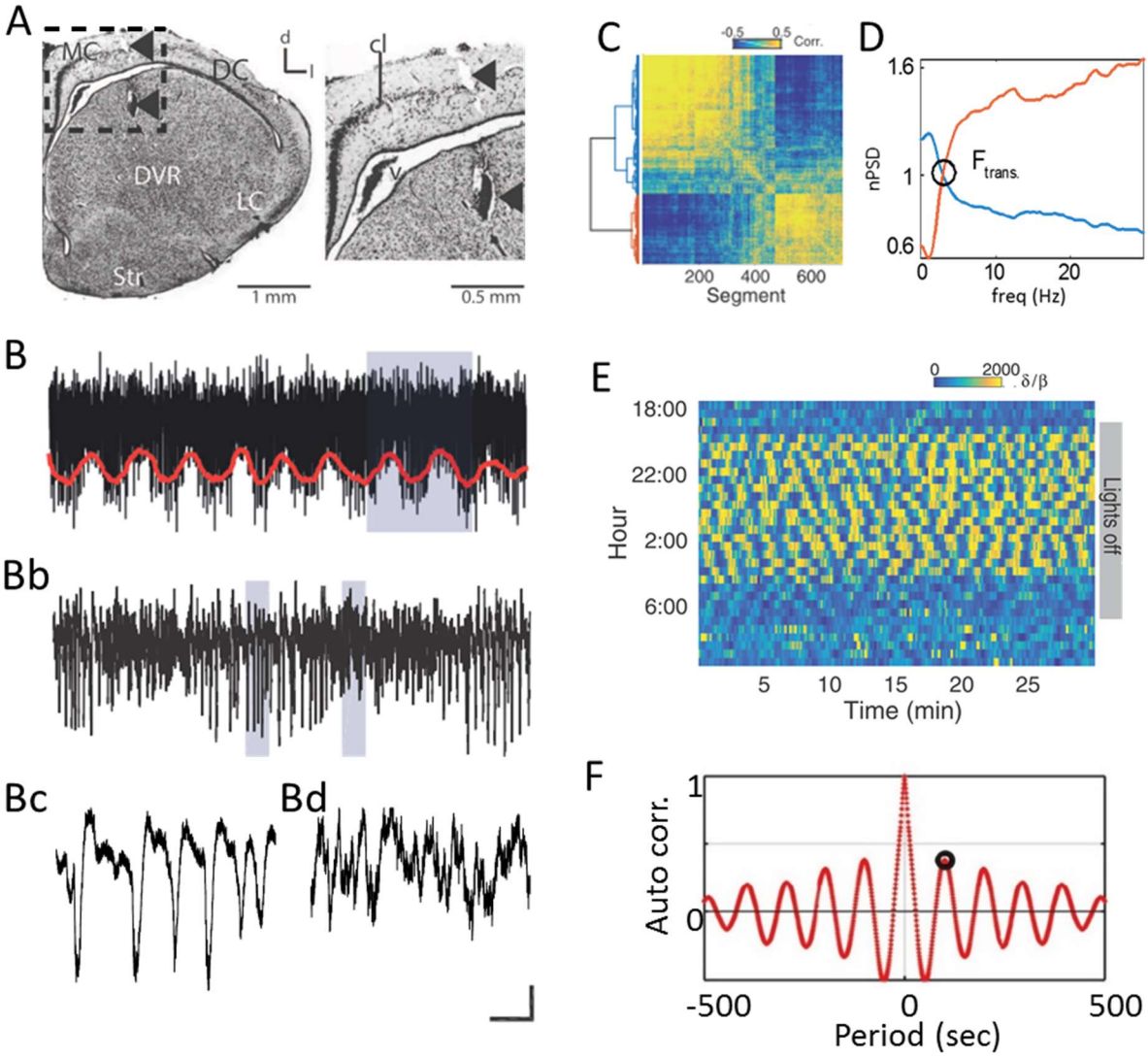

Figure 3.2: Two sleep states in lizards

(A) Coronal section through a lizard's forebrain (right hemisphere), showing the electrode track (along the two arrowheads) and main anatomical features. The area framed at left is magnified in the right panel (d, dorsal; l, lateral; DC, dorsal cortex; DVR, dorsal ventricular ridge; LC, lateral cortex; MC, medial cortex; Str, striatum;) **(B)** Slow time base. The LFP envelope oscillates slowly, as evident in the order-filtered trace (red). The shaded area is expanded in (Bb). (Bb) Two alternating epochs are apparent, with and without large negative LFP spikes, with intermediate-sized deflections in between. The shaded areas are expanded in (Bc) and (Bd). (Bc) Stereotypical negative LFP spikes with positive rebound occur regularly every 1 to 3 s. (Bd) The epoch alternating with that in (Bc) lacks stereotypical LFP spikes. The horizontal scale bar is 90 s for (B), 20 s for (Bb), 2 s for (Bc) and (Bd). The vertical scale bar is 300 µV for (B) and (Bb), and 200 µV for (Bc) and (Bd). **(C)** Night LFPs define two main spectral clusters. Shown is an ordered correlation matrix of spectral characteristics, calculated from 10-s data segments from one LFP channel over one night. Two dominant clusters are evident. The dendrogram is based on an Euclidian metric that uses Ward linkage. **(D)** Normalized power spectral density (nPSD) of the nighttime LFP for the two clusters in (C). Ftrans. is the frequency at which curves intersect (~4 Hz). One cluster dominates with higher-than-average power at low frequencies (δ band), defining SWS. The other cluster (β band) dominates with higher power at F > Ftrans. **(E)** Epochs of high and low δ power regularly oscillate throughout the night. Each horizontal row represents a 30-min segment (running left to right); successive 30-min segments run continuously from top to bottom. **(F)** Autocorrelation function of the e-sleep δ/β data in (E). The average period (circled) is around 80 s (27°C). (figure modified from (Shein-Idelson et al., 2016))

3.3) The durations of the two sleep states are temperature-dependent

Lizards, unlike mammals and birds, are poikilotherm animals (figure 3.3 A). Temperature is a critical factor in most chemical and biological reactions. I systematically tested the relationship between the period of the sleep-wake alternation rhythm and temperature across different animals and nights.

The period of the δ/β ratio oscillation depended on the temperature (figure 3.3 B): it increased from 87 to 175 seconds when the ambient temperature decreased from 31 to 23°C. The dependence of the period on temperature was well-fitted by a quadratic equation (figure 3.3 B). Added on this dependence, the period of the sleep cycle increased slowly throughout the night independently of the temperature. The increase was 1-1.5 sec/hour (figure 3.3 C).

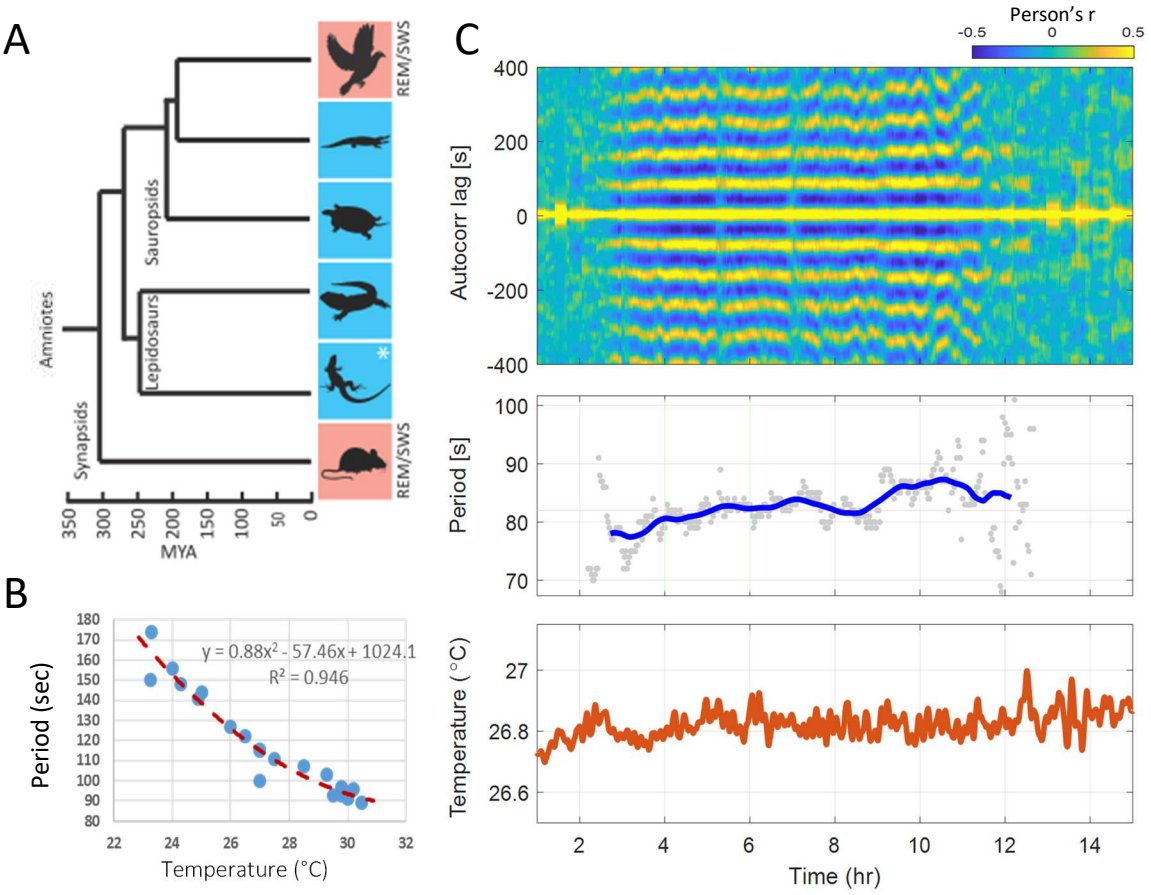

Figure 3.3: Period of the sleep cycle
(A) Cladogram of vertebrate evolution, indicating those classes (avians and mammals; pink boxes) in which the electrophysiological signatures of vertebrate sleep (SWS and REMS) have been established. These classes are also characterized by homeothermia. Blue boxes denote the non-avian reptiles, all of which are poikilotherms [from top to bottom: crocodilians; chelonians; tuatara (Sphenodon); and squamates (marked with an asterisk), including lizards and snakes]. Pogona is an agamid lizard. MYA, million years ago. The time scale follows (Striedter, 2003). **(B)** Relationship between period of sleep cycle and ambient temperature. The red dashed line is the 2nd order regression. Periods are the average over 2 hours of data, typically 3~4 hours since the beginning of the recording (9~11pm). **(C)** Top: same autocorrelogram as in figure 3.2 F, rotated by 90 degrees CCW. The X-axis is time in hours; the Y-axis is autocorrelation lag. Middle: quantification of the period as the function of time, for data above. The blue trace represents the piecewise average after smoothed by second-order Savitzky–Golay filter over a 10-min sliding window (1-min steps). Bottom: ambient temperature in the sleeping box.

3.4) Infra-slow oscillation

The stable period of SW-REM sleep alternation hinted at the existence of a slow oscillator in the DVR. The slow rhythm can be seen only after multiple steps of data processing, including segmentation, spectral analysis, power averaging, and division. Inspired by previous studies (Vanhatalo et al., 2004), I explored the possibility of recording ISOs during sleep directly. Conventional EEG and LFP recordings are done at frequencies ranging from 0.1 (or 0.5) to several hundred Hertz. A high-pass filter (>0.1-0.5 Hz) effectively solves problems such as DC voltage offsets when connecting electrodes to an AC-coupled amplifier. However, such filters reject also slow (<0.1Hz) rhythms and, depending on the filter type, may distort low-frequency signals.

Electrode materials have a significant influence on EEG signals. AgCl electrodes are considered optimal for DC-coupled electrographic recordings (Tallgren et al., 2005). However, high-density iridium oxide (IrOx) microelectrode arrays (silicon probes) offer many useful benefits such as enabling recording across multiple layers or areas. Yet all these approaches generate large DC shifts over time that lead to signals compensation. A previous study (Nasretdinov et al., 2017) for example, used a compensation chain made with two alkaline batteries and a potentiometer to compensate for DC offset, keeping the signal within the amplifier's input range. This manual method, unfortunately, is not practical for 16-20 hours of overnight recording.

The target frequency of my ISO recordings was in the 10 milli-Hertz (mHZ) range. To record such slow rhythms, electrode impedance was set to ~10 MOhm (at 2 Hz) with PEDOT plating (figure 3.4 A). After plating, the DC offset of a silicon probe remained in an acceptable range (<30 mV in 16-20 hours, except on 'bad' channels) (figure 3.4 B). Low-impedance electrodes also minimized noise during recordings.

Although the size of my LFP signals was similar, the signal-to-noise ratio thus increased considerably. The analog-to-digital converter of the recording system (Digital Lynx SX, Neuralynx Inc.) has a relatively broad input range (+/- 132 mV), which also allowed us to record the unfiltered LFP with no out-of-range signals.

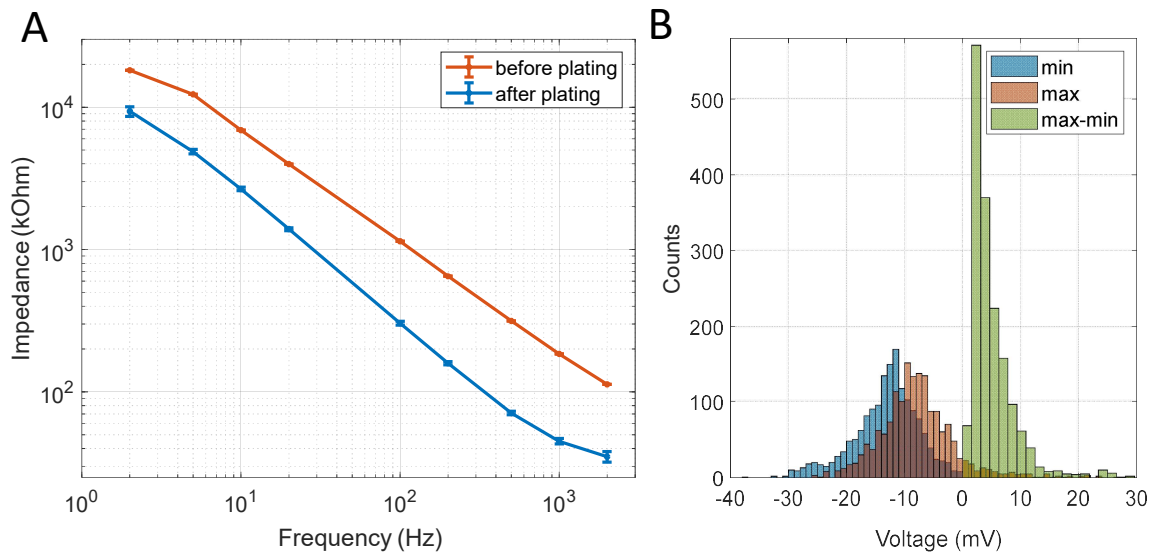

Figure 3.4: Impedance of electrodes
(A) Impedance test in 1X PBS before (red) and after (blue) PEDOT plating. The log-log scale shows the impedance at 2, 5, 10, 20, 100, 200, 500, 1000, and 2000 Hz. **(B)** The maximum and minimum voltage from all 64 channels across 26 overnight sessions from one animal. Red: maximum voltage from a single channel in one recording. Blue: minimum voltage from a single channel in one recording. Green: difference between the maximum and minimum voltages.

Visual inspection of the full-band EEG revealed prominent slow oscillation in all electrodes (figure 3.5 A, B). The slow rhythm's amplitude varied between 100 and >1000 µV, depending on the electrode area, impedance, implant location, and individual lizard. Spectral analysis revealed a band between 8 and 17 mHz (figure 3.5 C). The frequency of the slow rhythm varied between 5 and 20 mHz in different recordings. The corresponding period, between 50 and 200 seconds, was the same as for the sleep cycle, as measured from the δ/β ratio's periodicity.

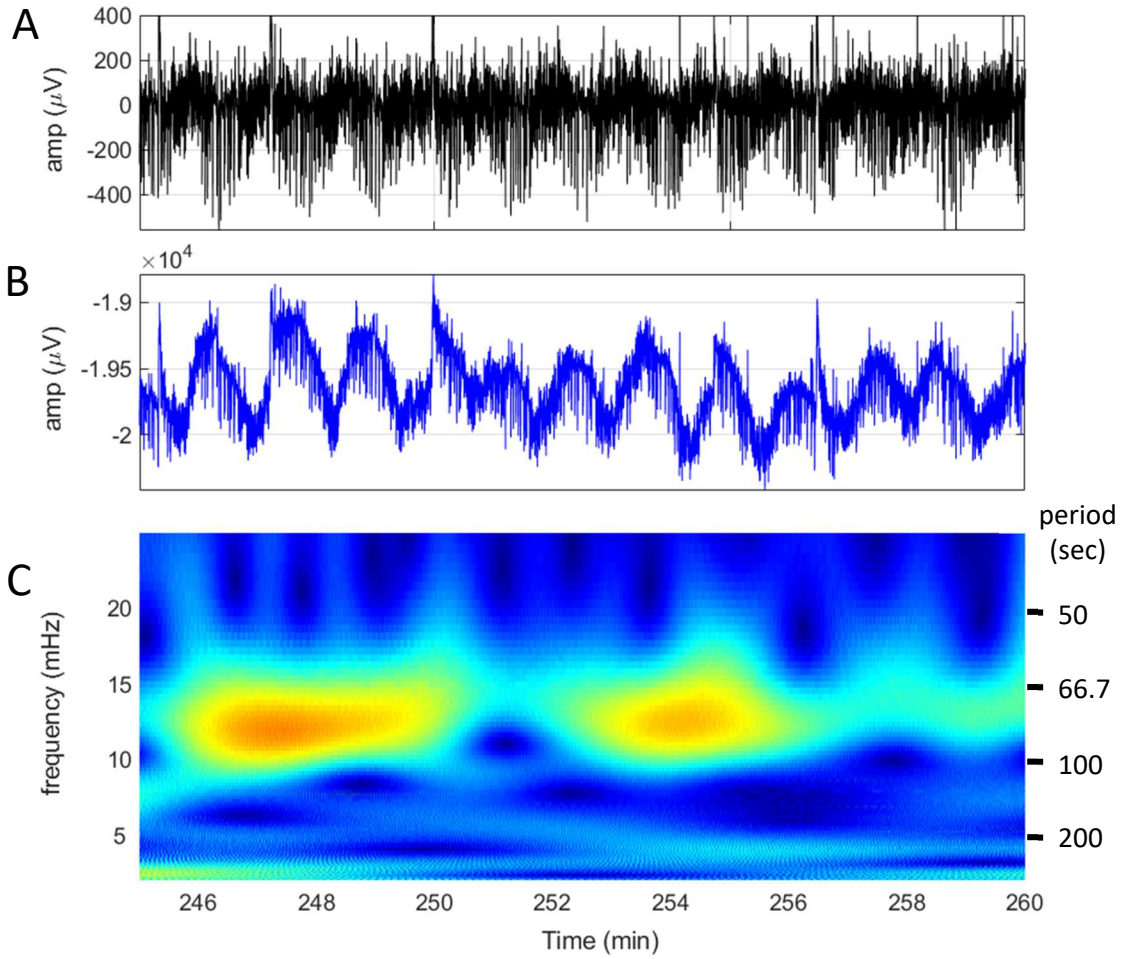

Figure 3.5: Full band EEG recording
(A) Band-passed (0.1-9000 Hz) EEG from DVR during sleep. **(B) F**ull-band EEG from the same electrode as in (A). **(C)** A wavelet spectrogram generated by using full-band EEG in (B) with Morse wavelet. The equivalent frequency range is between 2 and 25 mHz.

3.5) ISO power increases during sleep

Brainwaves reflect the synchronous activities of a large number of neurons. Brainwaves in different frequency bands can be linked to different behaviors, cognitive functions, and mental states. To examine the relationship between ISO and sleep, I calculated the power of the ISO between 2 and 20 mHz, using the root mean square (rms) in a 10-minute sliding window during overnight recordings. Figure 3.6 (A) shows an example of such an overnight recording. The ISO power started to increase ~30 minutes before the beginning of the dark phase and the corresponding rise in δ/β ratio. ISO power remained high for ~9 hours and was well correlated with the amplitude of the δ/β ratio.

Event-triggered averaging is a simple method to reveal a potential stimulus-response coupling. Only reproducible results show a significant signal after averaging. However, I encountered two technical problems when averaging data directly. First, the absolute amplitude of ISOs could change between days. Second, full-band LFP recordings are prone to artifacts, especially when the animals move (at the beginning and the end of the recording). Indeed, ISO power dramatically increased due to movement artifacts. To compare data from different days, I calculated z-scores to better account for the existence of artifactual outliers.

Despite differences between recordings concerning ambient temperature, start and end of recording times, the ISO power was always well correlated with the power of the δ/β power ratio. The mean of z-scored ISO power increased within an hour before the beginning of the dark phase (figure 3.6 B). The high-power period lasted 8-10 hours and ended 3-4 hours before the end of the dark phase. When applying the same method to the δ/β power ratio, the mean of z-scored δ/β power ratio showed an almost identical pattern during the dark phase (figure 3.6 C). These results revealed a synchronous change in the power of ISO and δ/β power ratio on long time scales.

To further test the relationship between ISO and sleep, I perturbed sleep by picking up the lizard in the middle of the night. ISO power decreased to the same amplitude as it is when the animal is naturally awakened at the end of the night (figure 3.7 A). The effect of the manipulation lasted for about 40 minutes until the animal resumed a relaxed posture (lying on the floor with its legs extended) indicative of sleep (figure 3.7 B). During the sleep interruption, the δ/β ratio stayed in between those in SW and REM states. The cycle of δ/β ratio did not recover until 40 to 50 minutes after the perturbation. ISO amplitude started increasing ~10 minutes after the disturbance but reached the baseline amplitude only about 40-50 minutes

later. Thus, a 5-minute sleep interruption had a long-lasting effect on both signal amplitude and stability (figure 3.7 C).

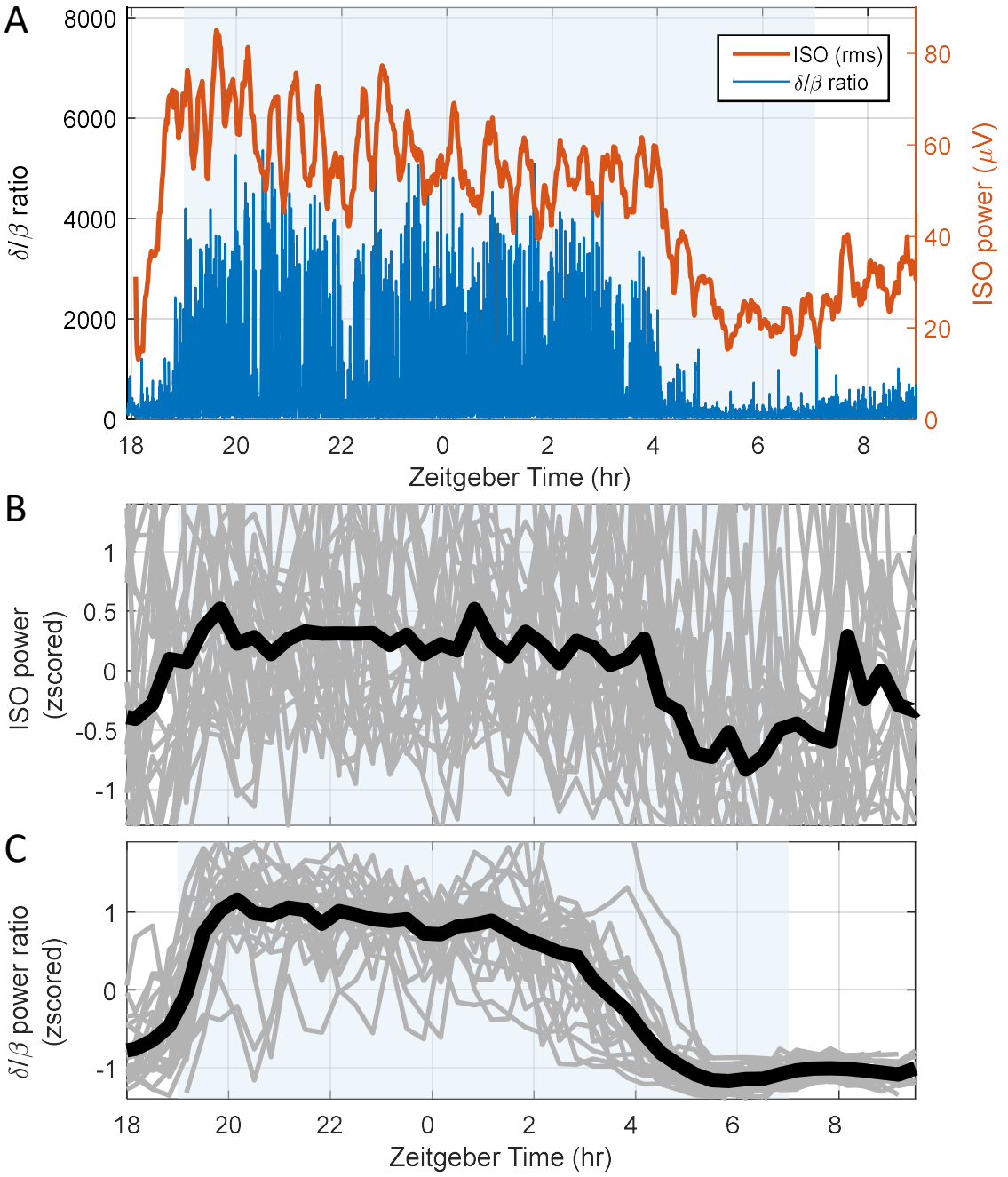

Figure 3.6: The power of ISO correlates with sleep
(A) An example of one overnight recording. Magenta line: ISO power (here as root-mean-square) over a 10-minute sliding window with 1-minute steps. Blue: δ/β ratio. Shaded box: dark phase between 7 pm and 7 am. **(B)** The z-scored ISO power from one implanted lizard. All data are from the same electrode. Gray lines: data from different days. Thick black line: mean of all data aligned to the Zeitgeber time. The first and the last recording are more than a month apart. The ambient temperature varied between 23 and 31°C. **(C)** The z-scored δ/β ratio power from the same data as in (B).

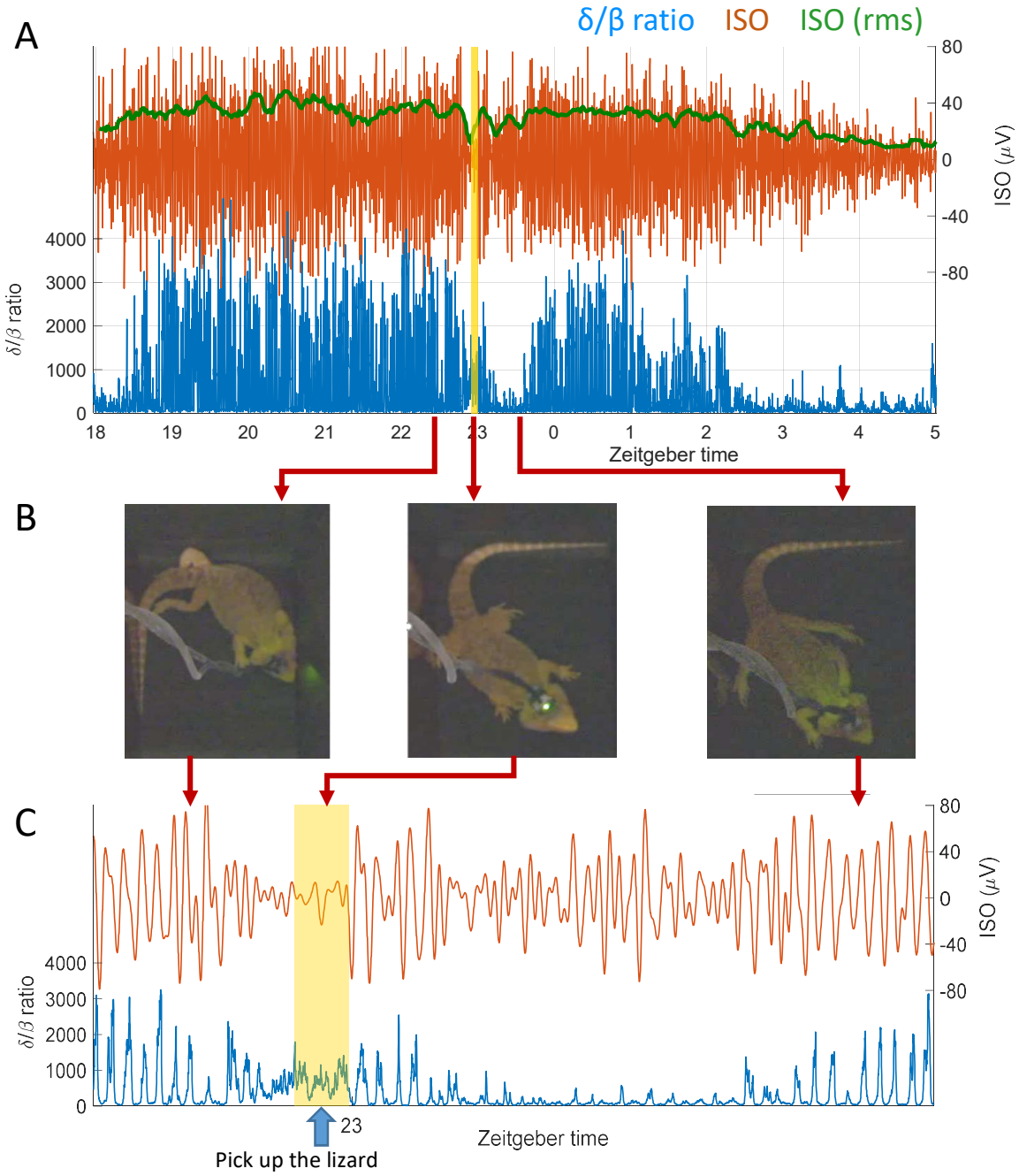

Figure 3.7: Sleep perturbation reduces the power of ISO
(A) An example of an overnight recording with imposed sleep disturbance (yellow shaded area, around 0 am) for ~5 min. **(B)** Lizard posture before (left), in the middle (middle), and after (right) the sleep disturbance. In the middle, the lizard shows a push-up-like posture indicating interruption of sleep. The head is more visible, and the legs retract towards the body. During sleep, the legs stretch, and the head lies on the floor. **(C)** Zoom-in of the time around the sleep disturbance in (A).

3.6) Phase relationship between ISO and δ/β ratio

Both the δ/β power ratio and ISO are slow periodic signals. I looked into the relationship between the up- and down-states of both signals. Visual inspection of raw traces reveals the high correlation between these two signals (figure 3.8 A). Two features appear in a cross-correlogram of these two 10-minute datasets (figure 3.8 B). First, the periodicity of the cross-correlogram indicates that the periods of these oscillations are the same (92 seconds in this recording). Second, it reveals a significant phase shift between them, of about 11 seconds, ISO leading.

I used a 10-minute sliding window (1-minute steps) to calculate the cross-correlation all through the overnight recording. This scrolling cross-correlogram (figure 3.8 C) shows a very stable relationship between ISO and δ/β ratio. During sleep, the period of these two signals and the lag between them remained largely unchanged. The periodic correlation, however, was absent before and after sleep.

To further confirm this relationship between ISO and δ/β ratio, the sleep-box temperature was changed in the middle of the night. The δ/β power ratio decreased over time but was not necessarily correlated with the temperature change. From the scrolling auto-correlogram (figure 3.9 A), I measured that the period of the sleep cycle decreased from 153 to 102 seconds when the temperature was raised from 24 to 28.5 °C in the second half of the night ($t \approx 340$ mins). The opposite effect was observed when the temperature was lowered in the second half of the night (data not shown). These periods were consistent with recordings made at constant temperatures, as in part 3.3.

The period, but not the amplitude, of the ISO was temperature-dependent (figure 3.9 B). The scrolling auto-correlogram of the ISO was identical to that of the δ/β ratio. This indicates that the alternation of sleep states and ISO either are causally related, or are under the influence of the same source or mechanism. Interestingly, although the period of both signals decreased to ~67% of its original value at 24°C after the temperature increased, the lag between them did not shorten proportionally. The lag remained between 14 and 16 seconds before and after the temperature changes (figure 3.9 C and D).

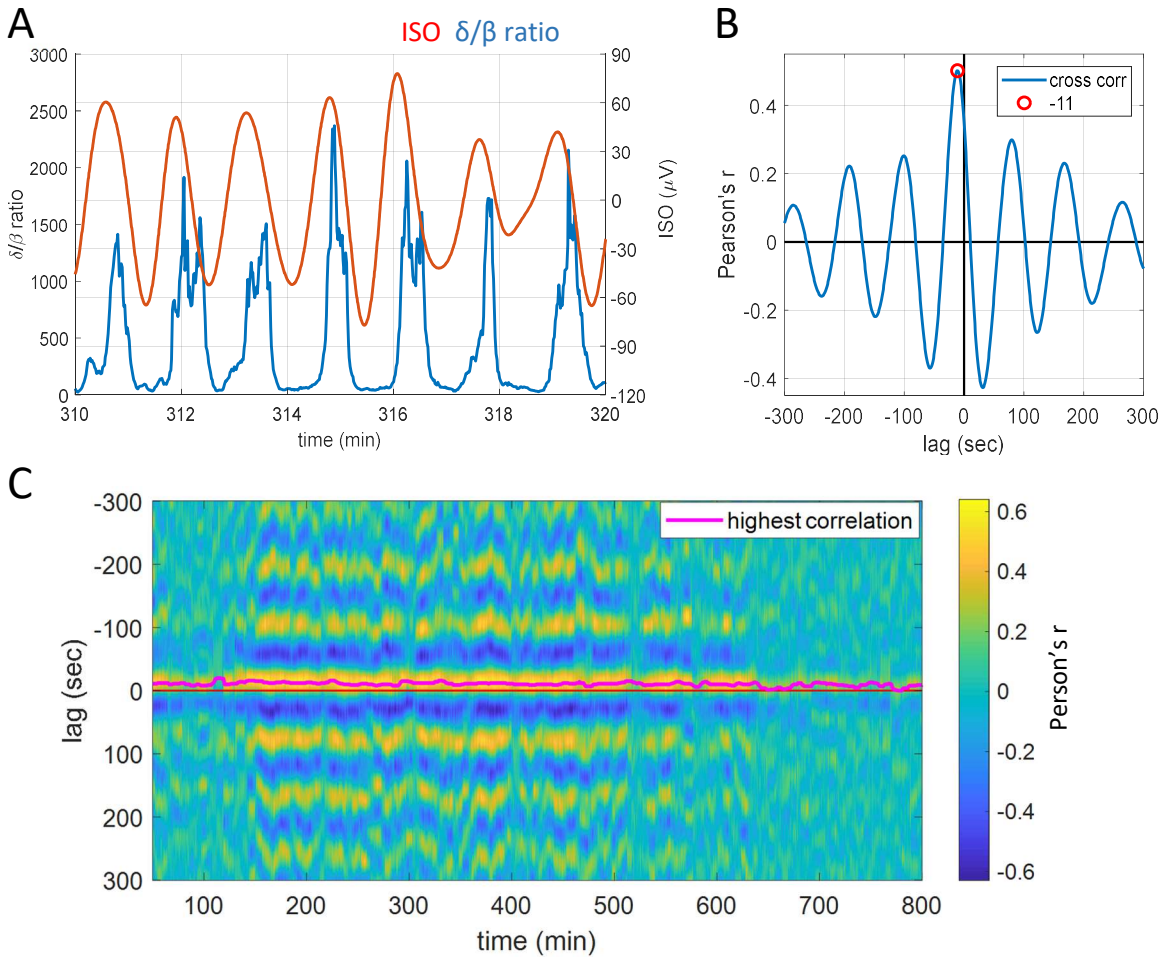

Figure 3.8: Phase relationship between ISO and δ/β power ratio
(A) Raw traces of δ/β ratio (blue) and ISO (red). Both signals are periodic and approximately synchronous. **(B)** Cross-correlogram of data in (A). The average period (between the two highest peaks) is around 92 seconds. The highest correlation (red circle) corresponds to a phase lag of 11 sec, ISO leading. **(C)** Sliding cross-correlogram, calculated as in (B), rotated by 90 degrees clockwise. The window length is 10 minutes, and the step size is 1 minute. X-axis: time in minutes; Y-axis: cross-correlation lag in seconds. The magenta line is the lag time (red circle in (B)) updated every minute. Correlation curve is smoothed using a medium filter (7-minute window).

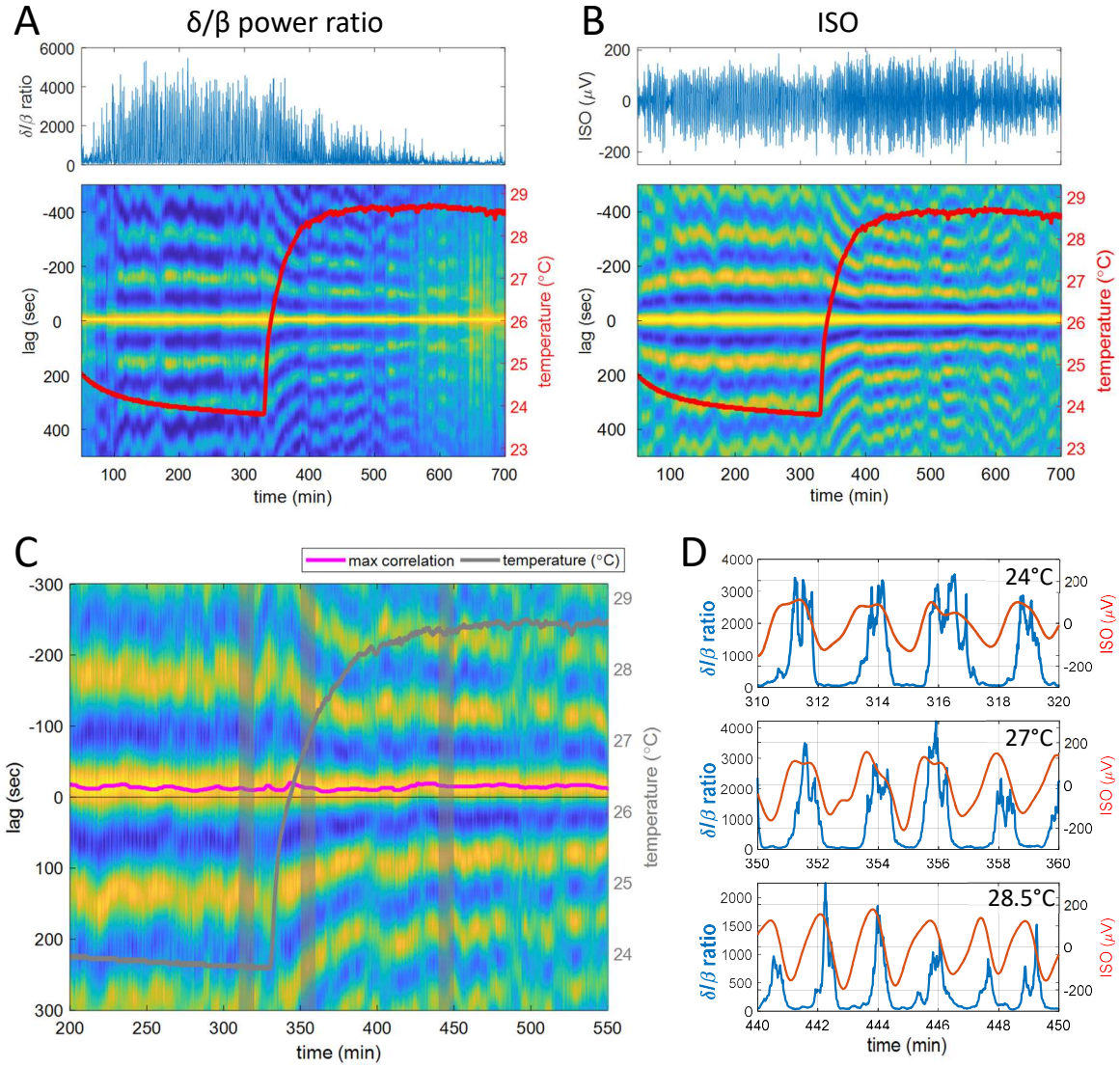

Figure 3.9: Frequency of ISO and δ/β oscillation are both temperature-dependent
(A) Top: δ/β ratio of an overnight recording. Bottom: the sliding auto-correlogram from the δ/β ratio. All parameters are the same as in figure 3.8 (C). The red line is the temperature of the sleeping box. **(B)** Top: ISO from the same electrode as in (A). Bottom: the sliding auto-correlogram of the ISO. All parameters are the same as in figure 3.8 (C). The red line is the temperature of the sleeping box. **(C)** Sliding cross-correlogram of ISO and δ/β ratio. Magenta: time of maximum correlation. Gray: Temperature of the recording rig. Raw traces of three shaded areas are shown in (D). **(D)** The δ/β ratio (blue) and ISO (red) at different temperatures.

After an animal had recovered from surgery, it could provide high-quality data for over a month. Figure 3.10 illustrates sleep recordings from one animal and the same electrodes over 5 weeks. The ambient temperature was different in each recording. The mean period of the sleep cycle and ISO varied between 89 and 158 seconds. The latency between them varied between 9 and 19 seconds. When plotting lag vs. period, no clear correlation stood out (Pearson's correlation coefficient (ρ) is -0.0437. *p*-value = 6.436x10^-9). But ISO always led, whatever the sleep cycle period (figure 3.10 B).

The leading and lagging signals (δ/β ratio or ISO) never changed when recorded from the same electrodes in the same animal over time. However, the leading signal could be different in different animals/recordings. In 4 implanted lizards with multiple recordings, ISO led δ/β ratio in two animals but lagged in the other two (figure 3.11 B). The average time lags between the two signals were also different between animals when recording under the same ambient temperature. Those differences hint that the connection between ISO and δ/β ratio is more complicated than a simple causal relationship.

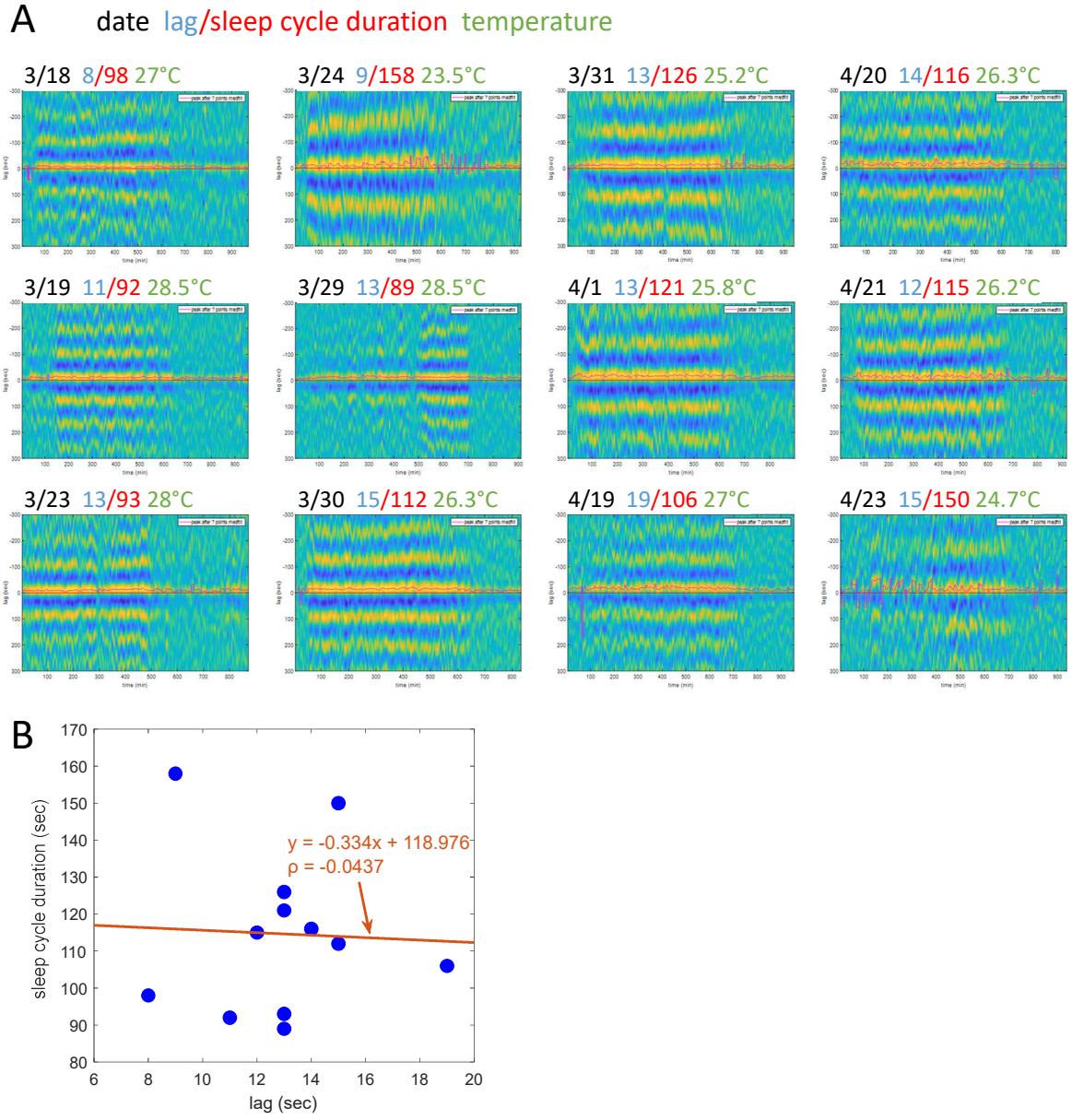

Figure 3.10: Phase relationship between ISO and δ/β ratio
(A) Sliding cross-correlograms of recordings from one lizard. All data plotted are from the same electrodes. The ambient temperature is constant for each recording for at least 4 hours during sleep, but different between days. The recording date, lag between signals, sleep cycle duration, and ambient temperature are color-coded and listed above each sub-figure. Lags and periods are averages over 100 minutes when periodic activity was clearly visible. **(B)** Scatter plot of lag vs. sleep period. Pearson's correlation coefficient (ρ) is -0.0437. *p*-value = 6.436x10^-9 (two-tailed t-test).

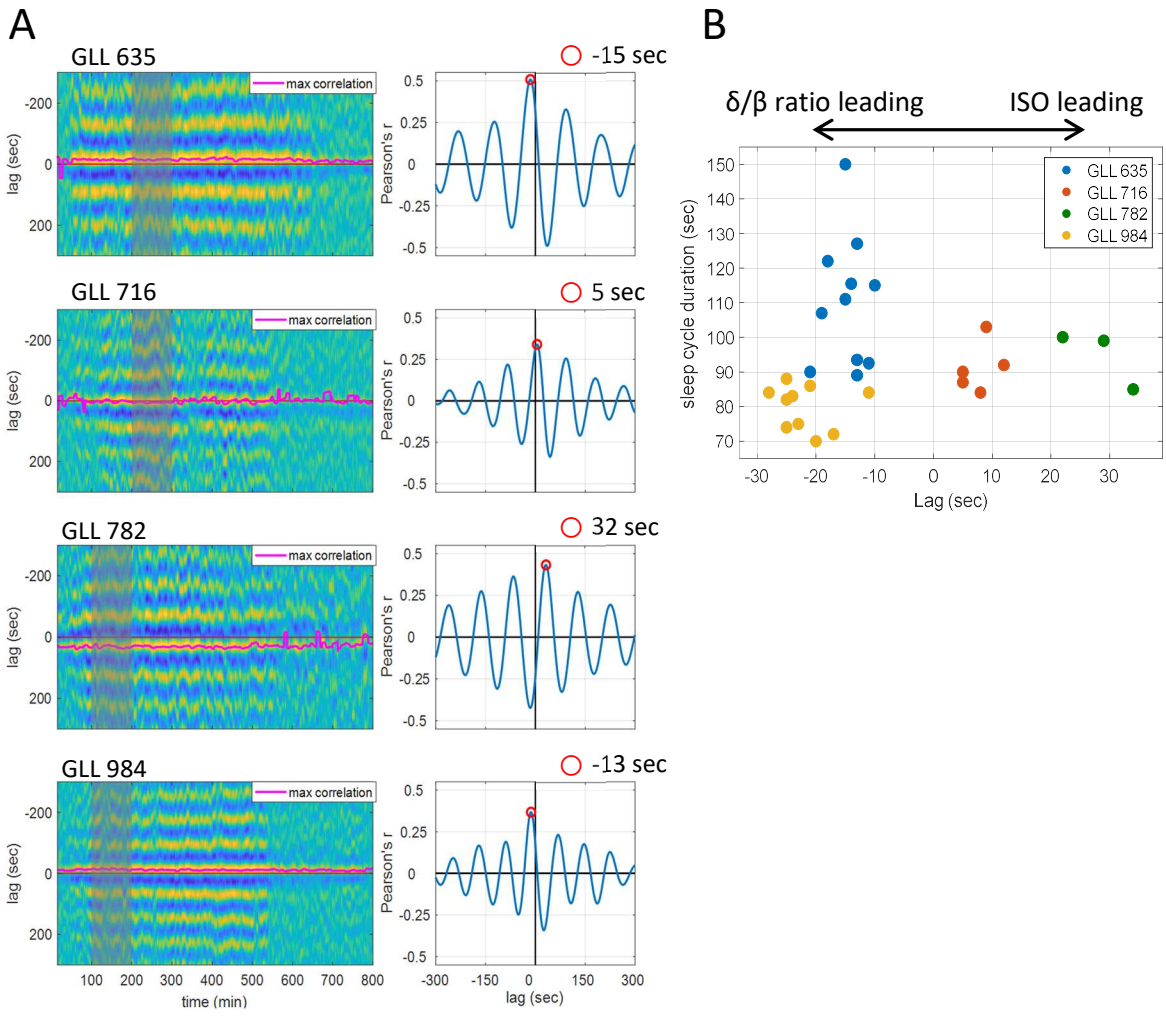

Figure 3.11: Phase relationship between ISO and δ/β ratio from different lizards
(A) Representative results from four implanted animals. All recordings were done at constant, but different temperatures. Left: sliding cross-correlogram between ISO and δ/β ratio. The window length is 10 minutes, and scrolling steps are 1 minute. The shaded box is the period used by the average cross-correlogram on the right. Right: average cross-correlogram over 100 minutes. The red cycle labels the point with the highest correlation value. The lag time of the highest correlation (red circle) is listed above. **(B)** Scatter plot of the sleep cycle duration and the lag between ISO and δ/β ratio. Each dot is one overnight recording from one animal. Lag times are from the averaged cross-correlogram as in (A, right). The period is the time difference between the two highest correlation points from the average cross-correlogram in (A, right). The positive lag indicates that ISO leads δ/β ratio; the negative lag indicates that δ/β ratio lead ISO. The highest correlations needed to be larger than 0.3 to be considered. All data points of GLL635/716/984 are from the same electrodes. Data from GLL782 are from two electrodes 23 µm away.

3.7) ISO latency along the horizontal and vertical axes

An inconsistent phase relationship between recordings or animals could have several explanations. One potential reason is a difference in impedances between electrodes from one animal to another. Indeed, a different impedance could lead to different filtering properties. Filtering changes not only the amplitude of a signal but also introduces phase delays. Because the frequency ranges of the δ/β ratio and of the ISO are three orders of magnitude apart, this could explain different lags between animals. Unfortunately, this hypothesis proved incorrect. Take GLL-716 and GLL-984 as an example. Identical probes (NeuroNexus A1x32-poly2) were used in both implantations. The average impedance of all 32 channels was 1.272±0.372 and 1.289±0.355 MOhm (1000Hz), respectively, right before sacrifice. The ISO amplitude of the deepest channels were both between 50 and 100 µV. However, the average lags between the two animals were 7.8 and -21.9 seconds, the leading signals being different (figure 3.11 B).

Another possibility is the location of the implant. It is nearly impossible to implant a probe in precisely the same location repeatedly. The reasons are: 1) The lizard skull does not have useful landmarks such as bregma and lambda in rodents. 2) The surface of the brain is smooth without convolutions to serve as landmarks. 3) Brain size changes with age. Therefore, the distance from a fixed point in the brain is not reliable. 4) The lateral ventricle is 500-1000 µm wide, allowing the brain to move in all three dimensions. I could confirm implantation location only *post hoc*, using micro-lesions.

To understand whether probe location affects the phase relationship between ISO and δ/β ratio signals, I compared signals from different electrodes in different shanks. Figure 3.12 illustrates an eight-shank probe implanted along the anterior-posterior axis. Cross-correlograms showed that the ISO synchronized with the δ/β ratio in both electrodes, but the lag was shorter in the posterior electrode (13 seconds) than in the anterior electrode (28 seconds) (Figure 3.12 C, D).

Different lags between ISO and δ/β ratio from two sites could come from either signal. To know which signal caused a significant lag, I used the same processing pipeline to calculate the δ/β ratio and ISO from both electrodes. The δ/β ratios had different amplitudes in different positions, but the lag between them is minimal (figure 3.13 A). However, ISOs from different shanks showed significant lags (~13 seconds) despite having very similar amplitudes and waveforms. The lag between ISOs from different shanks was very stable across the entire recording (figure 3.13 B). The average cross-correlogram showed that two ISOs had the same frequency, but the anterior one was 13.1 sec behind the posterior one (figure 3.13 C).

Long lags between electrodes appeared not only along the horizontal axis but also along the vertical axis. ISO from a linear probe showed a ~10 second lag between a deep and a superficial channel (figure 3.13 D, E) that were 667 µm apart, the superficial channel leading. If the ISO were a propagating wave, its speed would be 30.5 µm/sec along the horizontal axis and 66.7 µm/sec along the vertical axis. This propagation speed is ~5 orders-of-magnitude slower than other known mesoscopic traveling waves such as the theta and alpha waves in human neocortex (Zhang et al., 2018) and the theta wave in rats hippocampal CA1 (Lubenov and Siapas, 2009). It is therefore unlikely to be due to electrical propagation.

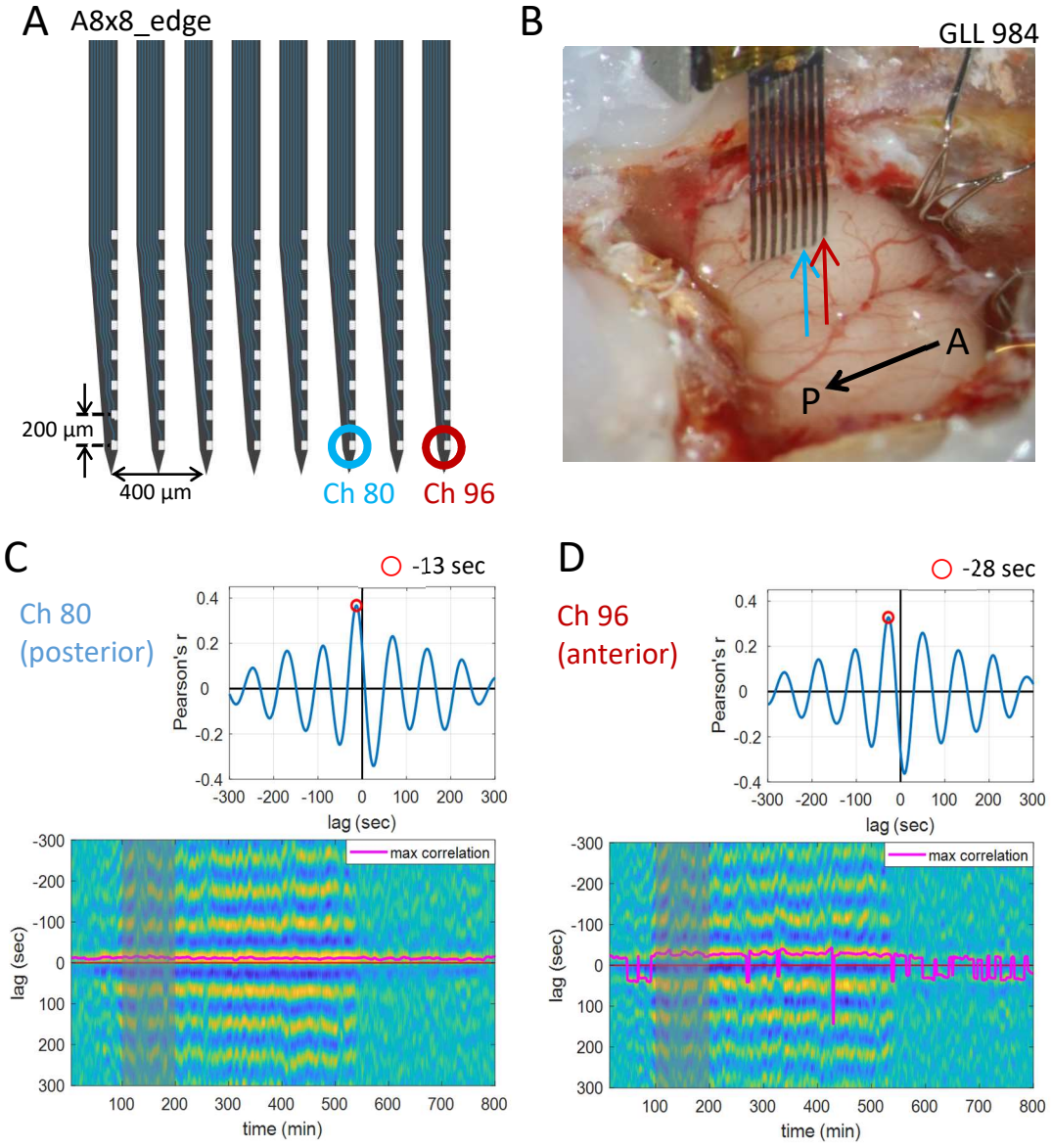

Figure 3.12: Lag between ISO and δ/β power ratio recorded from different probe shanks
(A) The configuration of an A8x8_edge probe from Neuronexus. **(B)** Implantation during the surgery. The probe is inserted into the DVR of the left hemisphere along the anterior-posterior axis. **(C,D)** Top: average cross-correlogram over 100 minutes during sleep from channels 80 and 96. Bottom: sliding cross-correlogram of the overnight recording. All parameters are the same as in figure 3.8 (B,C). Stepwise jumps of magenta trace due to local change of dominating side peak in cross correlation.

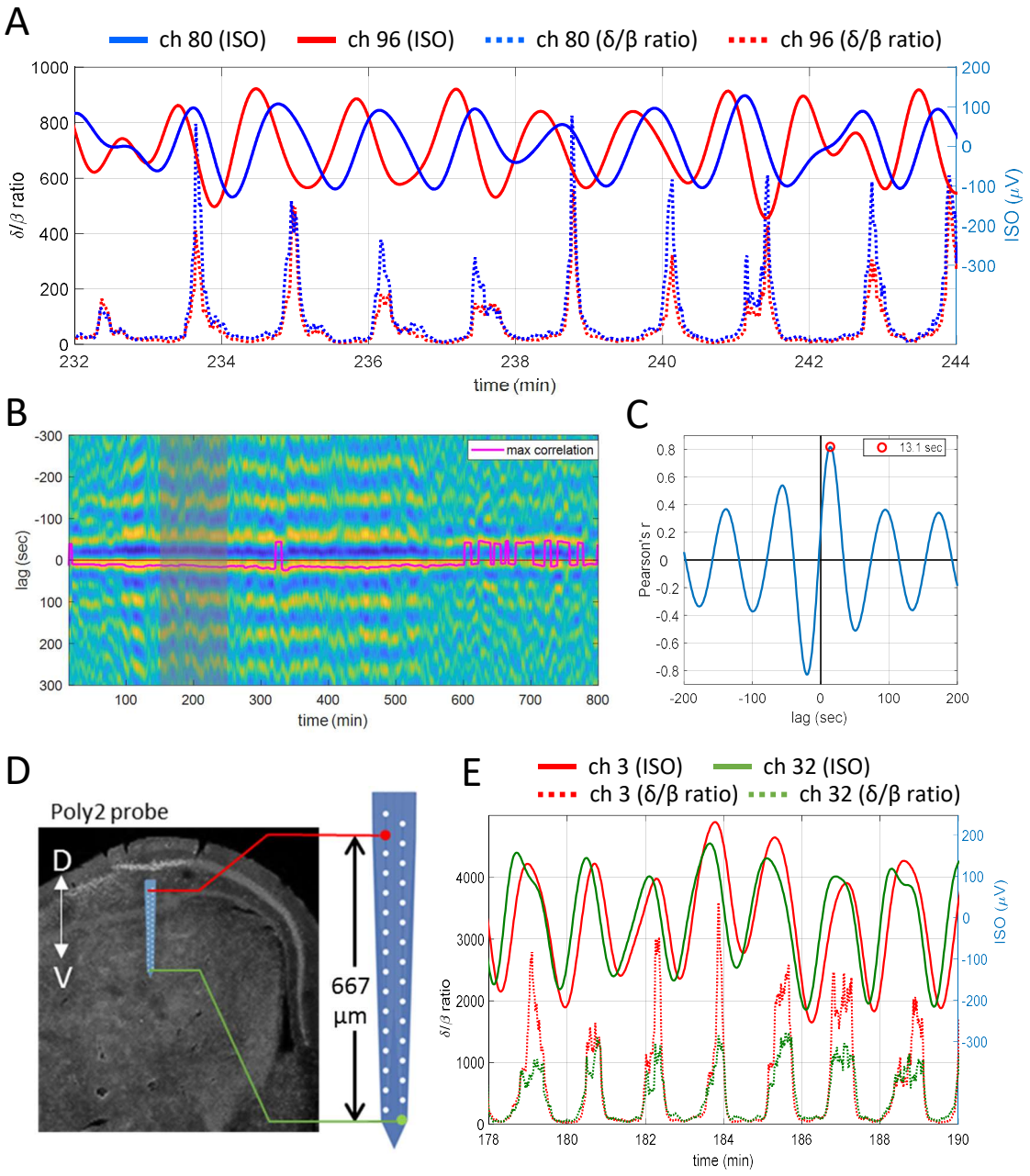

Figure 3.13: Latency of ISO recorded from different electrodes
(A) ISOs (solid lines) and δ/β power ratios (dashed lines) from channel 80 and 96 in the figure 3.12. **(B)** Sliding cross-correlogram between ISOs from channels 80 and 96. The magenta line is the highest correlation in each sliding window. The sliding window is 10 minutes, and the step size 1 minute. The shaded box labels the time used in (C). **(C)** Mean correlogram of the data in the shaded box in (B). The lag time of the highest correlation is 13.1 sec, posterior shank (channel 80) leading. **(D)** Left: illustration of the implantation of a poly2 probe from NeuroNexus. Right: configuration of the probe. The data from two electrode recording sites, channel 3 (red) and channel 32 (green), are shown in (E). **(E)** ISOs (solid lines) and δ/β ratios (dashed lines) from the two channels. Color scheme as in (D).

Chapter 4
In vitro recordings: Results

Whole-brain recording from freely moving animals with single-neuron resolution is the dream of many system neuroscientists. With the latest development of CMOS-based probes, it might be possible in the foreseeable future. The most recently developed Neuropixel probe can record neuronal activity through 384 parallel channels from 960 sites along its 10mm shank. Several groups developed executable methods to maximize recording density with the Neuropixel probes (Juavinett et al., 2019; Luo et al., 2020; Putzeys et al., 2019a). A rat can simultaneously carry up to 6 implanted probes, limited by space on its head and the weight an animal can carry without impacting its mobility (Siegle et al., 2021). Other techniques such as fMRI provide whole-brain activities but with low spatial and temporal resolution.

Reptilian brains offer another, complimentary approach – *ex vivo* recordings. The metabolic rate of an ectotherm animal is about one-tenth of a similar-sized endotherm. Their brains can also function properly at a low temperature, further decreasing oxygen and nutrients consumption, and thus, needs. Together, these features have allowed scientists to record neural activity from the retina, the cochlea, the olfactory bulb, cortex, brainstem and spinal cord in isolated turtle and lizard nervous systems (Connors and Kriegstein, 1986; Shein-Idelson et al., 2017; Stirling et al., 1998). In such preparation, it is also easier to introduce pharmacological agents or optogenetic manipulation into a precise location coincident with electrophysiological recording. Space and weight constraints are easier to solve in the *ex vivo* condition. Using this approach, I successfully recorded electrophysiological signals and got some exciting results that I now present in this chapter.

4.1) “Neutral” state of the isolated brain

Ex vivo recordings are new in the bearded dragon. Despite previous results in different species of lizard and turtle, it was essential to collect some necessary basic information from Pogona. The state of the isolated brain was one critical piece of information needed. In our approved protocol, a lizard has to be deeply anesthetized before brain extraction. To remove the anesthetic’s depressing effects, reptilian Ringer's solution was used to perfuse the brain after

decapitation, through neck arteries, for ~20 minutes before brain extraction. Despite such perfusion, there was a concern that *ex vivo* signals would be no different from those recording during anesthesia.

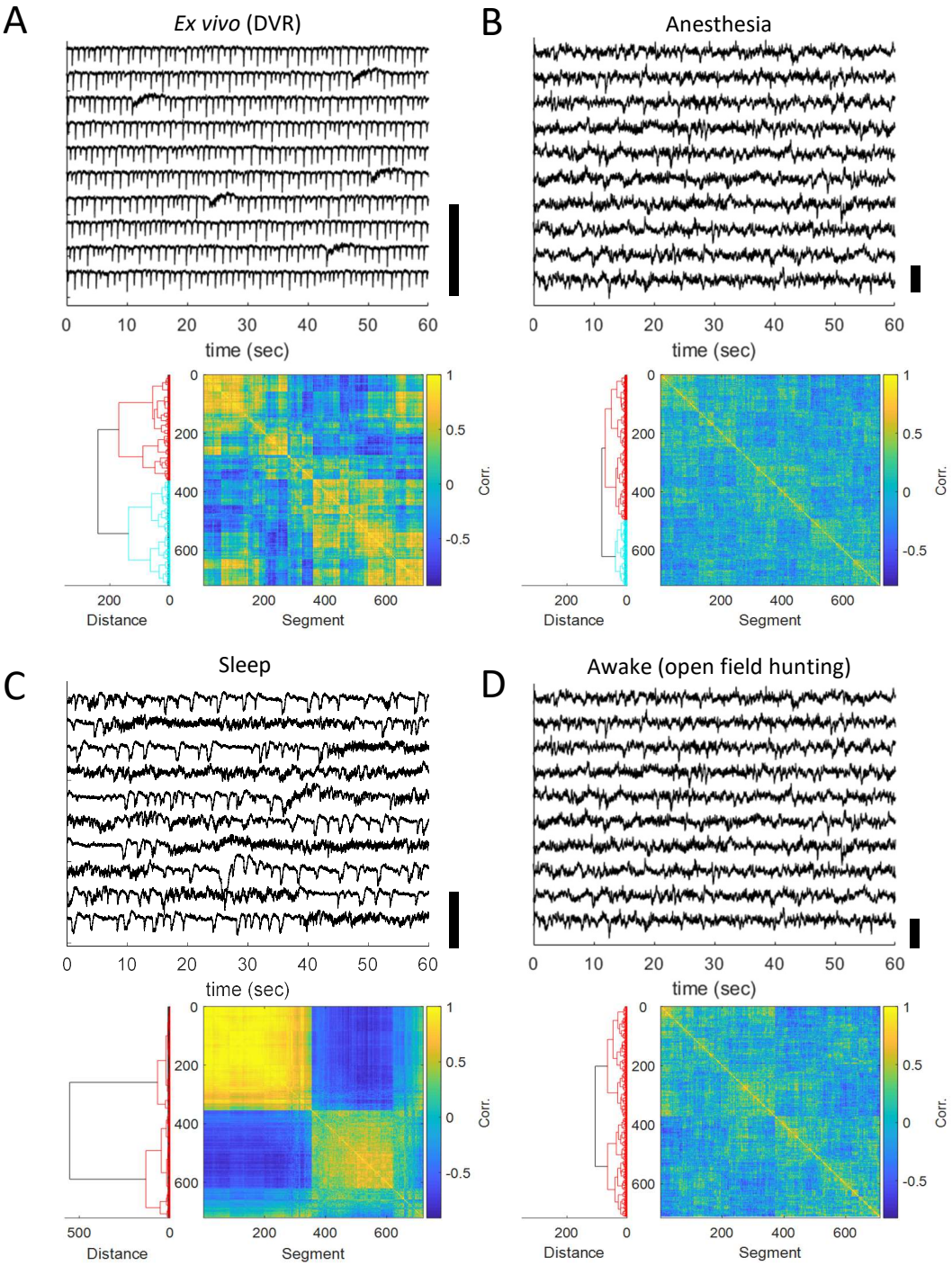

Figure 4.1: DVR LFP in different states

LFP, dendrogram, and correlation matrix (pairwise correlations between short data segments as in figure 3.2C) during **(A)** *ex vivo*, **(B)** anesthesia, **(C)** sleep, and **(D)** awake (hunting in an open field) states. Top: LFP filtered between 0.1 and 9000 Hz. Each row represents a 60-sec segment (running left to right); successive 60-sec segments run continuously from top to bottom. The solid vertical scale bars (right) are 1 mV in each panel. Bottom: Shown (right) is an ordered correlation matrix of spectral characteristics, calculated from 720 data segments. Each segment is 2-sec (A) or 10-sec (B,C,D) long from one LFP channel. The dendrogram (left) is based on a Euclidian metric (Ward linkage). Note that the dendrogram distance between the two major clusters is significantly longer in sleep than in the other three states.

To examine this possibility, I compared DVR LFPs recorded during *ex vivo*, anesthesia (intact animals, non-terminal), sleep, and awake states (freely moving). The *ex vivo* LFP showed a pattern distinct from all other states. It was characterized by concatenated large negative deflections interrupted by short (3-5 sec) bouts of broadband activity (figure 4.1A). Hierarchical clustering reveals two clusters as for sleep, but with shorter inter-cluster distance (figure 4.1C).

One recording was made during anesthesia, in a lizard that was lightly anesthetized with Ketamine (45 mg/kg, i.m.) and Midazolam (1.5 mg/kg, i.m.), that is, ~75% of the dosage of the initial anesthesia used to prepare *ex vivo* brains. This lizard lost its righting and toe-pinch reflexes but maintained spontaneous breathing and a weak corneal reflex. SWRs persisted during anesthesia, but the event frequency was significantly reduced (~0.2 sec^{-1}) compared with that in an *ex vivo* brain (~1 sec^{-1}) or during SW sleep (0.3-0.5 sec^{-1}). There was no broadband activity until the lizard recovered from anesthesia, 3-4 hours after administering the first anesthetic agent. Accordingly, there was no visible second cluster in the correlation matrix (figure 4.1B). It is noteworthy that the event frequency of *ex vivo* SWRs varied between 0.15 and 1 sec^{-1} in different animals. There was no clear relationship between event frequency and age, weight, gender, time of sacrifice, or ambient temperature.

The sleep DVR LFP contains two distinct states, each corresponding to REM and SW sleep. The occupancy of either state is roughly the same (figure 4.1C). When a lizard was hunting in an open-field maze, the DVR LFP showed continuous broadband activity similar to that during REM sleep (figure 4.1D). These results show that an isolated brain is in a “neutral” state, which cannot be categorized neatly into sleep, awake, or anesthesia.

SWRs are the most distinct LFP events in the lizard DVR. The LFP pattern during SW-sleep always shows consecutive SWR events. SWRs can also be observed during awake resting periods. In isolated brains, SWR-like events were different from those recorded during sleep. There were three major differences: First, the duration of sharp waves was 3-5 times shorter in *ex vivo* events. Second, the rebound following the trough of the SWR, typical of SWRs, was almost absent in *ex vivo* SWRs. Third, the ripple frequency was lower in *ex vivo* events (figure 4.2 A, B): during SW sleep, the ripple frequency is 40-140 Hz, but it was only 20-60 Hz in the *ex vivo* SWR-like events.

As we saw earlier, the δ/β power ratio is a good indicator of sleep state in Pogona. SWRs, the signature events of SW sleep in Pogona, can also be used to determine brain states. The periodic variation of SWR tracks that of the δ/β ratio during sleep (figure 4.2C). I did the same

measurement in *ex vivo* DVR recordings to look for potential periodic variations. Like the δ/β power ratio, SWR numbers fluctuated without any periodic regularity (figure 4.2D).

An isolated brain stayed in the "neutral" state for hours. However, LFP patterns could evolve significantly when extending a recording to 12-16 hours. Figure 4.3 illustrates this change in a long recording. In the first 7-8 hours, the LFP pattern was a mixture of SWRs and short bouts of broadband activity. In the 8th hour, the number of SWR-like events decreased dramatically from 15-18 to almost 0 after 1.5 hours (figure 4.3A). When I aligned the recording time with the Zeitgeber time, I observed that the number of SWRs decreased between 4 and 5 am, ~3 hours before the end of the dark phase (note that the lizard was no longer alive). It was similar to the time when the δ/β power ratio decreases during the night, at the end of a sleep recording (figure 3.6A). When zooming into the LFP, I observed that the second half of the recording did not possess SWRs. The LFP and spectrogram were similar to those characterizing the short broadband activities in the first 7-8 hours (figure 4.3 B,C). This result suggests that circadian rhythms controlling sleep-wake states may still function in an isolated brain. However, the circadian clock was beyond the scope of my project, and I did not look into it any further.

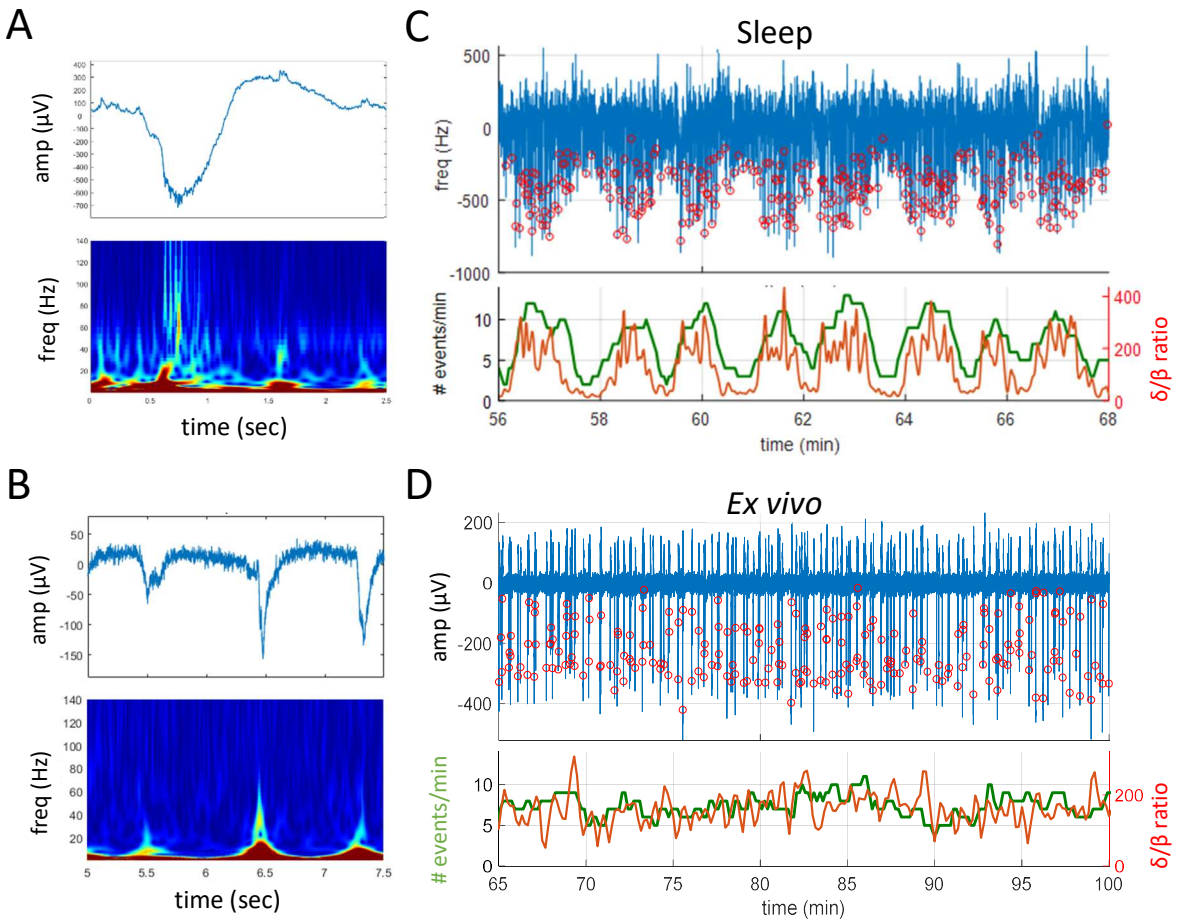

Figure 4.2: No state alternation during *ex vivo* recording
(A) Top: close-up view of DVR LFP during slow-wave sleep. A large-amplitude slow potential fluctuation and high-frequency ripple close to the trough resemble the mammalian SWR complex. Bottom: spectrogram of the LFP shown above (continuous wavelet analysis with Morlet wavelet). The frequency range of the ripple oscillation was between 40 and 100 Hz. **(B)** Top: close-up view of *ex vivo* DVR LFP. Time span same as in (A). SWRs are sharper than their counterparts during SW sleep. The rebounds following the troughs are almost absent. Bottom: spectrogram of the LFP. Ripple frequency is significantly lower than that during sleep. **(C)** Top: filtered LFP (blue) during sleep (frequency range: 0.1-6000Hz) and time of occurrence of SWRs (red circles). Bottom: δ/β power ratio (red) and smoothed number of SWRs (1-min sliding window, 10-sec steps). **(D)** The same analysis as in (C) applied to the *ex vivo* recording. The number of SWRs was calculated in a 15-sec window, sliding in 3-sec steps.

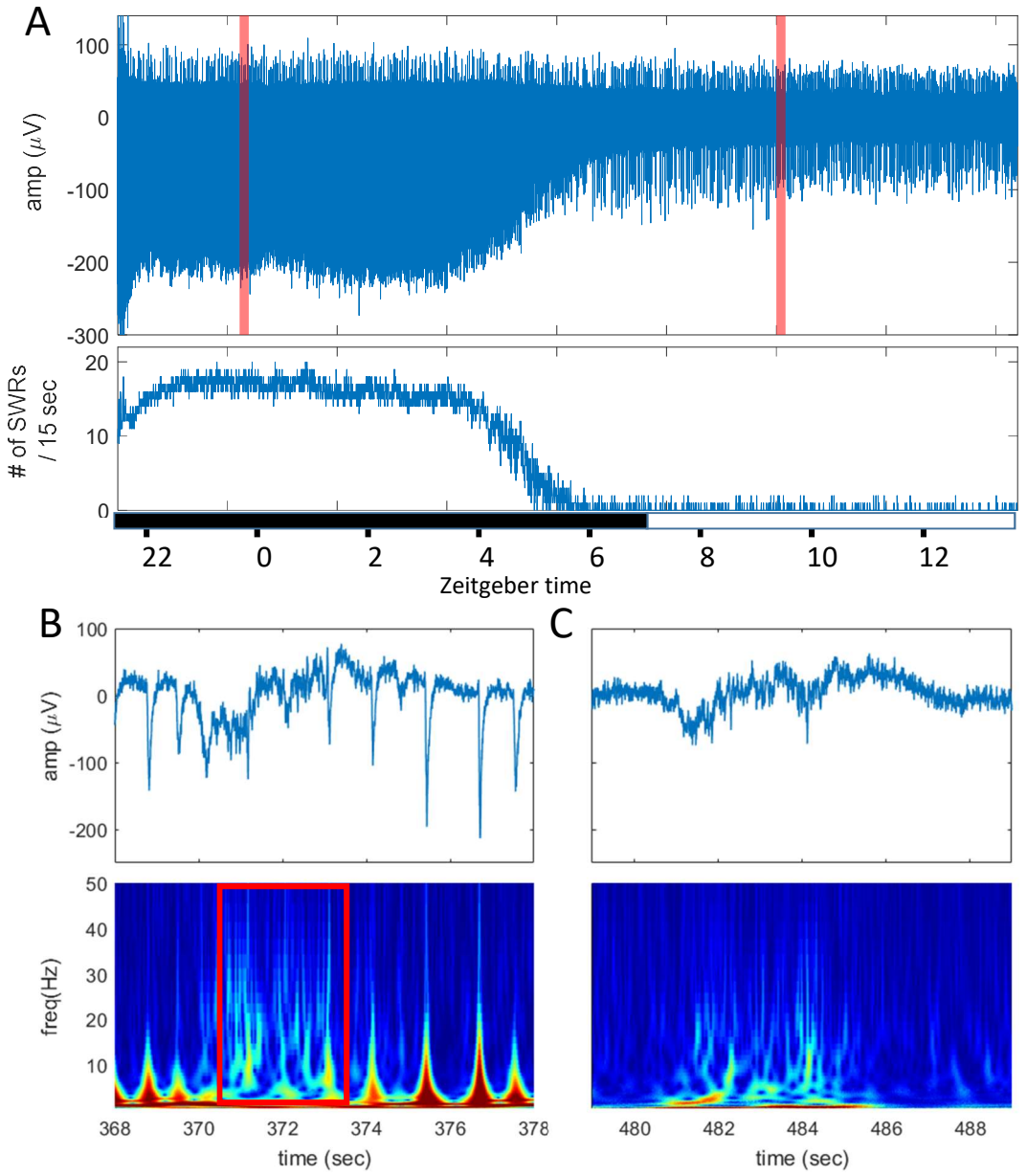

Figure 4.3: DVR LFP of an overnight recording from an isolated *ex vivo* brain
(A) Top: the bandpass filtered (0.1-9000Hz) LFP of an *ex vivo* recording from a single channel in DVR. Bottom: number of SWRs in a 15-sec window. Recording time was aligned to Zeitgeber time. The light-dark cycle in the terrarium is shown as a filled (dark) or open (light) bar underneath. The two red areas are expanded in (B) and (C). **(B)** 10-sec-long LFP recorded at ~11 PM (top); its spectrogram (bottom). The red box highlights a REM-like episode. **(C)** 10-sec-long LFP recorded at ~9 AM and its spectrogram. Note the similarity between (C) and the short bout of REM-like episode in (B).

4.2) Brainstem activity affects the DVR LFP in an isolated (*ex vivo*) brain

Ex vivo recordings enabled me to access the entire brain from any angle. We know from mammalian work (Héricé et al., 2019), that brain areas likely involved in sleep state alternation, such as the locus coeruleus (LC), sub-coeruleus (subC), laterodorsal tegmentum (LDT), periaqueductal gray (PAG), and raphe nuclei (RN), are located in the midbrain and the brainstem.

I simultaneously recorded LFP from LC, subC, PAG, and bilateral DVRs (figure 4.4A). PAG was very quiet in this *ex vivo* setting. I could record no specific pattern except "noise." LFPs from LC and subC contained low-amplitude and unsortable action potentials. The most distinct patterns from these two areas were short bouts of broadband activity across almost all electrodes in a two-shank probe. Signal amplitude was higher in the posterior shank than in the anterior one (figure 4.4B). According to the configuration of the silicon probe (500 µm spacing between shanks; 50 µm spacing between electrodes on one shank), broadband activity covered an area of at least 500 µm (anterior-posterior axis) by 600 µm (dorsal-ventral axis). This size was roughly the same as that occupied by LC and subC together. I used the average power between 40 and 100 Hz to detect broadband activity across the entire recording. The number of broadband-activity bouts in a 15-min window increased slightly over time (figure 4.4C). The duration of each event remained between 5 and 10 seconds (figure 4.4D).

From retrograde tracing results obtained by a lab colleague, Hsing-Hsi Li (unpublished data), we know that the DVR receives long-range, direct inputs from LC and subC. The number of retrogradely labeled LC/subC neurons appears to be higher on the ipsilateral side than on the contralateral one. When comparing the activities of DVR and LC/subC, I found that multiunit activity in DVR increased during brainstem broadband activity (figure 4.4E). This result is consistent with the hypothesis (but does not prove) that neuronal activity in the brainstem affects neuronal activity in DVR.

Bicuculline is an antagonist of gamma-aminobutyric acid A ($GABA_A$) receptors. It mimics network activity recorded during epilepsy by blocking the inhibitory action of $GABA_A$ receptors. To further confirm an interaction between the brainstem and DVR, I tried to manipulate neuronal activity in the brainstem by injecting bicuculline into the LC (figure 4.5AB). Three hours of baseline activity were recorded in DVR and brainstem areas before injection. I injected bicuculline twice into the left LC and once into the right LC. LFP recordings continued during drug injection. Baseline activity following injection was similar to that before injection. Event

frequency (SWRs) was ~4 in a 30-sec sliding window in both hemispheres. After the first injection into the left LC, signal amplitude in both DVRs decreased significantly (figure 4.5C). When zooming in on the LFP, I observed that SWRs disappeared in both DVRs soon after injection (figure 4.5D) and recovered slowly ~20 minutes later.

It took ~50 minutes until the number of SWRs returned to baseline levels. The second injection in the same location had a reduced effect. The number of SWRs in the ipsilateral (left) DVR decreased slightly, but that in the contralateral DVR did not change. When injecting bicuculline into the right LC, the number of SWRs decreased in both DVRs. The effect was more robust on the ipsilateral side than on the contralateral side. This result is consistent with the anatomical results mentioned before.

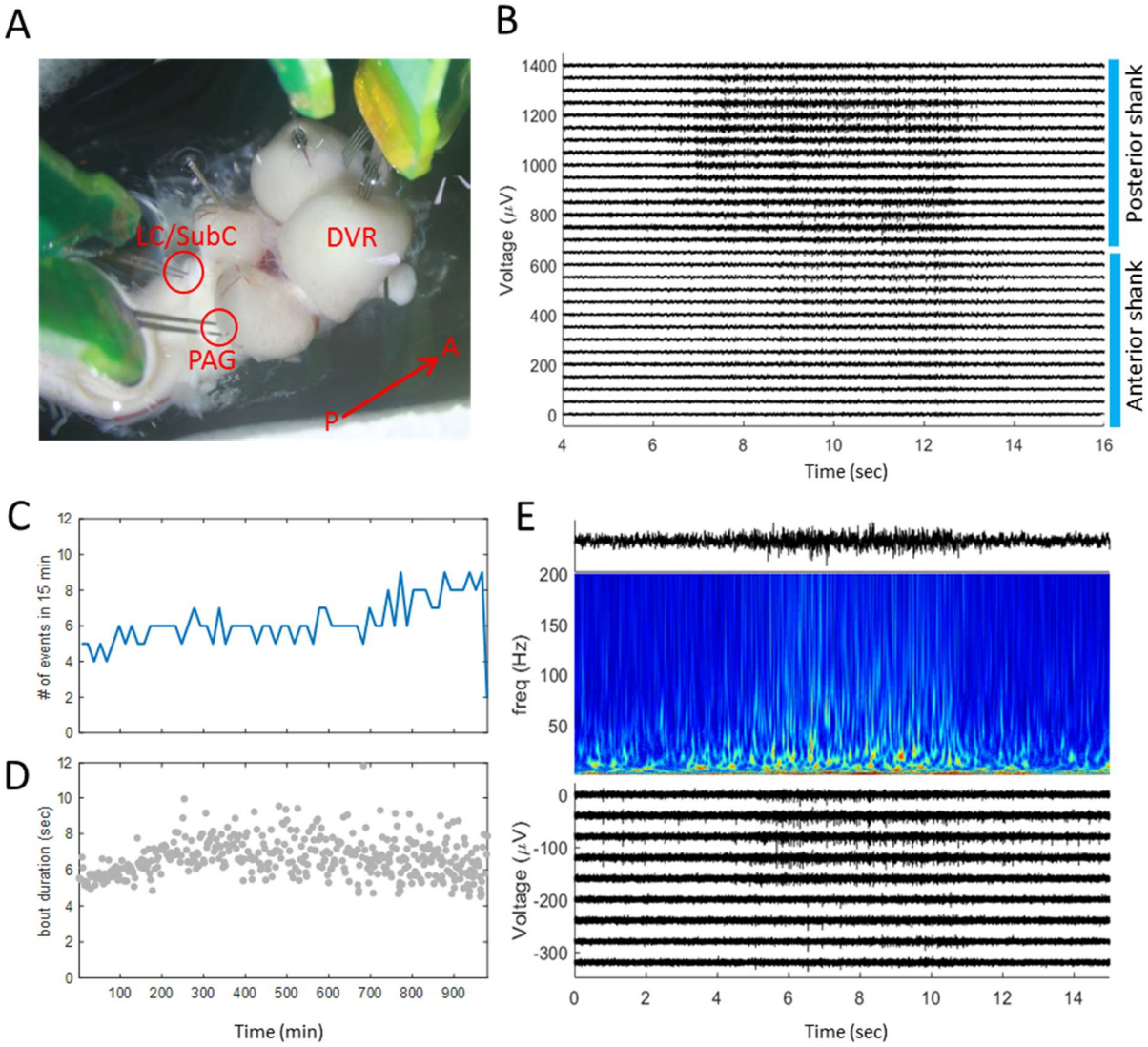

Figure 4.4: Broadband activity in the brainstem is correlated with an increase in firing rates in DVR
(A) Illustration of probe locations during *ex vivo* recording. **(B)** The bandpass filtered (0.1-9000 Hz) LFP in LC/subC along shanks. Signals from damaged channels were removed. A broadband LFP event occurred at 4-11 seconds. Amplitudes were larger in the posterior shank than in the anterior one. **(C)** The number of broadband events (15-min window) in a ~16-h recording. **(D)** Bout duration of each broadband event in LC/subC. **(E)** Top: mean LFPs from all channels in the posterior shank in (B). Middle: spectrogram of the mean LFP above. Bottom: forebrain LFPs filtered in the action potential range (300-2000 Hz). Note the increase in multiunit activities during the broadband activity in LC/subC.

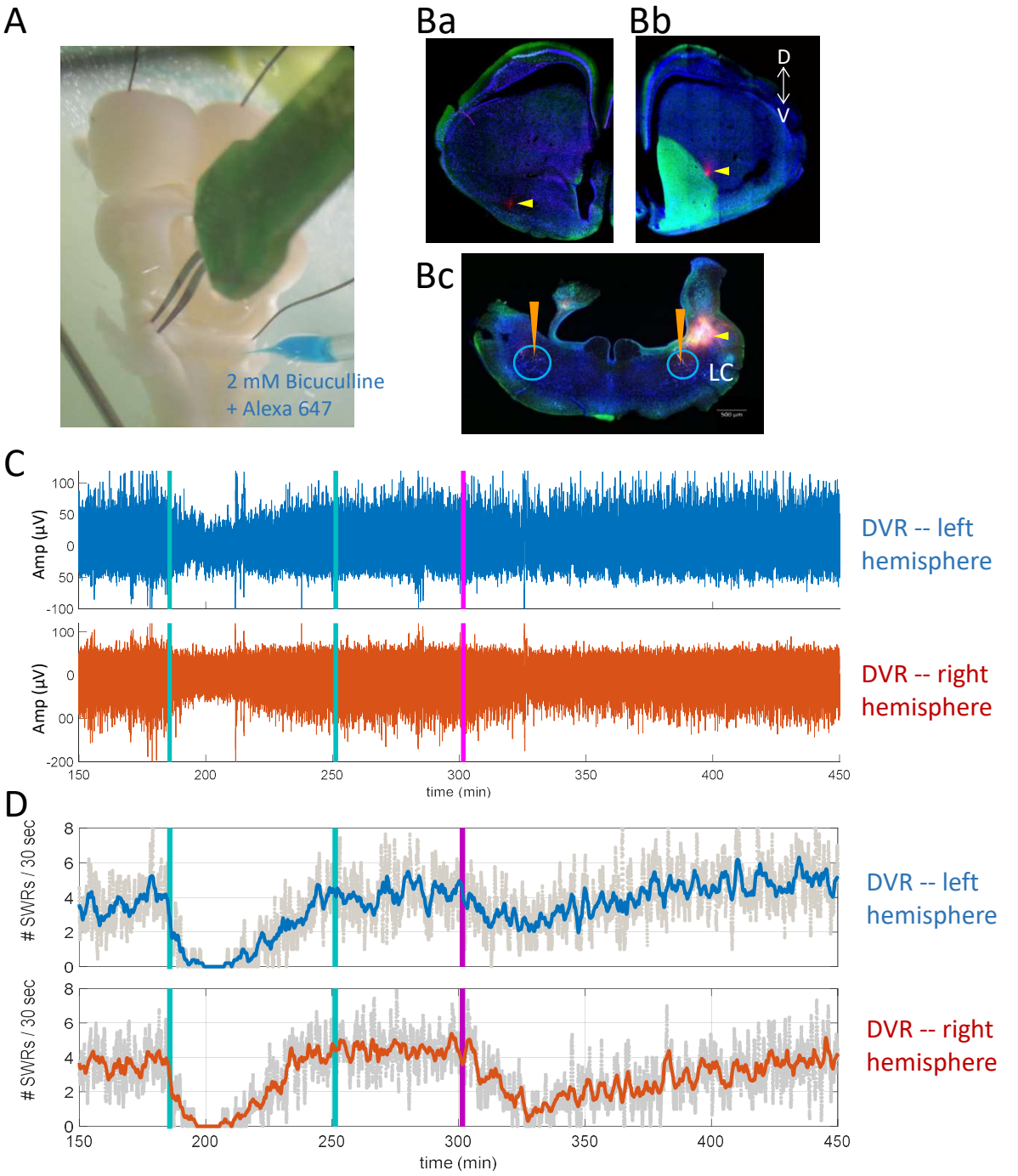

Figure 4.5: Neural activity induced in the brainstem affects the DVR LFP
(A) This representative photograph illustrates the *ex vivo* recording configuration together with the bicuculline injection pipette located in the brainstem. Alexa Fluor 647 was added to the bicuculline solution to label the injection area. **(B)** Coronal sections through a lizard's forebrain (Ba, left hemisphere; Bb, right hemisphere) and brainstem (Bc) show the electrode recording positions (yellow arrowheads). The electrode insertion sites in the left brainstem were in sections anterior and posterior to this section. Bicuculline injection sites are labeled with elongated triangles (Bc, orange). **(C)** Bandpass filtered (0.1-9000 Hz) LFPs from DVRs in the left (top) and right (bottom) hemispheres. Vertical lines indicate times of bicuculline injections in the left (cyan) and the right (magenta) LC. **(D)** Number of SWRs calculated in a 30-sec window (gray) sliding in 1-sec step. Smoothed traces of SWR numbers are color-coded as in (C).

4.3) Infra-slow oscillation

The sleep-related ISO was an unexpected finding, as was its precise coupling to the sleep-states alternation described earlier. My results described in section 4.2 showed that the *ex vivo* brain does not show periodic state changes in the 1-3 minutes range. I thus predicted that ISOs would not be observed in an isolated brain.

Surprisingly, ISOs with a broader frequency range than *in* vivo recordings (0.7-50 mHz) exist in the isolated brain. Figure 4.6A shows an example of ISOs recorded bilaterally from DVR and in full LC (ISO in the right LC was hardly detectable). Histology showed that both left and right silicon probes were placed in similar locations. The reason why the right LC signal was small is unknown.

ISOs from bilateral DVRs and left LC were almost identical, except for the amplitude. The cross-correlogram between the three areas proved that their frequencies were almost identical. The lag between hemispheres was only 0.6 seconds, right DVR leading (figure 4.6 Ba). However, lags between the ISO from the left LC and ISOs from the ipsilateral and the contralateral DVRs were 29 and 29.3 seconds, respectively, DVR leading (figure 4.6 Bb, Bc).

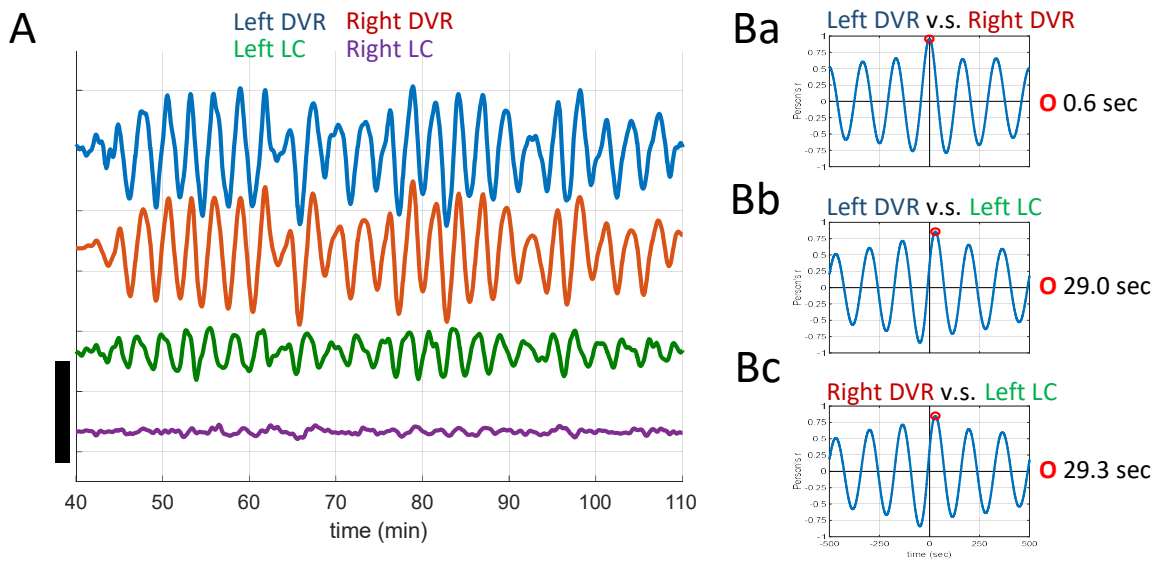

Figure 4.6: ISO in *ex vivo* recordings of DVR and LC
(A) ISOs recorded simultaneously from different locations. The scale bar at left is 500 µV. **(B)** Cross-correlograms between left and right DVRs (Ba), DVR in the left hemisphere and left LC (Bb), and DVR in the right hemisphere and left LC (Bc). Red circles indicate lag times at the highest correlation.

Figure 4.7 illustrates an *ex vivo* recording using a two-shank probe. The *ex vivo* ISO from DVR remains their periodicity in both superficial and deep recording sites (figure 4.7 C, top). The cross-correlogram shows that synchronous slow rhythms have a subtle lag (figure 4.7 C, bottom). The average lag between them is only 1.6 sec in a 327-sec period (figure 4.7 D). This result, ISO in the superficial channel leads ISO in the deep channel, is consistent with *in vivo* ISO (figure 3.13 E). Compared to the *in vivo* recording lag (10 sec lag in a 96-sec period, figure 3.13 E), the lag during *ex vivo* recording is significantly shorter. Whether this difference is related to the mechanism of ISO generation or propagation is unknown.

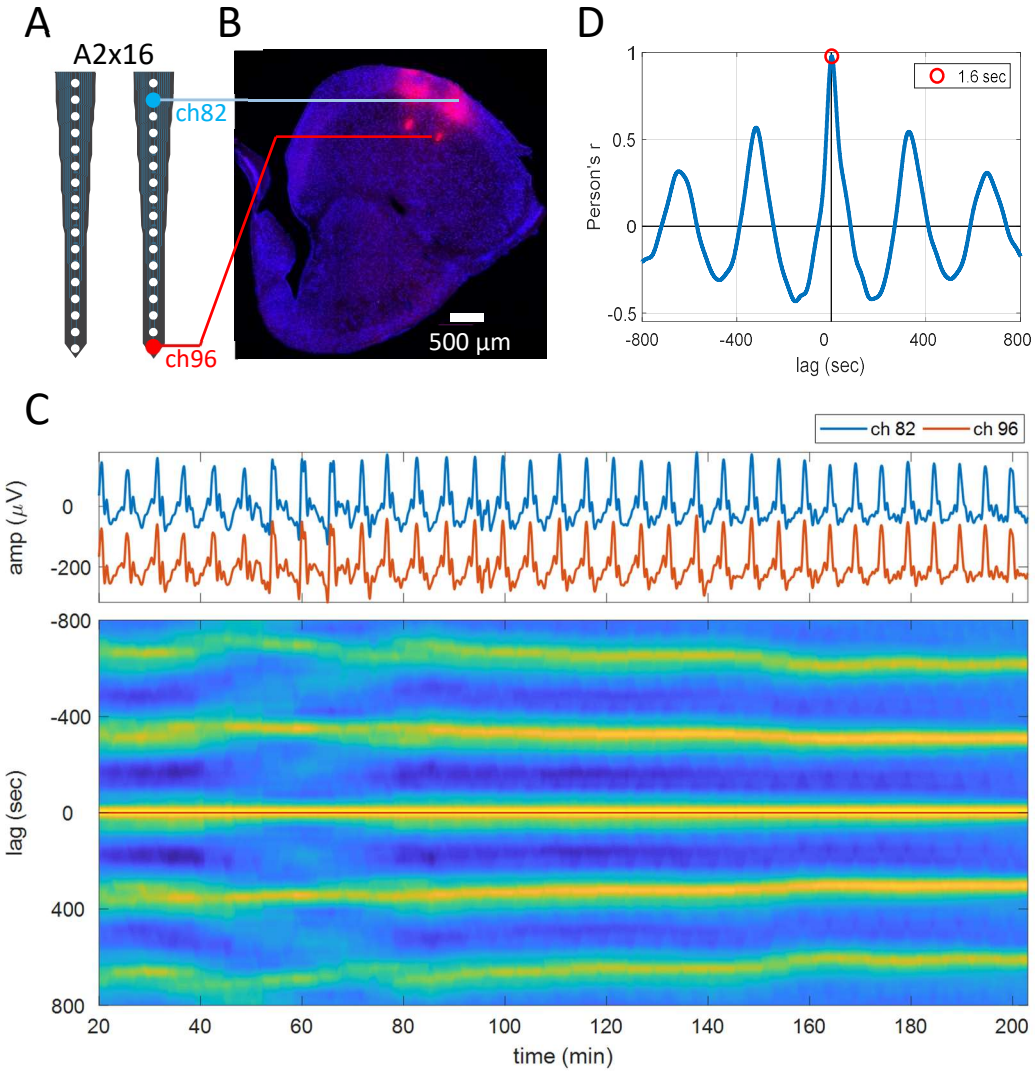

Figure 4.7: Latency of DVR ISO in different channels
(A) The configuration of an A2x16 probe from NeuroNexus that was used in this recording. **(B)** Histology of DVR (right hemisphere, the cortex is removed before recording). The white bar is 500 µm. Blue: DAPI staining; Red: electrodes track (DiI from the silicon probe). **(C)** Top: ISOs from a superficial channel (ch82) and a deep channel (ch96) as labeled electrodes in (A). Bottom: the sliding cross-correlogram between the superficial and the deep recording site. **(D)** Average cross-correlogram in (C, bottom). The red cycle labels the point with the highest correlation value. The legend box shows the lag time of the highest correlation (1.6 sec, superficial channel leading, in this recording).

Given an apparent coordination between DVRs and LC, I tried to identify whether either or both are the source of the oscillation, or perhaps lack of a putative, probably distributed oscillator. I used a simple physical separation experiment to address these questions.

A brain was trans-sectioned between the forebrain and the midbrain after six hours of recording. After sectioning, both segments were placed back in the same perfusion chamber, and all probes were inserted into the same locations. ISOs were present in the forebrain and the brainstem before and after the trans-section (figure 4.8A). ISO frequency increased significantly in the DVR in the first 30 minutes following the section. Then, it returned to its initial range and remained there until the end of the experiment (figure 4.8 B). The frequency of the brainstem ISO did not change much right after sectioning (figure 4.8 C). Once the DVR ISO frequency had stabilized (t = ~480 min), the lag between the two parts of a brain became unstable. The lag shifted, sometimes abruptly from -42.2 seconds (t = ~500 min) to 4.9 seconds (t = 650 min) (figure 4.8 D). Because the intrinsic frequencies of DVR and LC remained quite stable (Figure 4.8 B, C), the varying lag time after sectioning suggested the existence of a connection between two local ISO generators in an intact brain, one in the forebrain and one in the brainstem. In addition, these two generators seem to have the same intrinsic resonance.

To test the hypothesis that two independent but frequency-compatible ISO generators can interact with each other, I wanted to modify the activity of those neurons that project directly from the brainstem to the DVR. We injected a retrograde AAV containing the ChR2 gene into left and right DVRs. After 3-4 weeks of incubation, the brain was extracted under red light (to avoid activating a ChR2 before recording).

Figure 4.9 shows an example of ISOs from a rAAV-ChR2-infected brain in a dark perfusion chamber before and after the light stimulus. The ISO frequency increased slightly in the first 4 hours of recording. A blue light (470 nm) stimulus was delivered by an optical fiber placed on the brainstem's surface over LC. A 10-sec light pulse was repeated three times with a 12-sec interval between stimuli. The ISO waveform and frequency remained unchanged for ~30 minutes after the light stimuli. At t≈300 minutes, the sliding auto-correlogram lost its continuity (figure 4.9 B). Zooming in on the LFP, the periodic pattern was disrupted between t=285 and t=305 minutes (figure 4.9 C, middle). The second side peaks of the auto-correlogram almost disappeared (figure 4.9 D, middle), consistent with perturbed periodicity. Periodicity returned ~30 minutes later, but the ISO period decreased from 8.3 to 6.2 minutes (figure 4.9 D). This result demonstrates that the activity of brainstem neurons can disrupt DVR ISO with a long time lag in an *ex vivo* preparation.

Neurons in cortex and DVR are typically silent in most *ex vivo* recordings. Yet, figure 4.10 reflects a potential connection between ISO and neuron firing rates modulation. Twenty-one units were sorted from a two-hour recording. Spike trains were converted into firing rates and corresponding firing rates normalized individually (figure 4.10 A). At first sight, the firing rates of all units showed some periodicity. The trend was clear when averaging normalized firing rates of all units (figure 4.10 B). The auto-correlogram of the mean normalized firing rates showed a periodicity of ~7 minutes (figure 4.10 C). I recorded DVR ISOs were recorded from 23 of 32 *ex vivo* brains. This periodicity varied between 0.57 and 23 minutes. The mean period of all successful *ex* vivo ISO recordings was 7.05 minutes. The mode was 5 minutes (figure 4.10 D).

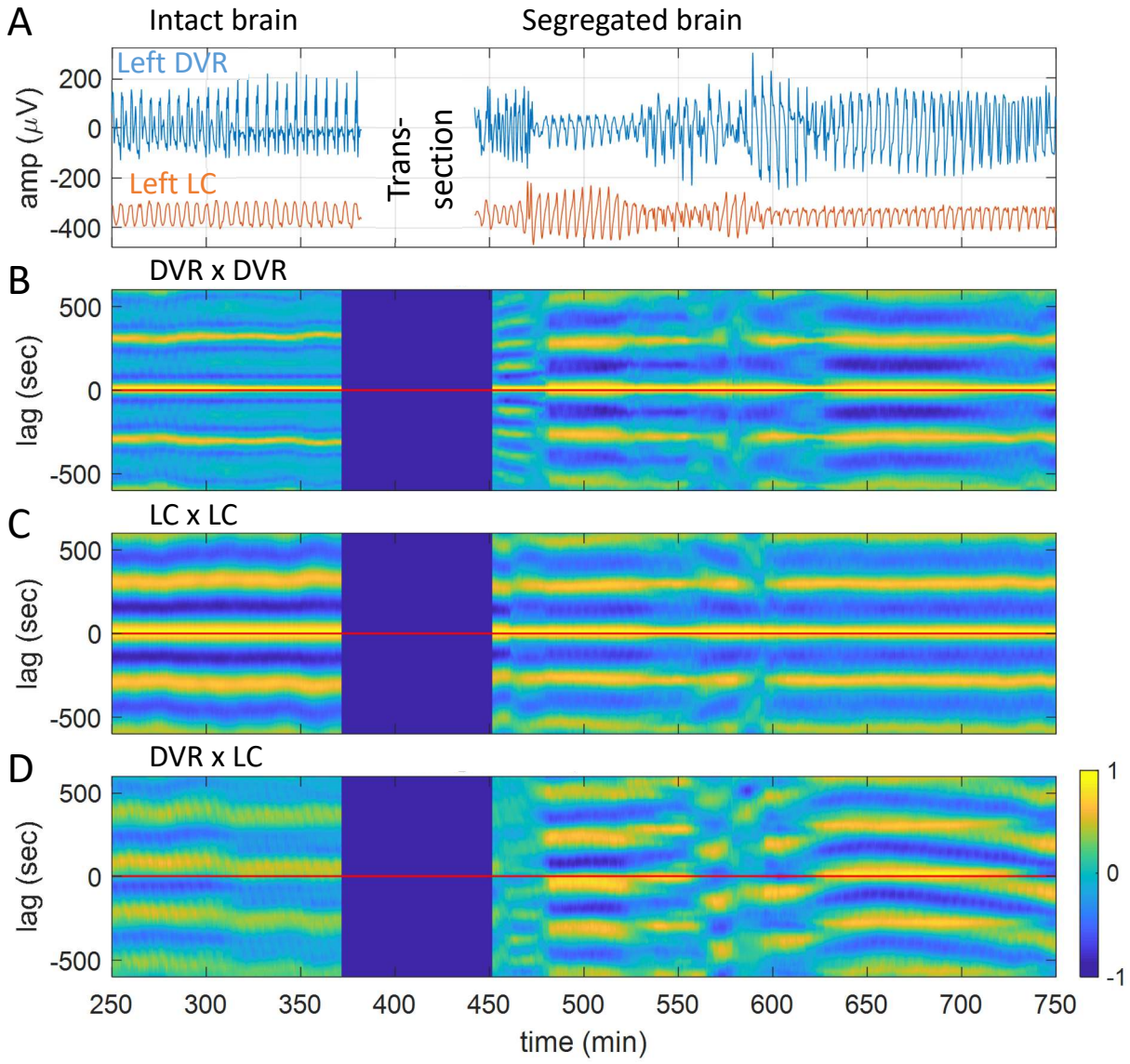

Figure 4.8: ISOs from the forebrain and the brainstem before and after trans-sectioning
(A) Mean ISOs from all electrodes in the DVR (blue, left hemisphere) and the brainstem (red, left side). Blank period represents the time needed to transect the brain and reposition the silicon probes. **(B)** Sliding auto-correlogram of DVR ISO in (A). Blue box represents time of sectioning and repositioning of probes. Mean durations of ISOs were 302.6 and 288.3 sec before and after cutting, respectively. Time ranges for averaging were 250-300 and 650-700 min, respectively. The autocorrelation was calculated over a 2400-sec window, sliding in 60-sec steps. The same parameters were used in (C) and (D). The red horizontal line indicates lag time 0. **(C)** Sliding auto-correlogram of the brainstem ISO in (A). The mean duration of ISOs was 300.4 and 287.8 sec before and after sectioning, respectively. **(D)** Sliding cross-correlogram of ISOs between DVR and the brainstem.

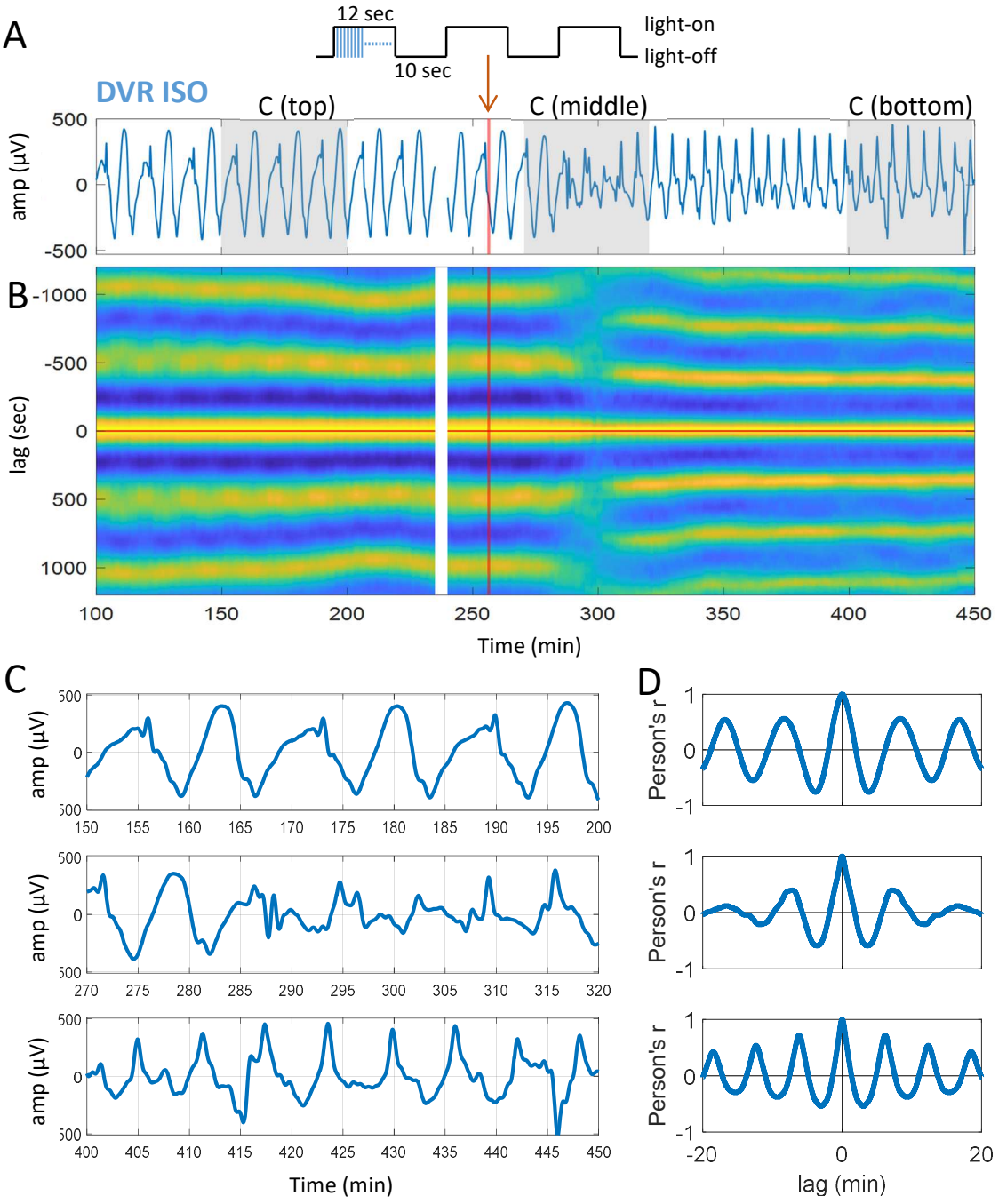

Figure 4.9: ChR2-evoked activity in the brainstem disrupts the DVR ISO in an *ex vivo* preparation
(A) ISO recorded in the DVR. Light stimuli were delivered at recording time ~255 min (red line). The gray shaded segments are expanded in (C). Inset: illustration of light stimulus (2ms pulse at 20 Hz). (Missing segment at t ≈ 240 minutes due to malfunction in the recording computer.) **(B)** Sliding auto-correlogram of the ISO in (A). Auto-correlation calculated over 2400-sec window, sliding in 60-sec steps. Note the discontinuity at t ≈ 300 min. **(C)** 50 minutes ISO data before (top), soon after (middle), and long after (bottom) light stimuli. **(D)** Auto-correlograms of ISOs in (C). The period of the ISO (the lag time of the second-highest correlation value) was 8.4, 7.8, and 6.2 min, respectively.

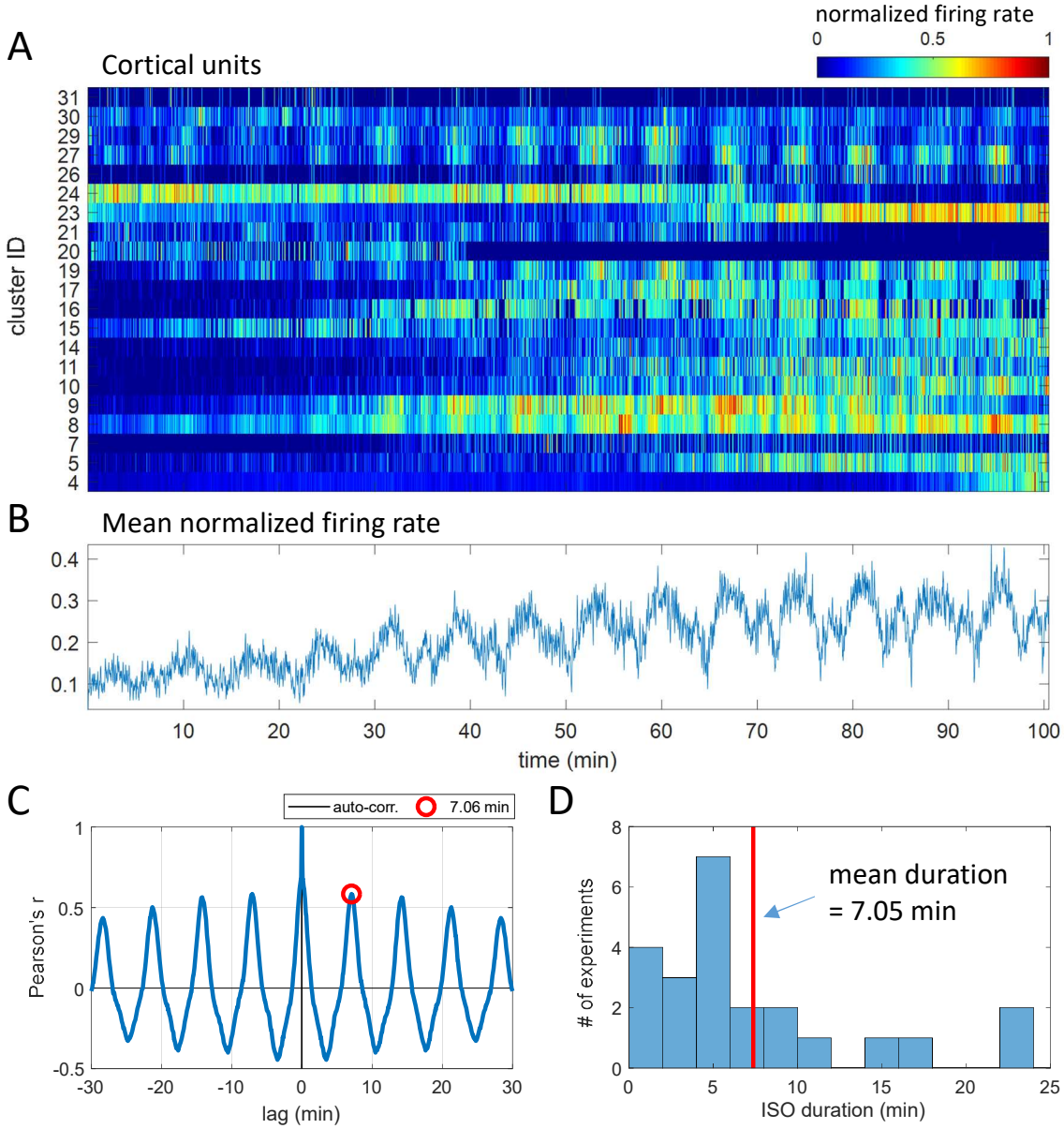

Figure 4.10: Slow rhythm in DVR neuron population firing rate (*ex vivo*)
(A) Normalized firing rates of all sorted forebrain units. **(B)** Mean of normalized firing rates in (A). **(C)** Auto-correlogram of (B). **(D)** Period of DVR ISOs from all successive *ex vivo* recordings (n=23).

Chapter 5
Discussion

5.1) Summary of results and potential limitations

Behavioral sleep has been described in metazoans from worms to humans. My data participated in establishing the existence of two sleep states in lizards. Lizard SW and REM sleep resemble a stripped-down version of the richer mammalian repertoire. The state alternation is very regular throughout the night, a pattern that has rarely been descried, if ever. The rhythm led to my discovery of an ISO in a frequency range between 5 and 20 mHz.

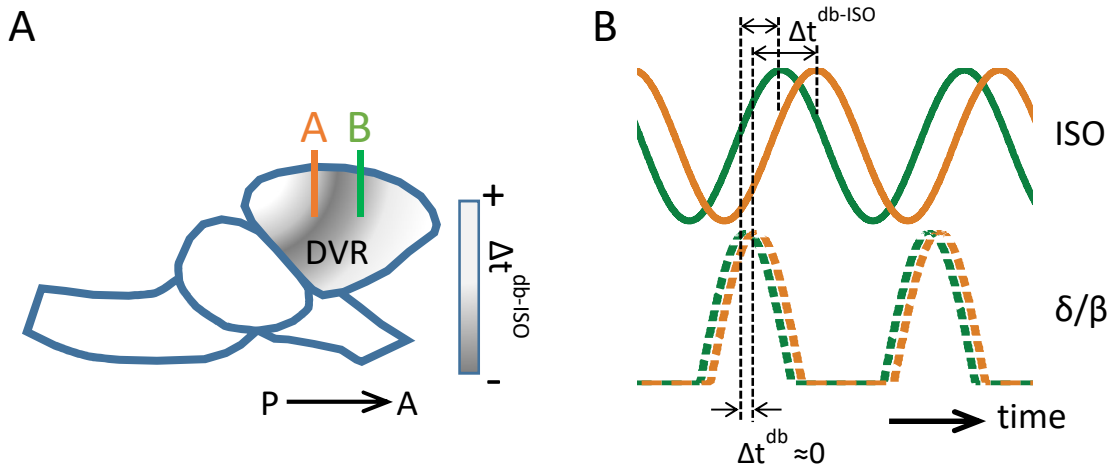

Figure 5.1: Summary of *in vivo* recordings
(A) Lateral view of a Pogona brain with recording electrodes in DVR. Color scheme in gray ($\Delta t^{db\text{-}ISO}$) indicates the variable lag between peaks of δ/β power ratio and ISO. **(B)** The relationship between ISO and δ/β power ratio. Color scheme as in (A). The Δt^{db} is the lag between δ/β ratio from site A to B. It is usually less than 1 sec. The $\Delta t^{db\text{-}ISO}$ is the lag between δ/β ratio and ISO from the same electrode. It varies between -30 and 35 sec, depends on the implantation location; from 4 lizards (see figure 3.11 B).

Figure 5.1 summarizes the relationship between two slow rhythms in DVR. Despite the fact that SWRs propagate from anterior to posterior DVR, the REM-SW sleep-state alternation, measured as δ/β power ratio (Δt^{db}), shows a very short lag between different electrodes. Lag (Δt^{db}) increases with the distance separating the electrodes. The *in vivo* ISO is synchronized with the δ/β power ratio recorded by the same electrode, but at a phase that depends on electrode

location. Based on my current results, DVR ISO seems to be a propagating wave that travels from the posterior-dorsal to the anterior-ventral at very low velocity (30-66.7 µm/sec).

Figure 5.2 summarizes results from *ex vivo* recordings. Despite the lack of sleep-state alternation (detected as δ/β oscillations *in vivo*), an ISO can be recorded *ex vivo* independently in both the forebrain (DVR) and the brainstem. They are phase-locked with very long time lags, DVR leading. DVR ISO also shows a short time lag between superficial and deep channels, superficial channels leading. This coordination disappears after severing the brain between the telencephalon and midbrain, but in an intact *ex vivo* preparation, ChR2-evoked activity in the brainstem appears to have a (delayed) effect on the forebrain ISO.

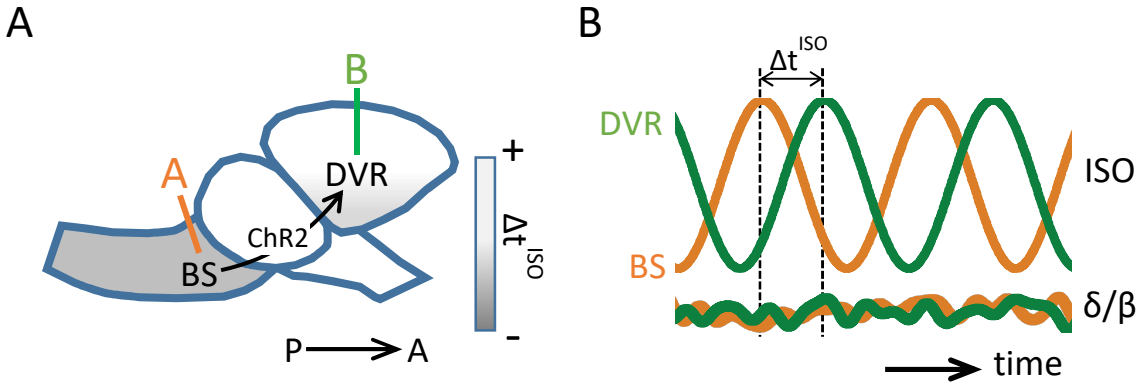

Figure 5.2: ISO in *ex vivo* recordings
(A) Schematic of ISO recordings in the lateral view of a Pogona brain. A and B are electrode locations in the brainstem (BS) and DVR, respectively. ChR2-evoked activity in the brainstem has a delayed effect on the DVR ISO (figure 4.8 A,B). Color scheme in gray indicates the lag between ISOs from DVR and the brainstem. **(B)** ISOs from the brainstem (orange) and the DVR (green) are synchronized with significant time lag (Δt^{ISO}), DVR leading. The δ/β power ration does not show significant change during *ex vivo* recordings. The Δt^{ISO} varies between 24 and 100 sec.

Together, my data shows an unnoticed very slow, propagating wave in the forebrain and the brainstem that can be closely linked to the sleep-state alternation. During sleep, one or more mechanisms generate ISOs in the brainstem and DVR. It is possible that the same mechanism also regulates the sleep state alternation. Two independent ISO generators in the brainstem and DVR are able to coordinate and synchronize with each other through direct connections. The mechanism(s) that generates, transmits and coordinates the ISO is unknown, but I will discuss several possibilities below (section 5.2).

Missing critical experiments are ones that would assess the interaction between the forebrain and the brainstem *in vivo* during sleep. The problem is a practical one: the lizard brain tilts at ~45 degrees along the anterior-posterior axis. Thick muscles cover the skull above the posterior half of the brain. With our current recording technology, it is next to impossible to reach the brainstem without severely impacting the animal's quality of life. It may be possible, at least *ex vivo*, to manipulate neuronal activity in the brainstem, in areas such as LC and LDT, with genetic or pharmaceutical methods, but I did not attempt to perform such experiments *in vivo*. The main reason is the lack of needed information among these areas. Most published research findings focus on sleep-awake regulation without differentiating between sleep states.

Ex vivo recordings represent an alternative solution that allows unrestricted access to the brain. One drawback is the potential influence of anesthesia before brain extraction. Individual lizards react to anesthetics differently. The dosage and time until deep anesthesia could be reached varied by two to three folds across animals. This may explain some of the inconsistency in my results during *ex vivo* experiments.

Another potential problem was the perfusate. Our Ringer recipe comes from a snake CSF and proved to be useful in lizard recordings. However, when extending the recording duration to 16-24 hours, the brain swelled up by at least 300 µm (7-8%). It might be helpful in the future to optimize the composition of the Pogona's CSF.

5.2) Potential mechanisms underlying the infra slow oscillation

The mechanisms underlying the ISO remain unknown. Here, I will review several possibilities and the arguments in support of or against each.

Three key observations are worthy of special mention. First, the ISO represents a very slow field potential variation. Unlike the δ/β ratio representing the power modulation ratio of brainwaves in the delta and beta bands, the ISO can be measured directly as a voltage fluctuation with the proper equipment. Second, ISOs are synchronized with the alternating sleep-states rhythm (δ/β ratio). This relationship remained when the ambient temperature was changed, although the phase delay changed (the time delay remained unchanged while the period of the rhythm decreased with increasing temperature) (figure 3.9). The sleep states and ISO may therefore be causally linked or be under the influence of the same source. Third, whereas the δ/β rhythm did not display a large phase gradient over space (< 1 sec for a period of ~120 sec over 400 µm in DVR) (figure 3.13), ISO appears to be a slow propagating wave. I did not carry out

measurements throughout the entire DVR; it is therefore unclear whether the propagation of the ISO is a local event restricted to the 1-2 mm sampled or whether it sweeps through the entire DVR.

These observations point out three essential components that any hypothesis aiming to explain the ISO during sleep needs. First, how ISO, a very slow, DC-like electric potential, is generated in the brain? Second, how are these two slow periodic activities, ISO and sleep-state alternation (δ/β ratio), connected to each other during sleep? Third, how does the ISO propagate when the state of sleep remains similar across DVR?

5.2.1) Ensemble activity and diffusing factors

Neuronal activity in the brain, such as ionic fluxes through channels in the excitable membrane and intrinsic membrane potential oscillations, gives rise to transmembrane currents. Collective current sinks and sources can superimpose at a given location and shape extracellular field potentials. When large numbers of neurons act synchronously, the magnitude of small extracellular fields adds up and becomes a detectable signal at a distance, e.g., as LFP or EEG. To contribute substantially to the LFP, resonant or correlated neuronal activity must happen in nearby neurons within a short time window. The short duration of an action potential, about 1 ms, makes it extremely hard to form synchronous activity. However, the long-lasting afterhyperpolarizing potential (AHP), caused by calcium influx (Helmchen et al., 1999) and calcium-activated potassium currents (Hotson and Prince, 1980; Sah and Louise Faber, 2002), contribute to the extracellular field potential (Buzsaki et al., 1988b). During sleep, AHPs are hypothetically involved in generating the slow rhythm (0.1-0.5 Hz) in the cerebral cortex that propagates within and across different layers (Sanchez-Vives and McCormick, 2000). The mechanism that generates delta waves, described before in section 1.3, also involves long-lasting hyperpolarizations. Moreover, ion channels with slow dynamics, such as slow inactivating Na^+ channels, have been reported from lobsters to mammals (Silva, 2014). We do not yet know the detailed electrophysiological properties of Pogona neurons, but our transcriptomic data provide a detailed description of the genes express (Tosches et al., 2018a). Although the period of the ISO is longer than that of other slow rhythms mentioned above, the ISO could result directly from synchronous up-down shifts of membrane voltage, as in other faster oscillations in the DVR.

The neuronal activity might directly generate the extracellular electric potential, but the previous example, such as delta wave, is not synchronized with sleep-state (δ/β ratio) alternation. To connect ISO and sleep-state alternation, the population activity of sleep regulation areas has to be state-dependent. Sleep regulation can be divided into two levels. First, the circadian clock and homeostatic pressure regulating the sleep-wake cycle. Second, the alternation between REM and SW. Since the power of ISO is stronger during sleep and weaker during awake states (figure 3.6), brain areas with significantly different activities between awake and sleep states are likely involved in ISO generation. Those areas include but are not limited to the sublaterodorsal nucleus (SLD), ventrolateral PAG (vlPAG), ventral medulla, LDT, pedunculopontine tegmental nuclei (PPT), LC, and dorsal raphe nucleus (Héricé et al., 2019). All neurons or sub-populations in these areas are exclusively active during REM (REM-on) or SW (REM-off) stages.

Two models, the reciprocal interaction (RI) and the mutual inhibition (MI) models, could bridge the substantial temporal gap between individual and ensemble activities (Héricé et al., 2019). The RI model is the predator-prey model frequently used to describe the dynamics of biological systems in which two species interact, one as a predator and the other as prey. In the model system, predators thrive when there are plentiful prey but, ultimately, outstrip their food supply and decline. As the predator population declines, the prey population increases again. These dynamics continue in a cycle of growth and decline in both populations, with a phase lag. During sleep, REM-off neurons (predators) activity gradually decays due to self-inhibition, which results in increased activity of REM-on neurons (prey). The first suggestion of this kind is the REM-on neurons in the gigantocellular tegmental field (FTG) in the pons interacting with REM-off neurons in LC (McCarley and Hobson, 1975).

The MI model (or flip-flop switch model) consists of mutual interactions between two components. When the activity increases in one component, it inhibits the other group. In this model, each inhibiting component stabilizes the system in a particular state through a self-reinforcing mechanism. Additional inputs to inhibitory components, such as circadian rhythm and/or homeostasis, play a key role in shifting the balance of mutual inhibition, that is, state change. This model was initially proposed for sleep-wake regulation (Saper et al., 2001) and extended to REM-SW regulation. The interactions between LDT/PPT and LC/RN (McCarley et al., 1995) or the vlPAG/lateral pontine tegmentum (LPT) and precoeruleus/SLD (Lu et al., 2006) belong to this model.

State-dependent neuronal population activity could hypothetically explain ISO generation and its synchrony to sleep states, but this hypothesis does not explain how the ISO propagates in DVR. However, the propagation speed suggests a slow-moving mechanism, e.g., extracellular factors diffusion. Inter-neuronal interactions are mainly mediated by chemical signals. Small-molecule neurotransmitters such as GABA and glutamate are responsible for fast, millisecond-scale on/off, interaction. Peptide transmitters are responsible for slow, typically seconds to minutes, but continuously variable in the brain (Salio et al., 2006). In sleep research, the hunt for sleep-inducing substrates, so-called 'hypnotoxin,' started as early as 1910 when Legendre and Piéron reported that transfusion of CSF from sleep-deprived dogs induced behavioral sleep in recipient dogs (Legendre, 1913). It led to discovering the delta sleep-inducing peptide (DSIP) (Graf and Kastin, 1984). When DSIP was infused into CSF, it increased the time of SW sleep and reduced the latency to the first SWS episode. No effect was observed for REM sleep (Drucker-Colin, 1973). Orexin/hypocretin, for another example, released by the lateral hypothalamus (LH), has been known to be crucial for sleep-wake regulation (Guillaumin and Burdakov, 2021) and stabilize REM sleep by activating the SLD network (Feng et al., 2020). Orexin-evoked postsynaptic depolarization can persist for seconds to minutes, presumably due to slow diffusion and breakdown, no known reuptake mechanisms, and the long half-lives of intracellular messengers generated by its downstream G-protein coupled receptors (GPCRs) (Schöne et al., 2014).

All together, the state-dependent ensemble activity of DVR neurons could hypothetically generate an ISO directly through extracellular ion imbalance or collective current sink and source; or indirectly through extracellular diffusing factors such as neuropeptides. It would explain why the ISO and δ/β ratio are synchronized with each other. The extracellular diffusing factors released by neurons would potentially propagate the ISO wave by changing neuron properties as it invades new territories.

This hypothesis shows some weaknesses when applied to the *ex vivo* recording. First, ISO exists during *ex vivo* recording with no states alternation (figure 4.2 C, 4.6 A). This contradicts the hypothesis that state-dependent ensemble activity initiates the ISO signal. *Ex vivo* LFP is concatenated by continuous SWRs generated in the claustrum without an apparent broadband activity (Norimoto et al., 2020). One possible explanation is that the mechanism silencing the claustrum during REM sleep does not function properly in the *ex vivo* setting. The sleep-states alternation, regardless of whether it exists or not, cannot be seen by measuring the power ratio between different frequency bands. The other explanation is that ISO is generated by the collective membrane properties change after a diffusing factor(s) reaches the recording area. As

long as the mechanism controlling a periodic release of diffusing factor(s) is intact, an ISO will occur in DVR. My *ex vivo* population firing rate recordings (figure 4.10 A-C) support the hypothesis of hidden states alternation. Second, the propagation speed of *ex vivo* ISO is slower than *in vivo* ISO. The speed should be similar in both recording settings if passive diffusion were the primary mechanism of ISO propagation. It is possible that an active mechanism present only in living animals, such as heartbeats or breathing, also contributes to the movement of extracellular factor(s). This idea can be linked to the hypothesis described in the next section.

5.2.2) Conductivity changes by waste clearance mechanism

ISO is an electric signal between an electrode and a reference wire. The extracellular space in the brain is filled with an electrically conducting solution composed of different ions, glucose, proteins, and metabolic waste. The conductivity (or its inverse, electrical resistivity) varies with the concentration of the electrolyte and the resulting movements of electronically charged particles. If the conductivity somehow changed in different sleep states, the LFP would change accordingly. Waste clearance mechanisms in the brain would thus offer a possibility to change the conductivity of the brain.

The brain parenchyma is bathed in interstitial fluid (ISF) that is a filtrate of plasma secreted at the blood-brain barrier. The ISF delivers oxygen and nutrients to neurons and acts as a vehicle for the rapid removal of metabolic wastes such as CO_2 and lactic acid. The CSF is mainly produced by choroid plexus epithelial cells located in each ventricle. It provides buoyancy and buffer against injury, maintains homeostasis of the central nervous system, and acts as a sink for the ISF. Part of the CSF is returned to the vascular system by entering the dural venous sinuses via arachnoid granulations. Some CSF enters the brain parenchyma via the periarterial spaces of the penetrating arteries. This part of CSF is important for the clearance of neurotoxic wastes such as albumin, amyloid beta (Aβ), and tau protein.

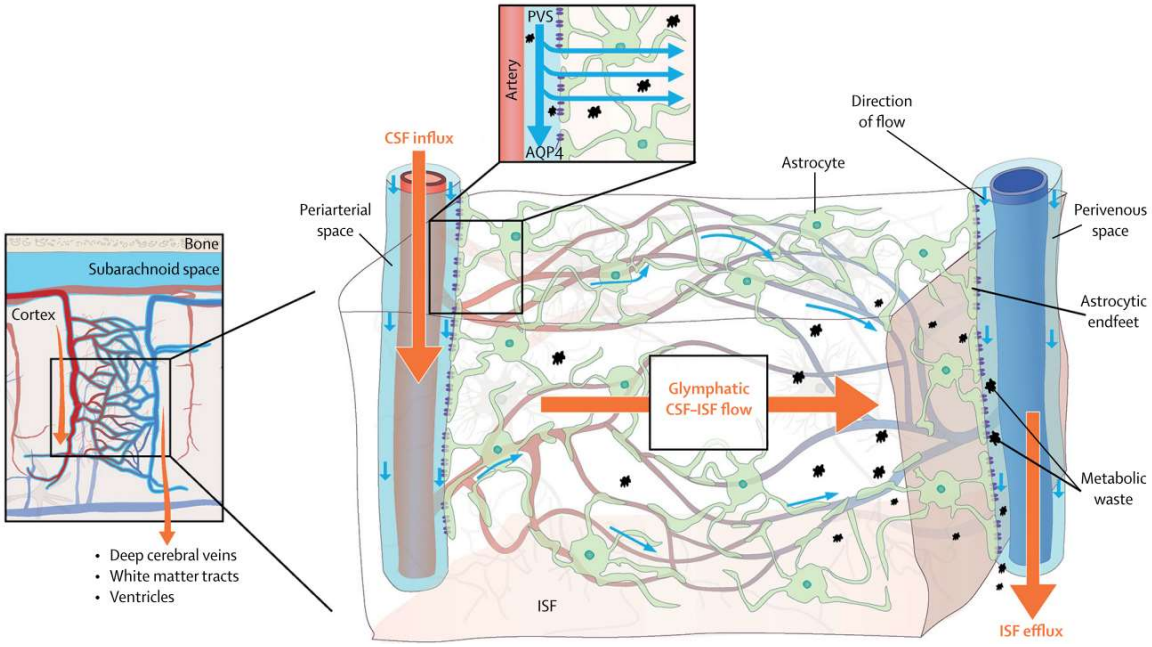

Figure 5.3: Schematic illustration of glymphatic pathway
The directional bulk flow of CSF-ISF mixture moves from penetrating arteries toward veins in the brain while carrying metabolic wastes. PVS=perivascular space. (figure from Rasmussen et al., 2018)

The glymphatic pathway is a fluid clearance pathway used to clear metabolic wastes in the central nervous system by CSF and ISF exchange (Kaur et al., 2021). According to this model, the CSF flows into the periarterial spaces. The periarterial spaces around penetrating arteries are bounded by the end-feet of astrocytes and the endothelium and smooth muscle of the vessel walls. Water and small molecular solutes enter the astrocytes through aquaporin (Aqp4) channels in the astrocyte end-feet membranes. From the astrocyte, the water and small molecular solutes are distributed to the ISF. The CSF-ISF mixture, along with the parenchymal solute, leaves the brain parenchyma through venous perivascular spaces. The drainage of CSF-ISF mixture carries with waste products of brain metabolism such as Aβ, soluble proteins, lipids, ions, and small molecules (Bacyinski et al., 2017). Glymphatic activity is high during natural sleep (Xie et al., 2013) and during the high delta power and low heart rate under ketamine/xylazine anesthesia (Hablitz et al., 2019). No study that I am aware of has directly measured glymphatic activity during the different stages of sleep. However, since the CSF influx into the periarterial space is the driving force of the glymphatic pathway, the CSF dynamic in different sleep states might shed light on the state-dependent glymphatic activity.

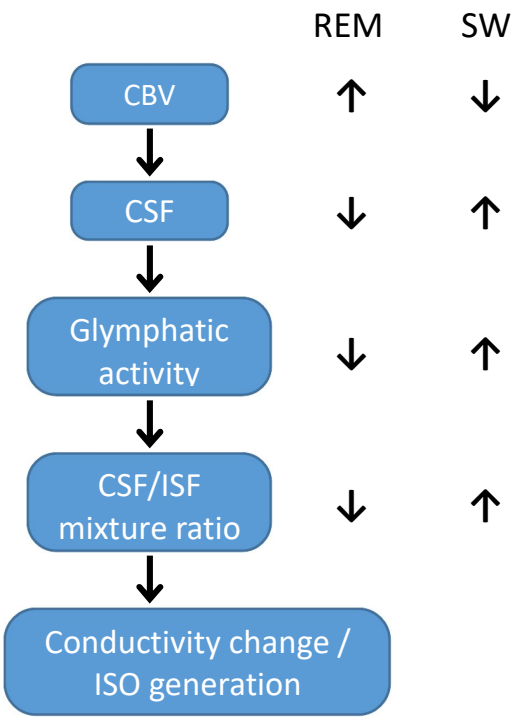

Figure 5.4: hypothetical model links sleep state alternation and ISO generation. Diagram of model linking the dynamic of CBV to the conductivity change that potentially generate ISO.

Monitoring CSF dynamics in brain parenchyma is not an easy task. Fultz et al. measured CSF flow by analyzing the signal intensity between the fresh CSF and the CSF that experienced multiple radiofrequency pulses. Together with EEG recording, they showed for the first time that human slow waves are coupled to and precede CSF oscillation (Fultz et al., 2019). One indirect method to detect CSF dynamics is to measure the cerebral blood volume (CBV). Because of constant intracranial volume, more CSF flows into the head when less volume is occupied by the blood (Piechnik et al., 2009; Scouten and Constable, 2008). During rodent REM sleep, the brain-wide CBV increases markedly compared to a quiet wake state (Bergel et al., 2018). In the somatosensory cortex, the CBV and arteriole diameter increase during REM sleep in comparison with SW sleep and awake (Turner et al., 2020), likely due to the neurovascular coupling (Drew et al., 2020).

Altogether, the EEG dynamics in different sleep states could be associated with CBV and CSF flow changes. The CSF dynamics would influence the glymphatic activity and potentially change tissue conductivity by changing the CSF and ISF's mixing ratio. The ISO signal could thereby be a secondary effect of different types of neuronal activity during the different states of sleep (figure 5.4).

The glymphatic pathway seems to happen within the brain parenchyma and fails to explain the ISO propagation. However, a larger scale waste clearance mechanism external to the brain parenchyma raises another possibility. It was generally believed that the central nervous system does not contain a lymphatic system and thus relies on alternative routes such as the glymphatic pathway to clear waste products. The presence of the meningeal lymphatic vessels was first mentioned by Paolo Mascagni at the end of the 18th century, re-introduced several times in the 1950s, 1960s, and 1990s, and finally been confirmed in 2015 by Louveau et al. (Louveau et al., 2015) and Aspelund et al. (Aspelund et al., 2015) (also see the review (Da

Mesquita et al., 2018)) (figure 5.5). They demonstrated that the meningeal lymphatic vessels can carry fluid and immune cells to the deep cervical lymph nodes (dCLNs) and may help clean interstitial wastes and CSF/ISF from the brain parenchyma after they travel through the glymphatic pathway. A similar CSF/ISF clearance mechanism was also found along cranial and spinal nerves (Fahmy et al., 2021; Ma et al., 2017).

As mentioned in section 5.2, it is unclear whether the propagation of the ISO is a local event restricted to the 1-2 mm sampled, or it whether sweeps through the entire DVR. If the CSF/ISF has to travel a long distance from arteries to external lymphatic vessels and leave the parenchyma, the moving direction of ISO will converge from arteries to major lymphatic vessels. With my current data, I am unfortunately not able to detect the propagating direction of ISO in the entire hemisphere.

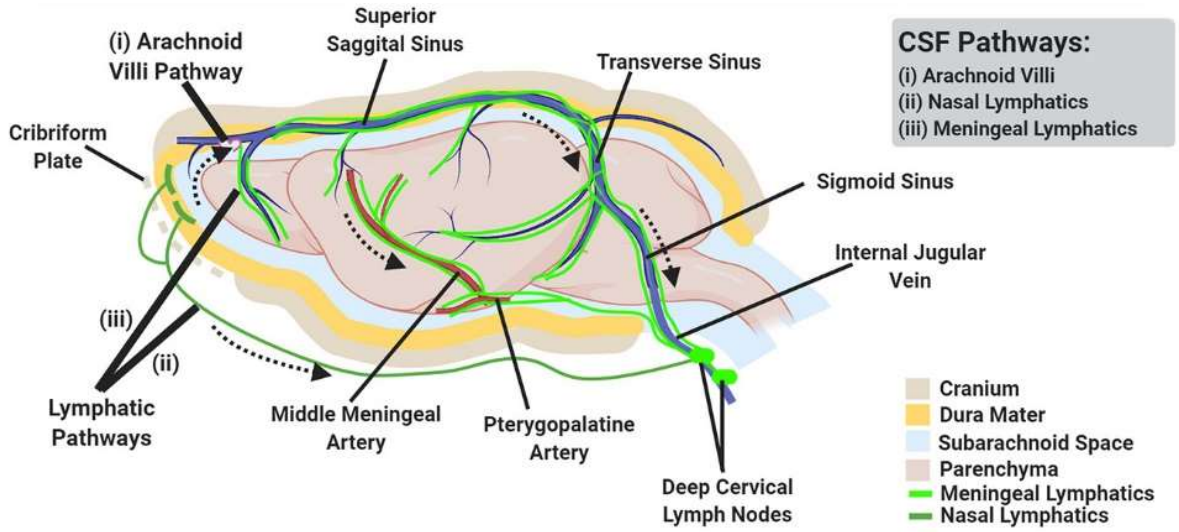

Figure 5.5: Waste clearance external to the brain parenchyma
Schematic of the CSF pathway involved in brain waste clearance, including 1) the arachnoid villi, 2) the nasal lymphatics, and 3) the meningeal lymphatics. (figure from Kaur et al., 2021)

In summary, the state-dependent dynamics of CBV and CSF could potentially change the mixture ratio of CSF and ISF through the glymphatic pathway. This would lead to conductivity changes in different states of sleep, thus recorded as ISO in DVR. The waste clearance mechanism involving removal of CSF/ISF may also travel from arteries to meningeal lymphatics and would be recorded as a slow propagating potential in DVR.

I will now try to apply the waste clearance hypothesis of an induced ISO to my *ex vivo* data. CSF is generated as plasma filtered from the blood through epithelial cells in each ventricle. Despite the absence of blood pressure to push the blood through epithelial cells, they can still actively

transport substances into ventricles in an isolated brain. The loss of blood pressure might slow down or reduce the amount of CSF generation but not necessarily stop it. In an isolated brain, the ventricle and the circulation system in the brain are mostly intact. CSF and Ringer's solution can still enter the brain as in *in vivo* recordings. Less CSF entering the parenchyma would slow down the bulk flow of CSF-ISF. This would potentially explain why the propagation speed of ISO is significantly different between *ex vivo* and *in vivo* recordings. However, similar to the previous section (5.2.1), the CBV and CSF dynamics correlate with the sleep-states alternation. This theory will not stand when there is no states alternation in *ex vivo* settings.

5.2.3) Potential change induced by intracranial pressure

The CBV and CSF circulatory dynamics provide another potential mechanism of ISO generation related to the intracranial pressure (ICP) and Cushing reflex. However, this mechanism cannot explain the slow propagation of, and the *ex vivo* ISO. Whether ICP fluctuation can work together with other mechanisms mentioned above is unknown. Even so, it still offers an unconventional idea for ISO generation.

In 1960, Lundberg identified spontaneous rhythmic oscillations of ICP that last 5-20 minutes (plateau or A wave) or 0.5-2 minutes (B wave) in human patients with severe acute traumatic brain injury (Lundberg, 1960). Rosner hypothesized a similar mechanism of both waves using the so-called "vasodilatory cascade model" (El-Adawy and Rosner, 1989; Rosner, 1986). This model introduces a simple feedback loop between ICP, arterial blood pressure (ABP), and cerebral perfusion pressure (CPP). Based on the Monro-Kellie hypothesis, the cranial compartment is inelastic and the volume inside the cranium is fixed. The cranium and its constituents (blood, CSF, and brain) create a state of volume equilibrium, such that any increase in one should cause a decrease in one or both of the remaining two (Mokri, 2001). In the brain, the relationship between pressure of different fluids in the cranium can be simplified to an equation: CPP = ABP-ICP.

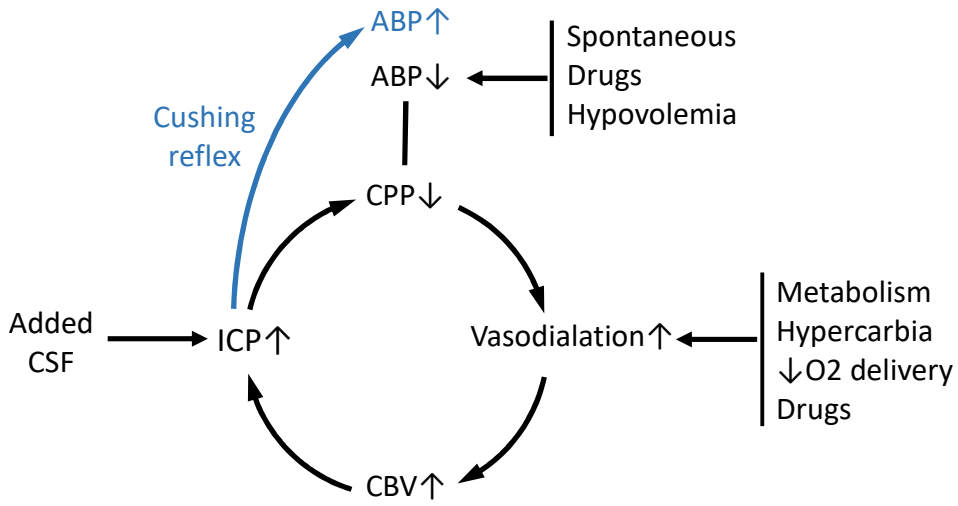

Figure 5.6: Rosner's model of intracranial wave
Schematic of the ICP wave occurrence based on the vasodilatory cascade. The Crushing reflex is the key to terminate the ABP reduction. (Figure modified from (Rosner, 1986)).

In normal conditions, the CPP is fairly constant. Rosner's hypothesis (figure 5.6) starts from a spontaneous drop in ABP that causes a reduction in CPP. The CPP reduction can cause brain ischemia and lead to the activation of the sympathetic system. It then elevates blood pressure and causes vasodilation to restore blood flow to the ischemic brain when cerebral autoregulation is intact. Vasodilation then results in an increase in CBV and a rise in ICP. The Cushing reflex, i.e., an increase in ABP in response to high ICP, brings the ABP back up and terminates the pressure wave. The CPP then back to the level before the spontaneous drop in ABP. Although ICP waves were recorded in patients with brain injury, they might also appear in normal conditions. In healthy macaque monkeys, the ICP increases during REM sleep and lasts ~7 minutes while the blood pressure decreases. Monkey ICP waves apparently resemble the plateau wave described by Lundberg (Gücer and Viernstein, 1979).

Two previous reports provide a potential link between ICP waves and ISO generation. ISO is an extracellular field potential that relies on a resistance/impedance change over time and a current source. Simultaneous recording of ICP and subdural impedance during sleep show that the fluctuation of impedance follows the dynamics of ICP. The ICP changes lead to the impedance change by minutes (Cooper and Hulme, 1966). Measurement of the electrical potential difference between blood and CSF has been done in different animals. The potential, CSF positive to blood, probably derives from ion transport across the blood-brain barrier. The spontaneously change mainly due to dynamics of pH and K^+ ion concentration in the blood and

CSF (Held et al., 1964; Sørensen et al., 1978; Voipio et al., 2003). In cats and humans, changes in the breathing pattern and CO2 content in the air lead to the change of blood pH and CSF-blood potential (Nita et al., 2004; Sørensen et al., 1978). Pogona does not show significant differences in breathing rate across different sleep states. However, the neuronal ensemble activity can change the K^+ concentration in the CSF. Whether it is enough to change the CSF-blood potential and generate ISO is unknown.

The dynamics of blood pressure are related to sleep states. In normal human subjects and cats, the sympathetic-nerve activity, heart rate, and blood pressure declined significantly during deep SW sleep. During REM sleep, heart rate and blood pressure return to those recorded during wakefulness (Sei et al., 1994; Somers et al., 1993). These changes were not observed in the wild-type rats (Perry et al., 2011) but in homozygous and heterozygous adenosine A_{2A}-receptor (A2AR) knockout mice (Sakata et al., 2005). I do not know whether the blood pressure of Pogona is sleep-states dependent. If so, the spontaneous drop in ABP that initiates Rosner's model of intracranial wave could be linked to the change of sleep states.

5.3) Prediction and suggestion for future studies

The previous section listed several possible mechanisms, including neuron population interaction, extracellular factors diffusion, the interaction between vasodynamic and ICP, and blood pH/K^+ level fluctuations. Each can generate ISO independently. It is very likely that multiple mechanisms act together in the brain. There are three studies I would suggest to help understand the ISO better. I will discuss their potentials and limitations below.

5.3.1) Source localization with the 3D electrode array

One very useful piece of information would be the source location of the ISO. From the results of large-scale single-cell sequencing, the lizard forebrain can be sub-divided into multiple regions by their gene expressing profiles (Tosches et al., 2018b). If one can pinpoint the source location, properties of local neurons and connectomics could hint at the potential mechanism of ISO generation. My data indicates that the source is located in an area posterior and dorsal to the recording sites. However, it is far away from the precision needed.

The most straightforward method would be to implant a large 3D electrode array into the brain and record EEG from the whole brain during sleep. Newly developed high-density probes make

it possible to do so (Jun et al., 2017b; Putzeys et al., 2019b; Steinmetz et al., 2020). However, CMOS-based recording systems all have built-in high pass filters with a frequency of ~0.5 Hz. The ISO with a frequency of 5 to 20 mHz was removed by the filter (personal experience). The traditional silicon probe with iridium oxide electrodes and PEDOT plating or silver chloride are better choices. Extensive coverage could be achieved by using a customized 3D array with lower spatial resolution. The source location of ISO can be estimated by applying an inverse solution (estimating the current density or activity values of the source that generated a measured electric potential) developed for EEG and ECoG analysis, such as eLORETA (Pascual-Marqui, 2007), wMNE (Iwaki and Ueno, 1998) and dSPM (Dale et al., 2000). The physical location of each electrode can be accessed by using microCT or microlesion post-mortem. Putting the estimated location onto a 3D model brain would allow one to narrow down the source of ISO. A lesion or optogenetic manipulation experiment could further confirm the estimated result.

The lack of knowledge about detailed brain anatomy and of systematic measurement of the brain's electrical properties make it difficult to estimate source location precisely. One has to assume a constant conductivity of the brain. However, a brain is generally both inhomogeneous and anisotropic. This significantly reduces accuracy of source localization. Another problem comes from the inverse solution itself. A very large number of source functions will yield the same potential distribution. Any inverse solution must in part depend on additional independent information obtained from different methods, such as MRI or positron emission tomography (PET), or on presumptive solution constraints, such as limiting the number of discrete locations (Nunez et al., 2019).

5.3.2) Microdialysis

Extracellular diffusing factors, such as neuropeptides or gradients of ion concentration, are possible factors for ISO generation and propagation. There are various methods to detect the dynamics of known extracellular factors. Genetically encoded fluorescent biosensors are available to detect neurotransmitters and neuromodulators such as dopamine, norepinephrine, glutamate, acetylcholine, and GABA (Jing et al., 2019; Wang et al., 2018). Fast-scan cyclic voltammetry-based methods have been successfully used to detect electrochemically active biogenic amines such as dopamine, epinephrine, norepinephrine, and 5-HT (Wightman, 2006). Similar electrochemical methods, together with specialized microelectrodes, are able to detect the pH, O_2, NO, glutamate, glucose, and many other substances (Borland and Michael, 2007).

Chemical dyes or nanosensors allow us to specifically detect extracellular ion concentrations (Chang et al., 2012; Liu et al., 2020; Maysinger et al., 2015).

However, the mechanism of ISO generation is yet unknown. Microdialysis, in this case, might be better suited for finding an unknown candidate. Microdialysis collects solution and small-size molecules from the extracellular fluid. Substances diffuse inversely along the concentration gradient through a semipermeable membrane at the tip of the microdialysis probe. The sample is then carried by continuous flow of the perfusate in the dialysis tube. The content and concentration of various substances in the collected dialysis fluid are then analyzed by external testing equipment, such as mass spectrometry and high-performance liquid chromatography.

There are multiple drawbacks to this method. Microdialysis has a low temporal and spatial resolution compared to electrochemical or fluorescence-based biosensors. The temporal resolution is determined by the length of the sampling intervals (usually a few minutes), but the sleep state alternation happens every 1-3 minutes in Pogona. The collection rate of diffusing factors would be too low. A tiny sample size makes online monitoring very challenging. The spatial resolution is determined by the membrane length and diameter of the probe. The size of commercially available probes for small animals is 200-500 µm (diameter) by 0.5-4 mm (membrane length) (Harvard Bioscience Inc. and Amuza Inc.). From the propagation speed, the ISO needs ~11 seconds to travel this distance. The time given to collect diffusate is thus even shorter than given above.

The technical difficulties can be solved. Since the sleep pattern is stable and repetitive, it can be monitored by a probe implanted in close proximity. Viewing ISO online can be achieved by improving the recording software. The necessary volume can be collected by pooling the fluid from the same state of sleep or ISO. Microdialysis can provide useful information for future experiments.

5.3.3) Imaging the vasomotion and detecting non-neuronal factors

ISO generation could result from non-neuronal factors such as glymphatic pathway, ICP, pH, and conductivity dynamics. Many state-of-the-art devices and materials allow us to monitor them altogether during *in vivo* recording.

The two-photon microscope is the most common method used to image blood vessels and hemodynamics. However, the animal has to be head-fixed during imaging. From my previous experience, it is not possible to head-fix a lizard. A lizard can hurt itself badly when struggling on

a head-fixing device. Recording from the freely moving animal with an implantable miniaturized microscope and electrophysiological recording is the only option with the technology currently available. In 2019, Janaka Senarathna et al. published a miniature multi-contrast microscope that can image the hemodynamics in freely moving rodents. The spatial resolution with a high-magnification adapter can reach 0.5 μm with a frame rate of 15 Hz (Senarathna et al., 2019). In mice, the arterioles' diameter, compared with the awake resting state, increases by 5-10 μm during different sleep states (Turner et al., 2020). The change is significant enough to be detected by the implantable microscope.

The same device can simultaneously detect hemodynamics and other fluorescence signals. The concentration of oxy- and deoxy-hemoglobin can be estimated by reflectance images illuminated by LED with different wavelengths (Lin et al., 2013). The extracellular ion concentration can be imaged via fluorescent indicators. Other physiological signals such as pH, ICP, and conductivity can easily be monitored by connecting their sensors to a potentiometer. With broadband EEG recordings, one can see the sleep state, ISO, vasodyniamics, cerebral blood flow, and extracellular ion concentration fluctuation simultaneously. The results might provide useful information on the mechanism underlying ISOs.

Reference

Achermann, P., and Borbély, A.A. (1997). Low-frequency (< 1 Hz) oscillations in the human sleep electroencephalogram. Neuroscience *81*, 213–222.

Akaike, T. (1982). Periodic bursting activities of locus coeruleus neurons in the rat. Brain Research *239*, 629–633.

Aladjalova, N.A. (1957). Infra-Slow Rhythmic Oscillations of The Steady Potential of the Cerebral Cortex. Nature *179*, 957.

Aladjalova, N.A. (1964). Progress in brain research. (Amsterdam; New York: Elsevier).

Albrecht, D., and Gabriel, S. (1994). Very slow oscillations of activity in geniculate neurones of urethane-anaesthetized rats: NeuroReport *5*, 1909–1912.

Albrecht, D., Royl, G., and Kaneoke, Y. (1998). Very slow oscillatory activities in lateral geniculate neurons of freely moving and anesthetized rats. Neuroscience Research *32*, 209–220.

Allison, T., and Goff, W. (1968). Sleep in a primitive mammal, the spiny anteater. Psychophysiology *5*, 200–201.

Allison, T., Van Twyver, H., and Goff, W.R. (1972). Electrophysiological studies of the echidna, Tachyglossus aculeatus. I. Waking and sleep. Arch Ital Biol *110*, 145–184.

Amzica, F., and Steriade, M. (1997). The K-complex: Its slow (<1-Hz) rhythmicity and relation to delta waves. Neurology *49*, 952–959.

Amzica, F., and Steriade, M. (1998). Electrophysiological correlates of sleep delta waves1Correspondence and reprint requests may be addressed to either author.1. Electroencephalography and Clinical Neurophysiology *107*, 69–83.

Andersen, P., Johansen, K., and Krog, J. (1960). Electroencephalogram during arousal from hibernation in the birchmouse. American Journal of Physiology-Legacy Content *199*, 535–538.

Aserinsky, E. (1996). The discovery of REM sleep. J Hist Neurosci *5*, 213–227.

Aserinsky, E., and Kleitman, N. (1953). Regularly occurring periods of eye motility, and concomitant phenomena, during sleep. Science *118*, 273–274.

Aspelund, A., Antila, S., Proulx, S.T., Karlsen, T.V., Karaman, S., Detmar, M., Wiig, H., and Alitalo, K. (2015). A dural lymphatic vascular system that drains brain interstitial fluid and macromolecules. Journal of Experimental Medicine *212*, 991–999.

Astic, L., Sastre, J.-P., and Brandon, A.-M. (1973). Etude polygraphique des etats de vigilance chez le foetus de Cobaye. Physiology & Behavior *11*, 647–654.

Ayala-Guerrero, F., and Huitrón-Reséndiz, S. (1991). Sleep patterns in the lizard Ctenosaura pectinata. Physiology & Behavior *49*, 1305–1307.

Ayala-Guerrero, F., and Mexicano, G. (2008). Sleep and wakefulness in the green iguanid lizard (Iguana iguana). Comparative Biochemistry and Physiology Part A: Molecular & Integrative Physiology *151*, 305–312.

Babiloni, C., Barry, R.J., Başar, E., Blinowska, K.J., Cichocki, A., Drinkenburg, W.H.I.M., Klimesch, W., Knight, R.T., Lopes da Silva, F., Nunez, P., et al. (2020). International Federation of Clinical Neurophysiology (IFCN) – EEG research workgroup: Recommendations on frequency and topographic analysis of resting state EEG rhythms. Part 1: Applications in clinical research studies. Clinical Neurophysiology *131*, 285–307.

Bacyinski, A., Xu, M., Wang, W., and Hu, J. (2017). The Paravascular Pathway for Brain Waste Clearance: Current Understanding, Significance and Controversy. Front. Neuroanat. *11*.

Baker, S.N. (2007). Oscillatory interactions between sensorimotor cortex and the periphery. Curr Opin Neurobiol *17*, 649–655.

Bauer, H., Korunka, C., and Leodolter, M. (1989). Technical requirements for high-quality scalp DC recordings. Electroencephalography and Clinical Neurophysiology *72*, 545–547.

Bergel, A., Deffieux, T., Demené, C., Tanter, M., and Cohen, I. (2018). Local hippocampal fast gamma rhythms precede brain-wide hyperemic patterns during spontaneous rodent REM sleep. Nat Commun *9*, 1–12.

Berger, H. (1929). Über das Elektrenkephalogramm des Menschen. Archiv f. Psychiatrie *87*, 527–570.

Berger, R.J., and Phillips, N.H. (1995). Energy conservation and sleep. Behavioural Brain Research *69*, 65–73.

Biswal, B., Yetkin, F.Z., Haughton, V.M., and Hyde, J.S. (1995). Functional connectivity in the motor cortex of resting human brain using echo-planar MRI. Magn Reson Med *34*, 537–541.

Blake, H., and Gerard, R.W. (1937). BRAIN POTENTIALS DURING SLEEP. American Journal of Physiology-Legacy Content *119*, 692–703.

Blumberg, M.S., Lesku, J.A., Libourel, P.-A., Schmidt, M.H., and Rattenborg, N.C. (2020). What Is REM Sleep? Current Biology *30*, R38–R49.

Borland, L.M., and Michael, A.C. (2007). An Introduction to Electrochemical Methods in Neuroscience. In Electrochemical Methods for Neuroscience, A.C. Michael, and L.M. Borland, eds. (Boca Raton (FL): CRC Press/Taylor & Francis), p.

Buschman, T.J., and Miller, E.K. (2007). Top-Down Versus Bottom-Up Control of Attention in the Prefrontal and Posterior Parietal Cortices. Science *315*, 1860–1862.

Butler, A.B. (1980). Cytoarchitectonic and Connectional Organization of the Lacertilian Telencephalon with Comments on Vertebrate Forebrain Evolution. In Comparative Neurology of the Telencephalon, S.O.E. Ebbesson, ed. (Boston, MA: Springer US), pp. 297–329.

Buzsaki, G. (2011). Hippocampus. Scholarpedia *6*, 1468.

Buzsáki, G. (2015). Hippocampal sharp wave-ripple: A cognitive biomarker for episodic memory and planning. Hippocampus *25*, 1073–1188.

Buzsáki, G., and Draguhn, A. (2004). Neuronal Oscillations in Cortical Networks. Science *304*, 1926–1929.

Buzsaki, G., Bickford, R.G., Ponomareff, G., Thal, L.J., Mandel, R., and Gage, F.H. (1988a). Nucleus basalis and thalamic control of neocortical activity in the freely moving rat. J. Neurosci. *8*, 4007–4026.

Buzsaki, G., Bickford, R.G., Ponomareff, G., Thal, L.J., Mandel, R., and Gage, F.H. (1988b). Nucleus basalis and thalamic control of neocortical activity in the freely moving rat. J. Neurosci. *8*, 4007–4026.

Chang, K.-S., Sun, C.-J., Chiang, P.-L., Chou, A.-C., Lin, M.-C., Liang, C., Hung, H.-H., Yeh, Y.-H., Chen, C.-D., Pan, C.-Y., et al. (2012). Monitoring extracellular K+ flux with a valinomycin-coated silicon nanowire field-effect transistor. Biosensors and Bioelectronics *31*, 137–143.

Coenen, A., Fine, E., and Zayachkivska, O. (2014). Adolf Beck: A Forgotten Pioneer in Electroencephalography. Journal of the History of the Neurosciences *23*, 276–286.

Connors, B.W., and Kriegstein, A.R. (1986). Cellular physiology of the turtle visual cortex: distinctive properties of pyramidal and stellate neurons. J Neurosci *6*, 164–177.

Cooper, R., and Hulme, A. (1966). Intracranial pressure and related phenomena during sleep1. J Neurol Neurosurg Psychiatry *29*, 564–570.

Corner, M.A. (1977). Sleep and the beginnings of behavior in the Animal Kingdom—Studies of Ultradian motility cycles in early life. Progress in Neurobiology *8*, 279–295.

Csicsvari, J., Hirase, H., Czurkó, A., Mamiya, A., and Buzsáki, G. (1999). Oscillatory Coupling of Hippocampal Pyramidal Cells and Interneurons in the Behaving Rat. J. Neurosci. *19*, 274–287.

Curio, G., Mackert, B.-M., Burghoff, M., Koetitz, R., Abraham-Fuchs, K., and Härer, W. (1994). Localization of evoked neuromagnetic 600 Hz activity in the cerebral somatosensory system. Electroencephalography and Clinical Neurophysiology *91*, 483–487.

Da Mesquita, S., Fu, Z., and Kipnis, J. (2018). The meningeal lymphatic system: a new player in neurophysiology. Neuron *100*, 375–388.

Dale, A.M., Liu, A.K., Fischl, B.R., Buckner, R.L., Belliveau, J.W., Lewine, J.D., and Halgren, E. (2000). Dynamic Statistical Parametric Mapping: Combining fMRI and MEG for High-Resolution Imaging of Cortical Activity. Neuron *26*, 55–67.

Dantzler, W. (1969). Effects of K, Na, and ouabain on urate and PAH uptake by snake and chicken kidney slices. American Journal of Physiology-Legacy Content *217*, 1510–1519.

Dash, M.B., Ajayi, S., Folsom, L., Gold, P.E., and Korol, D.L. (2018). Spontaneous Infraslow Fluctuations Modulate Hippocampal EPSP-PS Coupling. ENeuro *5*.

De Luca, M., Beckmann, C.F., De Stefano, N., Matthews, P.M., and Smith, S.M. (2006). fMRI resting state networks define distinct modes of long-distance interactions in the human brain. NeuroImage *29*, 1359–1367.

De Vera, L., González, J., and Rial, R.V. (1994). Reptilian waking EEG: slow waves, spindles and evoked potentials. Electroencephalography and Clinical Neurophysiology *90*, 298–303.

Dement, W. (1958). The occurrence of low voltage, fast, electroencephalogram patterns during behavioral sleep in the cat. Electroencephalogr Clin Neurophysiol *10*, 291–296.

Dietsch, G. (1932). Fourier-Analyse von Elektrencephalogrammen des Menschen. Pflügers Arch. *230*, 106–112.

Donner, T.H., Siegel, M., Fries, P., and Engel, A.K. (2009). Buildup of Choice-Predictive Activity in Human Motor Cortex during Perceptual Decision Making. Current Biology *19*, 1581–1585.

Drew, P.J., Duyn, J.H., Golanov, E., and Kleinfeld, D. (2008). Finding coherence in spontaneous oscillations. Nat Neurosci *11*, 991–993.

Drew, P.J., Mateo, C., Turner, K.L., Yu, X., and Kleinfeld, D. (2020). Ultra-slow Oscillations in fMRI and Resting-State Connectivity: Neuronal and Vascular Contributions and Technical Confounds. Neuron *107*, 782–804.

Drucker-Colin, R.R. (1973). Crossed perfusion of a sleep inducing brain tissue substance in conscious cats. Brain Research *56*, 123–134.

El-Adawy, Y., and Rosner, M.J. (1989). Vasodilatory Cascade: ICP Response to CPP Level and Reduction Rate. In Intracranial Pressure VII, J.T. Hoff, and A.L. Betz, eds. (Berlin, Heidelberg: Springer), pp. 842–844.

Elbert, T. (1993). Slow Cortical Potentials Reflect the Regulation of Cortical Excitability. In Slow Potential Changes in the Human Brain, W.C. McCallum, and S.H. Curry, eds. (Boston, MA: Springer US), pp. 235–251.

Engel, A.K., and Fries, P. (2010). Beta-band oscillations—signalling the status quo? Current Opinion in Neurobiology *20*, 156–165.

Fahmy, L.M., Chen, Y., Xuan, S., Haacke, E.M., Hu, J., and Jiang, Q. (2021). All Central Nervous System Neuro- and Vascular-Communication Channels Are Surrounded With Cerebrospinal Fluid. Front Neurol *12*, 614636.

Feng, H., Wen, S.-Y., Qiao, Q.-C., Pang, Y.-J., Wang, S.-Y., Li, H.-Y., Cai, J., Zhang, K.-X., Chen, J., Hu, Z.-A., et al. (2020). Orexin signaling modulates synchronized excitation in the sublaterodorsal tegmental nucleus to stabilize REM sleep. Nat Commun *11*, 3661.

Ferguson, J.E., Boldt, C., and Redish, A.D. (2009). Creating low-impedance tetrodes by electroplating with additives. Sensors and Actuators A: Physical *156*, 388–393.

Filippov, I.V., and Frolov, V.A. (2004). Very slow potentials in the lateral geniculate complex and primary visual cortex during different illumination changes in freely moving rats. Neuroscience Letters *373*, 51–56.

Filippov, I.V., Williams, W.C., and Frolov, V.A. (2004). Very slow potential oscillations in locus coeruleus and dorsal raphe nucleus under different illumination in freely moving rats. Neuroscience Letters *363*, 89–93.

Fox, M.D., and Raichle, M.E. (2007). Spontaneous fluctuations in brain activity observed with functional magnetic resonance imaging. Nat Rev Neurosci *8*, 700–711.

Frank, M.G., and Heller, H.C. (2019). The Function(s) of Sleep. In Sleep-Wake Neurobiology and Pharmacology, H.-P. Landolt, and D.-J. Dijk, eds. (Cham: Springer International Publishing), pp. 3–34.

Fuentealba, P., and Steriade, M. (2005). The reticular nucleus revisited: Intrinsic and network properties of a thalamic pacemaker. Progress in Neurobiology *75*, 125–141.

Fultz, N.E., Bonmassar, G., Setsompop, K., Stickgold, R.A., Rosen, B.R., Polimeni, J.R., and Lewis, L.D. (2019). Coupled electrophysiological, hemodynamic, and cerebrospinal fluid oscillations in human sleep. Science *366*, 628–631.

Gaffey, C.T., and Mullins, L.J. (1958). Ion fluxes during the action potential in Chara. The Journal of Physiology *144*, 505–524.

Girardeau, G., Benchenane, K., Wiener, S.I., Buzsáki, G., and Zugaro, M.B. (2009). Selective suppression of hippocampal ripples impairs spatial memory. Nature Neuroscience *12*, 1222–1223.

Graf, M.V., and Kastin, A.J. (1984). Delta-sleep-inducing peptide (DSIP): A review. Neuroscience & Biobehavioral Reviews *8*, 83–93.

Green, J.D., Maxwell, D.S., Schindler, W.J., and Stumpf, C. (1960). Rabbit eeg "theta" rhythm: its anatomical source and relation to activity in single neurons. Journal of Neurophysiology *23*, 403–420.

Greicius, M.D., Krasnow, B., Reiss, A.L., and Menon, V. (2003). Functional connectivity in the resting brain: A network analysis of the default mode hypothesis. PNAS *100*, 253–258.

Grooms, J.K., Thompson, G.J., Pan, W.-J., Billings, J., Schumacher, E.H., Epstein, C.M., and Keilholz, S.D. (2017). Infraslow Electroencephalographic and Dynamic Resting State Network Activity. Brain Connectivity *7*, 265–280.

Gücer, G., and Viernstein, L.J. (1979). Intracranial pressure in the normal monkey while awake and asleep. Journal of Neurosurgery *51*, 206–210.

Guillaumin, M.C.C., and Burdakov, D. (2021). Neuropeptides as Primary Mediators of Brain Circuit Connectivity. Frontiers in Neuroscience *15*, 229.

Guthrie, P.B., Knappenberger, J., Segal, M., Bennett, M.V.L., Charles, A.C., and Kater, S.B. (1999). ATP Released from Astrocytes Mediates Glial Calcium Waves. J. Neurosci. *19*, 520–528.

Hablitz, L.M., Vinitsky, H.S., Sun, Q., Stæger, F.F., Sigurdsson, B., Mortensen, K.N., Lilius, T.O., and Nedergaard, M. (2019). Increased glymphatic influx is correlated with high EEG delta power and low heart rate in mice under anesthesia. Science Advances *5*, eaav5447.

He, J. (2003). Slow oscillation in non-lemniscal auditory thalamus. J Neurosci *23*, 8281–8290.

Held, D., Fencl, V., and Pappenheimer, J.R. (1964). ELECTRICAL POTENTIAL OF CEREBROSPINAL FLUID. Journal of Neurophysiology *27*, 942–959.

Helmchen, F., Svoboda, K., Denk, W., and Tank, D.W. (1999). In vivo dendritic calcium dynamics in deep-layer cortical pyramidal neurons. Nat Neurosci *2*, 989–996.

Helps, S.K., Broyd, S.J., James, C.J., Karl, A., Chen, W., and Sonuga-Barke, E.J.S. (2010). Altered spontaneous low frequency brain activity in Attention Deficit/Hyperactivity Disorder. Brain Research *1322*, 134–143.

Héricé, C., Patel, A.A., and Sakata, S. (2019). Circuit mechanisms and computational models of REM sleep. Neuroscience Research *140*, 77–92.

Hobson, J.A. (2005). Sleep is of the brain, by the brain and for the brain. Nature *437*, 1254–1256.

Hoops, D. (2015). A perfusion protocol for lizards, including a method for brain removal. MethodsX *2*, 165–173.

Hotson, J.R., and Prince, D.A. (1980). A calcium-activated hyperpolarization follows repetitive firing in hippocampal neurons. Journal of Neurophysiology *43*, 409–419.

Huntley, A.C. (1987). Electrophysiological and behavioral correlates of sleep in the desert iguana, Dipsosaurus dorsalis hallowell. Comparative Biochemistry and Physiology Part A: Physiology *86*, 325–330.

Hutchison, W.D., Dostrovsky, J.O., Walters, J.R., Courtemanche, R., Boraud, T., Goldberg, J., and Brown, P. (2004). Neuronal Oscillations in the Basal Ganglia and Movement Disorders: Evidence from Whole Animal and Human Recordings. J. Neurosci. *24*, 9240–9243.

Iber, C., Sonia, A.-I., Chesson, A.L., Quan, S.F., and American Academy of Sleep Medicine. (2007). The AASM manual for the scoring of sleep and associated events : rules, terminology and technical specifications (Westchester, IL: American Academy of Sleep Medicine).

IFSECN (1974). International federation of societies for electroencephalography and clinical neurophysiology. Electroencephalography and Clinical Neurophysiology *37*, 521.

Iwaki, S., and Ueno, S. (1998). Weighted minimum-norm source estimation of magnetoencephalography utilizing the temporal information of the measured data. Journal of Applied Physics *83*, 6441–6443.

Jackson, N., and Muthuswamy, J. (2008). Artificial dural sealant that allows multiple penetrations of implantable brain probes. J. Neurosci. Methods *171*, 147–152.

Jessen, N.A., Munk, A.S.F., Lundgaard, I., and Nedergaard, M. (2015). The Glymphatic System – A Beginner's Guide. Neurochem Res *40*, 2583–2599.

Jing, M., Zhang, Y., Wang, H., and Li, Y. (2019). G-protein-coupled receptor-based sensors for imaging neurochemicals with high sensitivity and specificity. J Neurochem *151*, 279–288.

Johnson, B.R., Wyttenbach, R.A., Wayne, R., and Hoy, R.R. (2002). Action Potentials in a Giant Algal Cell: A Comparative Approach to Mechanisms and Evolution of Excitability. J Undergrad Neurosci Educ *1*, A23–A27.

Jouvet, M. (1962). Research on the neural structures and responsible mechanisms in different phases of physiological sleep. Arch Ital Biol *100*, 125–206.

Jouvet, M. (1965). PARADOXICAL SLEEP--A STUDY OF ITS NATURE AND MECHANISMS. Prog Brain Res *18*, 20–62.

Jouvet, M. (1967). Neurophysiology of the states of sleep. Physiological Reviews *47*, 117–177.

Jouvet, M., and Klein, M. (1964). Analyse polygraphique du sommeil de la tortue. CR Acad. Sci.(Paris) *258*, 2175–2178.

Jouvet, M., Michel, F., and Courjon, J. (1959). On a stage of rapid cerebral electrical activity in the course of physiological sleep. C R Seances Soc Biol Fil *153*, 1024–1028.

Juavinett, A.L., Bekheet, G., and Churchland, A.K. (2019). Chronically implanted Neuropixels probes enable high-yield recordings in freely moving mice. ELife *8*, e47188.

Jun, J.J., Mitelut, C., Lai, C., Gratiy, S.L., Anastassiou, C.A., and Harris, T.D. (2017a). Real-time spike sorting platform for high-density extracellular probes with ground-truth validation and drift correction. BioRxiv 101030.

Jun, J.J., Steinmetz, N.A., Siegle, J.H., Denman, D.J., Bauza, M., Barbarits, B., Lee, A.K., Anastassiou, C.A., Andrei, A., Aydın, Ç., et al. (2017b). Fully integrated silicon probes for high-density recording of neural activity. Nature *551*, 232–236.

Kaur, J., Fahmy, L.M., Davoodi-Bojd, E., Zhang, L., Ding, G., Hu, J., Zhang, Z., Chopp, M., and Jiang, Q. (2021). Waste Clearance in the Brain. Frontiers in Neuroanatomy *15*, 53.

Kawamura, H., and Sawyer, C.H. (1965). Elevation in Brain Temperature during Paradoxical Sleep. Science *150*, 912–913.

Kleitman, N. (1929). Sleep. Physiological Reviews *9*, 624–665.

Knyazev, G.G. (2012). EEG delta oscillations as a correlate of basic homeostatic and motivational processes. Neuroscience & Biobehavioral Reviews *36*, 677–695.

Kovac, S., Speckmann, E.-J., and Gorji, A. (2018). Uncensored EEG: The role of DC potentials in neurobiology of the brain. Progress in Neurobiology *165–167*, 51–65.

Lázár, Z.I., Dijk, D.-J., and Lázár, A.S. (2019). Infraslow oscillations in human sleep spindle activity. J Neurosci Methods *316*, 22–34.

Lecci, S., Fernandez, L.M.J., Weber, F.D., Cardis, R., Chatton, J.-Y., Born, J., and Lüthi, A. (2017). Coordinated infraslow neural and cardiac oscillations mark fragility and offline periods in mammalian sleep. Science Advances *3*, e1602026.

Lee, A.K., and Wilson, M.A. (2002). Memory of Sequential Experience in the Hippocampus during Slow Wave Sleep. Neuron *36*, 1183–1194.

Lee Kavanau, J. (2002). REM and NREM sleep as natural accompaniments of the evolution of warm-bloodedness. Neuroscience & Biobehavioral Reviews *26*, 889–906.

Legendre, R. (1913). Recherche sur le besoin de sommeil consecutive a une veille prolongee. Z Allgem Physiol *14*, 235.

Lehtelä, L., Salmelin, R., and Hari, R. (1997). Evidence for reactive magnetic 10-Hz rhythm in the human auditory cortex. Neuroscience Letters *222*, 111–114.

Leopold, D.A., Murayama, Y., and Logothetis, N.K. (2003). Very Slow Activity Fluctuations in Monkey Visual Cortex: Implications for Functional Brain Imaging. Cerebral Cortex *13*, 422–433.

Lesku, J.A., and Rattenborg, N.C. (2014). Avian sleep. Current Biology *24*, R12–R14.

Lesku, J.A., Meyer, L.C.R., Fuller, A., Maloney, S.K., Dell'Omo, G., Vyssotski, A.L., and Rattenborg, N.C. (2011). Ostriches Sleep like Platypuses. PLOS ONE *6*, e23203.

Leung, L.C., Wang, G.X., Madelaine, R., Skariah, G., Kawakami, K., Deisseroth, K., Urban, A.E., and Mourrain, P. (2019). Neural signatures of sleep in zebrafish. Nature *571*, 198–204.

Libourel, P.-A., and Barrillot, B. (2020). Is there REM sleep in reptiles? A key question, but still unanswered. Current Opinion in Physiology *15*, 134–142.

Libourel, P.-A., and Herrel, A. (2016). Sleep in amphibians and reptiles: a review and a preliminary analysis of evolutionary patterns. Biological Reviews *91*, 833–866.

Libourel, P.-A., Barrillot, B., Arthaud, S., Massot, B., Morel, A.-L., Beuf, O., Herrel, A., and Luppi, P.-H. (2018). Partial homologies between sleep states in lizards, mammals, and birds suggest a complex evolution of sleep states in amniotes. PLoS Biol *16*.

Lin, A.J., Ponticorvo, A., Konecky, S.D., Cui, H., Rice, T.B., Choi, B., Durkin, A.J., and Tromberg, B.J. (2013). Visible spatial frequency domain imaging with a digital light microprojector. J Biomed Opt *18*, 096007.

Liu, J., Li, F., Wang, Y., Pan, L., Lin, P., Zhang, B., Zheng, Y., Xu, Y., Liao, H., Ko, G., et al. (2020). A sensitive and specific nanosensor for monitoring extracellular potassium levels in the brain. Nature Nanotechnology *15*, 321–330.

Loomis, A.L., Harvey, E.N., and Hobart, G.A. (1937). Cerebral states during sleep, as studied by human brain potentials. Journal of Experimental Psychology *21*, 127–144.

Lörincz, M.L., Geall, F., Bao, Y., Crunelli, V., and Hughes, S.W. (2009). ATP-dependent infra-slow (<0.1 Hz) oscillations in thalamic networks. PLoS One *4*, e4447.

Louie, K., and Wilson, M.A. (2001). Temporally Structured Replay of Awake Hippocampal Ensemble Activity during Rapid Eye Movement Sleep. Neuron *29*, 145–156.

Louveau, A., Smirnov, I., Keyes, T.J., Eccles, J.D., Rouhani, S.J., Peske, J.D., Derecki, N.C., Castle, D., Mandell, J.W., Lee, K.S., et al. (2015). Structural and functional features of central nervous system lymphatic vessels. Nature *523*, 337–341.

Low, P.S., Shank, S.S., Sejnowski, T.J., and Margoliash, D. (2008). Mammalian-like features of sleep structure in zebra finches. PNAS *105*, 9081–9086.

Lu, J., Sherman, D., Devor, M., and Saper, C.B. (2006). A putative flip–flop switch for control of REM sleep. Nature *441*, 589–594.

Lubenov, E.V., and Siapas, A.G. (2009). Hippocampal theta oscillations are travelling waves. Nature *459*, 534–539.

Lucas, E., Sterman, M.B., and McGinty, D.J. (1969). SALAMANDER EEG-A MODEL OF PRIMITIVE SLEEP AND WAKEFULNESS. In Psychophysiology, (CAMBRIDGE UNIV PRESS 40 WEST 20TH STREET, NEW YORK, NY 10011-4211), pp. 230-.

van Luijtelaar, E.L.J.M., and Coenen, A.M.L. (1984). An EEG averaging technique for automated sleep-wake stage identification in the rat. Physiology & Behavior *33*, 837–841.

Lundberg, N. (1960). Continuous recording and control of ventricular fluid pressure in neurosurgical practice. Acta Psychiatr Scand Suppl *36*, 1–193.

Luo, T.Z., Bondy, A.G., Gupta, D., Elliott, V.A., Kopec, C.D., and Brody, C.D. (2020). An approach for long-term, multi-probe Neuropixels recordings in unrestrained rats. ELife *9*, e59716.

M. Eiland, M., I. Lyamin, O., and M. Siegel, J. (2001). State-related discharge of neurons in the brainstem of freely moving box turtles, Terrapene carolina major. Archives Italiennes de Biologie *139*, 23–36.

Ma, Q., Ineichen, B.V., Detmar, M., and Proulx, S.T. (2017). Outflow of cerebrospinal fluid is predominantly through lymphatic vessels and is reduced in aged mice. Nat Commun *8*, 1434.

Marshall, L., Mölle, M., Fehm, H.L., and Born, J. (1998). Scalp recorded direct current brain potentials during human sleep. European Journal of Neuroscience *10*, 1167–1178.

Mateo, C., Knutsen, P.M., Tsai, P.S., Shih, A.Y., and Kleinfeld, D. (2017). Entrainment of Arteriole Vasomotor Fluctuations by Neural Activity Is a Basis of Blood-Oxygenation-Level-Dependent "Resting-State" Connectivity. Neuron *96*, 936-948.e3.

Maysinger, D., Ji, J., Hutter, E., and Cooper, E. (2015). Nanoparticle-Based and Bioengineered Probes and Sensors to Detect Physiological and Pathological Biomarkers in Neural Cells. Front. Neurosci. *9*.

McCarley, R.W., and Hobson, J.A. (1975). Neuronal excitability modulation over the sleep cycle: a structural and mathematical model. Science *189*, 58–60.

McCarley, R.W., Greene, R.W., Rainnie, D., and Portas, C.M. (1995). Brainstem neuromodulation and REM sleep. Seminars in Neuroscience *7*, 341–354.

Meglasson, M.D., and Huggins, S.E. (1979). Sleep in a crocodilian, Caiman sclerops. Comparative Biochemistry and Physiology Part A: Physiology *63*, 561–567.

Moiseeva, N.I., and Aleksanian, Z.A. (1986). Slow-wave oscillations of the multi-unit activity average frequency in the human brain during drowsiness and sleep. Electroencephalography and Clinical Neurophysiology *63*, 431–437.

Mokri, B. (2001). The Monro–Kellie hypothesis: Applications in CSF volume depletion. Neurology *56*, 1746–1748.

Mölle, M., Marshall, L., Gais, S., and Born, J. (2002). Grouping of spindle activity during slow oscillations in human non-rapid eye movement sleep. J Neurosci *22*, 10941–10947.

Monto, S., Palva, S., Voipio, J., and Palva, J.M. (2008). Very Slow EEG Fluctuations Predict the Dynamics of Stimulus Detection and Oscillation Amplitudes in Humans. J. Neurosci. *28*, 8268–8272.

Mukhametov, L.M., Supin, A.Y., and Polyakova, I.G. (1977). Interhemispheric asymmetry of the electroencephalographic sleep patterns in dolphins. Brain Res *134*, 581–584.

Nakanishi, H., Sun, Y., Nakamura, R.K., Mori, K., Ito, M., Suda, S., Namba, H., Storch, F.I., Dang, T.P., Mendelson, W., et al. (1997). Positive correlations between cerebral protein synthesis rates and deep sleep in Macaca mulatta. Eur J Neurosci *9*, 271–279.

Narikiyo, K., Manabe, H., and Mori, K. (2014). Sharp wave-associated synchronized inputs from the piriform cortex activate olfactory tubercle neurons during slow-wave sleep. J Neurophysiol *111*, 72–81.

Narikiyo, K., Mizuguchi, R., Ajima, A., Shiozaki, M., Hamanaka, H., Johansen, J.P., Mori, K., and Yoshihara, Y. (2020). The claustrum coordinates cortical slow-wave activity. Nat Neurosci *23*, 741–753.

Nasretdinov, A., Lotfullina, N., Vinokurova, D., Lebedeva, J., Burkhanova, G., Chernova, K., Zakharov, A., and Khazipov, R. (2017). Direct Current Coupled Recordings of Cortical Spreading Depression Using Silicone Probes. Front. Cell. Neurosci. *11*.

Nicolau, M.C., Akaârir, M., Gamundí, A., González, J., and Rial, R.V. (2000). Why we sleep: the evolutionary pathway to the mammalian sleep. Progress in Neurobiology *62*, 379–406.

Nita, D.A., Vanhatalo, S., Lafortune, F.-D., Voipio, J., Kaila, K., and Amzica, F. (2004). Nonneuronal origin of CO2-related DC EEG shifts: an in vivo study in the cat. J. Neurophysiol. *92*, 1011–1022.

Norimoto, H., Fenk, L.A., Li, H.-H., Tosches, M.A., Gallego-Flores, T., Hain, D., Reiter, S., Kobayashi, R., Macias, A., Arends, A., et al. (2020). A claustrum in reptiles and its role in slow-wave sleep. Nature *578*, 413–418.

Norton, S., and Jewett, R.E. (1965). Frequencies of slow potential oscillations in the cortex of cats. Electroencephalography and Clinical Neurophysiology *19*, 377–386.

Novak, P., Lepicovska, V., and Dostalek, C. (1992). Periodic amplitude modulation of EEG. Neuroscience Letters *136*, 213–215.

Nunez, P.L., Nunez, M.D., and Srinivasan, R. (2019). Multi-Scale Neural Sources of EEG: Genuine, Equivalent, and Representative. A Tutorial Review. Brain Topogr *32*, 193–214.

Osterhout, W.J.V., and Hill, S.E. (1940). ACTION CURVES WITH SINGLE PEAKS IN NITELLA IN RELATION TO THE MOVEMENT OF POTASSIUM. Journal of General Physiology *23*, 743–748.

Parmeggiani, P.L. (2003). Thermoregulation and sleep. Front Biosci *8*, s557-567.

Parri, H.R., and Crunelli, V. (2001). Pacemaker calcium oscillations in thalamic astrocytes in situ. NeuroReport *12*, 3897–3900.

Pascual-Marqui, R.D. (2007). Discrete, 3D distributed, linear imaging methods of electric neuronal activity. Part 1: exact, zero error localization. ArXiv:0710.3341 [Math-Ph, Physics:Physics, q-Bio].

Penttonen, M., and Buzsáki, G. (2003). Natural logarithmic relationship between brain oscillators. Thalamus & Related Systems *2*, 145–152.

Penttonen, M., Nurminen, N., Miettinen, R., Sirviö, J., Henze, D.A., Csicsvári, J., and Buzsáki, G. (1999). Ultra-slow oscillation (0.025 Hz) triggers hippocampal afterdischarges in Wistar rats. Neuroscience *94*, 735–743.

Perry, J.C., Bergamaschi, C.T., Campos, R.R., Andersen, M.L., Montano, N., Casarini, D.E., and Tufik, S. (2011). Sympathetic and angiotensinergic responses mediated by paradoxical sleep loss in rats. J Renin Angiotensin Aldosterone Syst *12*, 146–152.

Pfurtscheller, G., and Neuper, C. (1994). Event-related synchronization of mu rhythm in the EEG over the cortical hand area in man. Neuroscience Letters *174*, 93–96.

Piechnik, S.K., Evans, J., Bary, L.H., Wise, R.G., and Jezzard, P. (2009). Functional changes in CSF volume estimated using measurement of water T2 relaxation. Magnetic Resonance in Medicine *61*, 579–586.

Piéron, H. (1913). Le problème physiologique du sommeil. (Paris: Masson).

Ponomarenko, A.A., Korotkova, T.M., and Haas, H.L. (2003). High frequency (200 Hz) oscillations and firing patterns in the basolateral amygdala and dorsal endopiriform nucleus of the behaving rat. Behavioural Brain Research *141*, 123–129.

Porkka-Heiskanen, T., Strecker, R.E., Thakkar, M., Bjørkum, A.A., Greene, R.W., and McCarley, R.W. (1997). Adenosine: A Mediator of the Sleep-Inducing Effects of Prolonged Wakefulness. Science *276*, 1265–1268.

Putzeys, J., Raducanu, B.C., Carton, A., Ceulaer, J.D., Karsh, B., Siegle, J.H., Helleputte, N.V., Harris, T.D., Dutta, B., Musa, S., et al. (2019a). Neuropixels Data-Acquisition System: A Scalable Platform for Parallel Recording of 10 000+ Electrophysiological Signals. IEEE Transactions on Biomedical Circuits and Systems *13*, 1635–1644.

Putzeys, J., Raducanu, B.C., Carton, A., Ceulaer, J.D., Karsh, B., Siegle, J.H., Helleputte, N.V., Harris, T.D., Dutta, B., Musa, S., et al. (2019b). Neuropixels Data-Acquisition System: A Scalable Platform for Parallel Recording of 10 000+ Electrophysiological Signals. IEEE Transactions on Biomedical Circuits and Systems *13*, 1635–1644.

Ramm, P., and Smith, C.T. (1990). Rates of cerebral protein synthesis are linked to slow wave sleep in the rat. Physiol Behav *48*, 749–753.

Rattenborg, N.C. (2007). Response to commentary on evolution of slow-wave sleep and palliopallial connectivity in mammals and birds: A hypothesis. Brain Research Bulletin *72*, 187–193.

Rattenborg, N.C., Lima, S.L., and Amlaner, C.J. (1999). Half-awake to the risk of predation. Nature *397*, 397–398.

Rattenborg, N.C., Lesku, J.A., and Martinez-Gonzalez, D. (2011). Evolutionary perspectives on the function of REM sleep. In Rapid Eye Movement Sleep, B.N. Mallick, S.R. Pandi-Perumal, R.W. McCarley, and A.R. Morrison, eds. (Cambridge: Cambridge University Press), pp. 58–70.

Revich, M., Isaacs, G., Evarts, E., and Kety, S. (1968). The Effect of Slow Wave Sleep and Rem Sleep on Regional Cerebral Blood Flow in Cats. Journal of Neurochemistry *15*, 301–306.

Rial, R.V., Akaârir, M., Gamundí, A., Nicolau, C., Garau, C., Aparicio, S., Tejada, S., Gené, L., González, J., De Vera, L.M., et al. (2010). Evolution of wakefulness, sleep and hibernation: From reptiles to mammals. Neuroscience & Biobehavioral Reviews *34*, 1144–1160.

Rodriguez, A., and Laio, A. (2014). Clustering by fast search and find of density peaks. Science *344*, 1492–1496.

Roffwarg, H.P., Muzio, J.N., and Dement, W.C. (1966). Ontogenetic Development of the Human Sleep-Dream Cycle. Science *152*, 604–619.

Rosner, M.J. (1986). The Vasodilatory Cascade and Intracranial Pressure. In Intracranial Pressure VI, J.D. Miller, G.M. Teasdale, J.O. Rowan, S.L. Galbraith, and A.D. Mendelow, eds. (Berlin, Heidelberg: Springer), pp. 137–141.

Roth, C., Achermann, P., and Borbély, A.A. (1999). Alpha activity in the human REM sleep EEG: topography and effect of REM sleep deprivation. Clinical Neurophysiology *110*, 632–635.

Ruskin, D.N., Bergstrom, D.A., Kaneoke, Y., Patel, B.N., Twery, M.J., and Walters, J.R. (1999). Multisecond Oscillations in Firing Rate in the Basal Ganglia: Robust Modulation by Dopamine Receptor Activation and Anesthesia. Journal of Neurophysiology *81*, 2046–2055.

Sah, P., and Louise Faber, E.S. (2002). Channels underlying neuronal calcium-activated potassium currents. Progress in Neurobiology *66*, 345–353.

Sakata, M., Sei, H., Eguchi, N., Morita, Y., and Urade, Y. (2005). Arterial Pressure and Heart Rate Increase during REM Sleep in Adenosine A2A-Receptor Knockout Mice, but not in Wild-Type Mice. Neuropsychopharmacol *30*, 1856–1860.

Salio, C., Lossi, L., Ferrini, F., and Merighi, A. (2006). Neuropeptides as synaptic transmitters. Cell Tissue Res *326*, 583–598.

Sanchez-Vives, M.V., and McCormick, D.A. (2000). Cellular and network mechanisms of rhythmic recurrent activity in neocortex. Nat Neurosci *3*, 1027–1034.

Saper, C.B., Chou, T.C., and Scammell, T.E. (2001). The sleep switch: hypothalamic control of sleep and wakefulness. Trends in Neurosciences *24*, 726–731.

Schöne, C., Apergis-Schoute, J., Sakurai, T., Adamantidis, A., and Burdakov, D. (2014). Coreleased orexin and glutamate evoke nonredundant spike outputs and computations in histamine neurons. Cell Rep *7*, 697–704.

Schuman, M. (1980). The Psychophysiological Model of Meditation and Altered States of Consciousness: A Critical Review. In The Psychobiology of Consciousness, J.M. Davidson, and R.J. Davidson, eds. (Boston, MA: Springer US), pp. 333–378.

Scouten, A., and Constable, R.T. (2008). VASO-based calculations of CBV change: Accounting for the dynamic CSF volume. Magnetic Resonance in Medicine *59*, 308–315.

Sei, H., Sakai, K., Kanamori, N., Salvert, D., Vanni-Mercier, G., and Jouvet, M. (1994). Long-term variations of arterial blood pressure during sleep in freely moving cats. Physiology & Behavior *55*, 673–679.

Senarathna, J., Yu, H., Deng, C., Zou, A.L., Issa, J.B., Hadjiabadi, D.H., Gil, S., Wang, Q., Tyler, B.M., Thakor, N.V., et al. (2019). A miniature multi-contrast microscope for functional imaging in freely behaving animals. Nature Communications *10*, 99.

Shein-Idelson, M., Ondracek, J.M., Liaw, H.-P., Reiter, S., and Laurent, G. (2016). Slow waves, sharp waves, ripples, and REM in sleeping dragons. Science *352*, 590–595.

Shein-Idelson, M., Pammer, L., Hemberger, M., and Laurent, G. (2017). Large-scale mapping of cortical synaptic projections with extracellular electrode arrays. Nature Methods *14*, 882–890.

Siegel, J.M. (2008). Do all animals sleep? Trends in Neurosciences *31*, 208–213.

Siegel, J.M., Manger, P.R., Nienhuis, R., Fahringer, H.M., and Pettigrew, J.D. (1998). Monotremes and the evolution of rapid eye movement sleep. Phil. Trans. R. Soc. Lond. B *353*, 1147–1157.

Siegel, J.M., Manger, P.R., Nienhuis, R., Fahringer, H.M., Shalita, T., and Pettigrew, J.D. (1999). Sleep in the platypus. Neuroscience *91*, 391–400.

Siegel, M., Donner, T.H., and Engel, A.K. (2012). Spectral fingerprints of large-scale neuronal interactions. Nat Rev Neurosci *13*, 121–134.

Siegle, J.H., Jia, X., Durand, S., Gale, S., Bennett, C., Graddis, N., Heller, G., Ramirez, T.K., Choi, H., Luviano, J.A., et al. (2021). Survey of spiking in the mouse visual system reveals functional hierarchy. Nature 1–7.

Silva, J. (2014). Slow Inactivation of Na+ Channels. In Voltage Gated Sodium Channels, P.C. Ruben, ed. (Berlin, Heidelberg: Springer), pp. 33–49.

Snyder, F., Hobson, J.A., Morrison, D.F., and Goldfrank, F. (1964). Changes in respiration, heart rate, and systolic blood pressure in human sleep. Journal of Applied Physiology *19*, 417–422.

Somers, V.K., Dyken, M.E., Mark, A.L., and Abboud, F.M. (1993). Sympathetic-Nerve Activity during Sleep in Normal Subjects. New England Journal of Medicine *328*, 303–307.

Sørensen, E., Olesen, J., Rask-Madsen, J., and Rask-andersen, H. (1978). The electrical potential difference and impedance between CSF and blood in unanesthetized man. Scandinavian Journal of Clinical and Laboratory Investigation *38*, 203–207.

Steinmetz, N.A., Aydin, C., Lebedeva, A., Okun, M., Pachitariu, M., Bauza, M., Beau, M., Bhagat, J., Böhm, C., Broux, M., et al. (2020). Neuropixels 2.0: A miniaturized high-density probe for stable, long-term brain recordings. BioRxiv 2020.10.27.358291.

Steriade, M., Nunez, A., and Amzica, F. (1993a). A novel slow (< 1 Hz) oscillation of neocortical neurons in vivo: depolarizing and hyperpolarizing components. J. Neurosci. *13*, 3252–3265.

Steriade, M., Nunez, A., and Amzica, F. (1993b). Intracellular analysis of relations between the slow (< 1 Hz) neocortical oscillation and other sleep rhythms of the electroencephalogram. J. Neurosci. *13*, 3266–3283.

Steriade, M., Contreras, D., Dossi, R.C., and Nunez, A. (1993c). The slow (< 1 Hz) oscillation in reticular thalamic and thalamocortical neurons: scenario of sleep rhythm generation in interacting thalamic and neocortical networks. J. Neurosci. *13*, 3284–3299.

Steriade, M., McCormick, D.A., and Sejnowski, T.J. (1993d). Thalamocortical oscillations in the sleeping and aroused brain. Science *262*, 679–685.

Stirling, R.V., Dunlop, S.A., and Beazley, L.D. (1998). An in vitro technique for electrophysiological mapping of reptilian retinotectal projections. Journal of Neuroscience Methods *81*, 85–89.

Striedter, G.F. (2016). Evolution of the hippocampus in reptiles and birds. J Comp Neurol *524*, 496–517.

Tallgren, P., Vanhatalo, S., Kaila, K., and Voipio, J. (2005). Evaluation of commercially available electrodes and gels for recording of slow EEG potentials. Clinical Neurophysiology *116*, 799–806.

Tauber, E.S., Roffwarg, H.P., and Weitzman, E.D. (1966). Eye Movements and Electroencephalogram Activity during Sleep in Diurnal Lizards. Nature *212*, 1612–1613.

Tauber, E.S., Rojas-Ramírez, J., and Peón, R.H. (1968). Electrophysiological and behavioral correlates of wakefulness and sleep in the lizard, Ctenosaura pectinata. Electroencephalography and Clinical Neurophysiology *24*, 424–433.

Tervo, D.G.R., Huang, B.-Y., Viswanathan, S., Gaj, T., Lavzin, M., Ritola, K.D., Lindo, S., Michael, S., Kuleshova, E., Ojala, D., et al. (2016). A designer AAV variant permits efficient retrograde access to projection neurons. Neuron *92*, 372–382.

Tosches, M.A., Yamawaki, T.M., Naumann, R.K., Jacobi, A.A., Tushev, G., and Laurent, G. (2018a). Evolution of pallium, hippocampus, and cortical cell types revealed by single-cell transcriptomics in reptiles. Science *360*, 881–888.

Tosches, M.A., Yamawaki, T.M., Naumann, R.K., Jacobi, A.A., Tushev, G., and Laurent, G. (2018b). Evolution of pallium, hippocampus, and cortical cell types revealed by single-cell transcriptomics in reptiles. Science *360*, 881–888.

Turner, K.L., Gheres, K.W., Proctor, E.A., and Drew, P.J. (2020). Neurovascular coupling and bilateral connectivity during NREM and REM sleep. ELife *9*, e62071.

Ungurean, G., Barrillot, B., Martinez-Gonzalez, D., Libourel, P.-A., and Rattenborg, N.C. (2020). Comparative Perspectives that Challenge Brain Warming as the Primary Function of REM Sleep. IScience *23*, 101696.

Vanhatalo, S., Tallgren, P., Becker, C., Holmes, M.D., Miller, J.W., Kaila, K., and Voipio, J. (2003). Scalp-recorded slow EEG responses generated in response to hemodynamic changes in the human brain. Clinical Neurophysiology *114*, 1744–1754.

Vanhatalo, S., Palva, J.M., Holmes, M.D., Miller, J.W., Voipio, J., and Kaila, K. (2004). Infraslow oscillations modulate excitability and interictal epileptic activity in the human cortex during sleep. Proc. Natl. Acad. Sci. U.S.A. *101*, 5053–5057.

Voigts, J., Siegle, J.H., Pritchett, D.L., and Moore, C.I. (2013). The flexDrive: an ultra-light implant for optical control and highly parallel chronic recording of neuronal ensembles in freely moving mice. Front. Syst. Neurosci. *7*.

Voipio, J., Tallgren, P., Heinonen, E., Vanhatalo, S., and Kaila, K. (2003). Millivolt-Scale DC Shifts in the Human Scalp EEG: Evidence for a Nonneuronal Generator. Journal of Neurophysiology *89*, 2208–2214.

Volgushev, M., Chauvette, S., Mukovski, M., and Timofeev, I. (2006). Precise Long-Range Synchronization of Activity and Silence in Neocortical Neurons during Slow-Wave Sleep. J. Neurosci. *26*, 5665–5672.

W. F. Flanigan, J. (1973). Sleep and Wakefulness in Iguanid Lizards, Ctenosaura pectinata and Iguana iguana; pp. 401–416. BBE *8*, 401–416.

Walker, J.M., and Berger, R.J. (1973). A Polygraphic Study of the Tortoise (Testudo denticulata). BBE *8*, 453–467.

Walker, M.P., and Stickgold, R. (2006). Sleep, Memory, and Plasticity. Annual Review of Psychology *57*, 139–166.

Walker, J.M., Glotzbach, S.F., Berger, R.J., and Heller, H.C. (1977). Sleep and hibernation in ground squirrels (Citellus spp): electrophysiological observations. American Journal of Physiology-Regulatory, Integrative and Comparative Physiology *233*, R213–R221.

Walter, W.G. (1936). THE LOCATION OF CEREBRAL TUMOURS BY ELECTRO-ENCEPHALOGRAPHY. The Lancet *228*, 305–308.

Wang, H., Jing, M., and Li, Y. (2018). Lighting up the brain: genetically encoded fluorescent sensors for imaging neurotransmitters and neuromodulators. Current Opinion in Neurobiology *50*, 171–178.

Warner, B.F., and Huggins, S.E. (1978). An electroencephalographic study of sleep in young caimans in a colony. Comparative Biochemistry and Physiology Part A: Physiology *59*, 139–144.

Wightman, R.M. (2006). Probing Cellular Chemistry in Biological Systems with Microelectrodes. Science *311*, 1570–1574.

Xie, L., Kang, H., Xu, Q., Chen, M.J., Liao, Y., Thiyagarajan, M., O'Donnell, J., Christensen, D.J., Nicholson, C., Iliff, J.J., et al. (2013). Sleep Drives Metabolite Clearance from the Adult Brain. Science *342*.

Zhang, H., Watrous, A.J., Patel, A., and Jacobs, J. (2018). Theta and Alpha Oscillations Are Traveling Waves in the Human Neocortex. Neuron *98*, 1269-1281.e4.